Mixed Abrasive Slurries of Ceria and Silica Nanoparticles formed by Electrostatic Attraction for Shallow Trench Isolation Chemical Mechanical Polishing

by

Korel Vanese Dawkins

A thesis submitted in partial fulfillment of the requirements for the degree of

Doctor of Philosophy

in

Chemical Engineering

Department of Chemical and Materials Engineering
University of Alberta

© Korel Vanese Dawkins, 2019

Abstract

Device isolation is achieved using shallow trench isolation (STI) which requires chemical mechanical planarization (CMP) of the excess and unwanted oxide layer and stopping on the underlying silicon nitride layer. The increasing stringent requirement of the STI CMP performance is the driving force behind developing new slurries used in this process, which enhances oxide-to–nitride polish rate selectivity with little to no surface defects. In this study, mixed abrasive slurries (MAS) of colloidal ceria and silica abrasives are used to achieve high oxide-to-nitride polish rate selectivity through a systematic investigation of the electrostatic interactions between particle-particle and particle-wafer surface, the characteristics of the colloidal stability of the suspensions and their impact on polish rate along with the use of additives in suppressing nitride polish rate and the associated pH range in which high selectivity is observed. A model for the material removal mechanism using MAS is proposed, based on an adaptation of the surface area and indentation based mechanism. Within a range of ceria-to-silica weight ratios, known as the transition range, the mixed abrasive slurries were observed to be unstable which corresponded with high material removal rates of both oxide and nitride films. Polishing above this range, produced high oxide removal rates but low nitride removal rates giving relatively high selectivity. Frictional forces during polishing are investigated by using the table motor current; the results demonstrate that this has an impact on polish rates especially of nitride surfaces which polish mechanism appears to be predominately mechanical. The overall rate of material removal is maximized by polishing with such mixed abrasive slurries in a synergistic ratio compared to the slurries containing a single kind of abrasive under the same conditions and at high weight ratios of MAS (≥ 0.2), STI CMP selectivity is enhanced.

Preface

Chapter 4 of this thesis has been published as K. Dawkins, R.W. Rudyk, Z. Xu and K. Cadien, "The pH-dependant attachment of ceria nanoparticles to silica using surface analytical techniques," *Journal of Applied Surface Science*, vol. 345 (2015), 249-255. I was responsible for the data collection and analysis as well as the manuscript composition. R.W. Rudyk assisted with the XPS data analysis and contributed to manuscript edits. Z. Xu and K. Cadien were the supervisory authors and were involved with concept formation and manuscript edit.

Dedication

Dedicated to the Memory

of

My loving Father, Earl Dawkins, for supporting me through my entire educational journey. You always believed in my ability to be successful in academia. You are gone but your belief in me has made this journey possible.

My Grandmother, Gladys Louise Howard, a strong and gentle soul who taught me that hard work is the key to success and that so much could be done with little.

My Uncle, Winston McFarlane, my greatest cheerleader.

Acknowledgements

Firstly, I would like to thank God for giving me the ability to complete this thesis and surrounding me with people that have made this journey an enlightening experience. I would like to gratefully acknowledge my supervisors Dr. Kenneth Cadien and Dr. Zhenghe Xu for their professional guidance, patience and encouragement. Dr. Cadien has been exceptionally supportive both academically and personally and has given me insightful suggestions and comments that have contributed immeasurably to the being of this thesis. I would also like to acknowledge my supervisory committee, Dr. Sean Sanders for his insightful comments. I would like to thank the faculty and staff of the Department of Chemical and Materials Engineering. Lily Laser, Kevin Heidebrecht, Les Dean, Jim Skwarok, Jie Ru and Lisa Carreiro all provided fundamental administrative and technical assistance to me.

I am very grateful to the staff of NanoFab, particularly the late Les Schowalter. My fellow students have been a constant source of support and encouragement. Special thanks to fellow group mates Lucy Nolan for many insightful discussions and guidance during the start of my program and Triratna Muneshwar for all the meaningful discussions and for his valuable help with the operations of the CMP tool. I would additionally like to acknowledge the financial assistance I received from the Natural Sciences and Engineering Research Council of Canada, and the University of Alberta.

A special thank you to my Edmonton Moravian Church family who have been a constant source of prayers, support and encouragement during my time in Edmonton. Finally, I would like to acknowledge my mom, Carol Smikle, and siblings for their love, support and encouragement throughout my pursuit of this degree.

Contents

List of Tables

List of Figures

Chapter 1 : Introduction

Chemical mechanical polishing also known as chemical mechanical planarization (CMP) is a relatively newer technology for the fabrication of devices in the semiconductor industry when compared to lithography or etching. Chemical Mechanical Polishing, was developed in the early 1980's [1] by IBM, initially used to address topography issues on silicon substrate in integrated circuit (IC) manufacturing. Since then, CMP has grown into a key enabling technology of virtually any material and has expanded to other applications such as shallow trench isolation (STI), copper damascene process and multilevel metallization among others. Presently, semiconductor devices are composed of multilayers and each layer must be globally planar before the next is deposited. CMP gained its' popularity because it is the only technique capable of producing globally planar surfaces and thus enables multilevel, interconnected structures which allowed for the continued shrinkage of microelectronic devices.

Shallow Trench Isolation is widely adapted as shrinks below 0.35 μm required new isolation. The performance requirement of STI CMP is more stringent due to the smaller proximity between transistors and demands precise control over the CMP process for device fabrication. The increasing need to achieve accurate polishing stop while minimizing over polishing in STI is the driving force behind optimizing CMP variables such as the polishing slurries. This includes finding new ways to increase the oxide-to-nitride selectivity by exploiting new chemicals such as surfactants and mixed abrasives used in CMP slurries. However, key factors such as slurry pH, slurry stability, abrasive particle type and size, abrasive concentration, and chemical additives are known to significantly affect the CMP mechanism[2] [34]

To develop CMP processes for STI CMP, a thorough understanding of all the variables that control the successful outcome of a CMP process must be reached. An example, is the need to investigate particle-particle and particle-wafer interactions in order to develop novel slurries for STI CMP. STI CMP has driven the development of high selectivity slurries that are capable of removing the oxide layer and stopping on the underlying nitride layer. Initially, silica based slurries were used for STI CMP, however they exhibit low polishing selectivity between silicon dioxide and silicon nitride substrates[5]. Ceria slurries are said to be the primary candidates for STI due to their preferential polishing of oxides over nitrides and enhancement in surface finish all due to ceria possessing the "chemical tooth"[6]. However, the use of ceria slurries in STI CMP comes with challenges such as micro-scratches due to the agglomeration of abrasive particles. More recently, mixed abrasive slurries (MAS) are promising for STI CMP. Mixed abrasive slurries of ceria and silica particles have shown an enhancement in silicon dioxide removal rates over single component slurries of either ceria or silica with less defects[7–10]. However, using these slurries also slightly increases the silicon nitride removal rates.

It is hypothesized that slurry additives such as surfactants can be utilized in such slurries to suppress nitride polishing rates while maintaining relatively high oxide polishing rates[11–20]. This research is aimed at developing a novel mixed abrasive slurry consisting of colloidal ceria and silica for STI CMP, based on fundamental understanding of the slurry stability, particle- particle and particle-wafer interactions. Material removal rates are found to be dependent on both ceria- to- silica weight ratio and slurry pH, which also affect the stability of the slurries through particle - particle interactions. The models proposed within this work to achieve high oxide-to-nitride selectivity which is necessary for STI CMP, are based on (i) electrostatic interactions, (ii) selective additive adsorption onto the nitride surface forming a passivation layer and (iii) reduction of the friction force during nitride CMP. To date, there are few studies on STI CMP by mixed ceria and silica slurries or the characteristics of such slurries such as its stability, which we aim to study in this research.

Scope of Dissertation

The main objective of this research is to develop a novel STI polishing slurry for the CMP of silicon dioxide and silicon nitride films with the ultimate goal of increasing the oxide-to-nitride polish rate selectivity. The colloidal stability of slurries is an important factor in STI CMP because it affects material removal rate as well as causing defects such as micro-scratches due to the agglomeration of particles present in poor stability slurries. Therefore, a secondary objective of this research is to perform an in-depth study through the experimentation of colloidal stability of the MAS of ceria and silica, the interactions between slurry particles and the interaction between slurry particles and the surface to be polished. Lastly, an investigation into the use of additives to suppress the nitride polish rate is performed. A synopsis of the work done for this research follows:

An introduction into CMP and STI CMP is presented in this chapter along with an outline of the work done in achieving oxide-to nitride selectivity for STI CMP using mixed abrasive slurries.

Chapter 2 reviews the literature on the fundamentals of the CMP process. The roles of the CMP components such as the pad, wafer and slurry are elaborated upon. The mechanical and chemical processes that constitute CMP are covered in greater details. A review of STI CMP process and slurry selectivity follows. The selectivity of mixed abrasive slurries for STI CMP is defined. Furthermore, the challenges we face in CMP today is discussed.

Chapter 3 details the materials and methods used for this research. CMP experiments are defined. Also, experiments and measurements using both particle characterization methods and surface characterization methods are presented.

Chapter 4 is a study of the electrostatic interaction between ceria particles and silicon dioxide wafer surfaces for its later removal during the cleaning process. It is shown that pH plays a major role in the adhesion of ceria particles to silica surfaces. The optimum pH for obtaining a clean silica surface, after exposure to a ceria slurry is pH > 9.6. The ceria particles used in this work are characterized and found to be composed of a ~31%:69% ratio of Ce(III):Ce(IV)

Chapter 5 examines the stability of mixed abrasive slurries and the oxide and nitride polish rates of said slurries as a function of slurry weight ratio. It is shown that maximum polish rates of both oxide and nitride films occur at the isoelectric point of the composite particles which corresponds to very unstable slurries. However, when the MAS resembles that of pure ceria which corresponds to stable slurries at higher slurry weight ratios, highest selectivity is achieved.

Chapter 6 demonstrates the use of additives to the MAS to maximize selectivity and the use of a different silica core particle. A model demonstrating the polishing mechanism using MAS is proposed and may explain why the use of additives with MAS proved to be only marginally effective in suppressing the nitride removal rate to a very low value.

Chapter 7 presents the relationship between the polishing rate and frictional force. Experimental results pertaining to this relationship are presented and discussed and conclusions are drawn.

Chapter 8 offers a conclusion of this work and recommendations for future work.

Chapter 2 : Literature Review

2.1 CMP Fundamentals

Chemical Mechanical Polishing is an excellent global planarization technique that uses a synergistic combination of chemical etching and mechanical forces producing globally planar surfaces with enhanced surface finish. CMP was adapted from optical lens polishing methods, i.e. telescope mirrors [21]. One of the earliest uses of CMP was in glass polishing. Outside of the semiconductor industry, CMP is popular in optical lens polishing.

The CMP process was initially developed to address topography issues on Si substrates in microelectronic fabrication by IBM in the early 80's. Before CMP, severe topography existed at interlayer dielectric (ILD) levels, which resulted in sloped wall vias limiting designs to only 2 or 3 levels of metal. This topography is disadvantageous because it increases the depth of focus during lithography[22,23]. Surface topography had to be reduced in order to print smaller features. With the shrinkage of device dimension and the number of components in the circuit increasing, CMP enabled multiple layers of metals, increased packing density, improved device speed, greater functionality and reduction in manufacturing cost.

A typical CMP system consists mainly of three components: polishing pad, wafer and the slurry with abrasive particles. A schematic presentation of the CMP components is shown in Figure 2-1. During CMP, the wafer to be polished is held upside down by a rotating carrier and pressed face down against the compliant rotating pad that serves as a conduit for the slurry with abrasive particles and chemical additives, which is introduced onto the pad by a peristaltic pump. Material removal is achieved by the synergistic combination of mechanical and chemical forces.

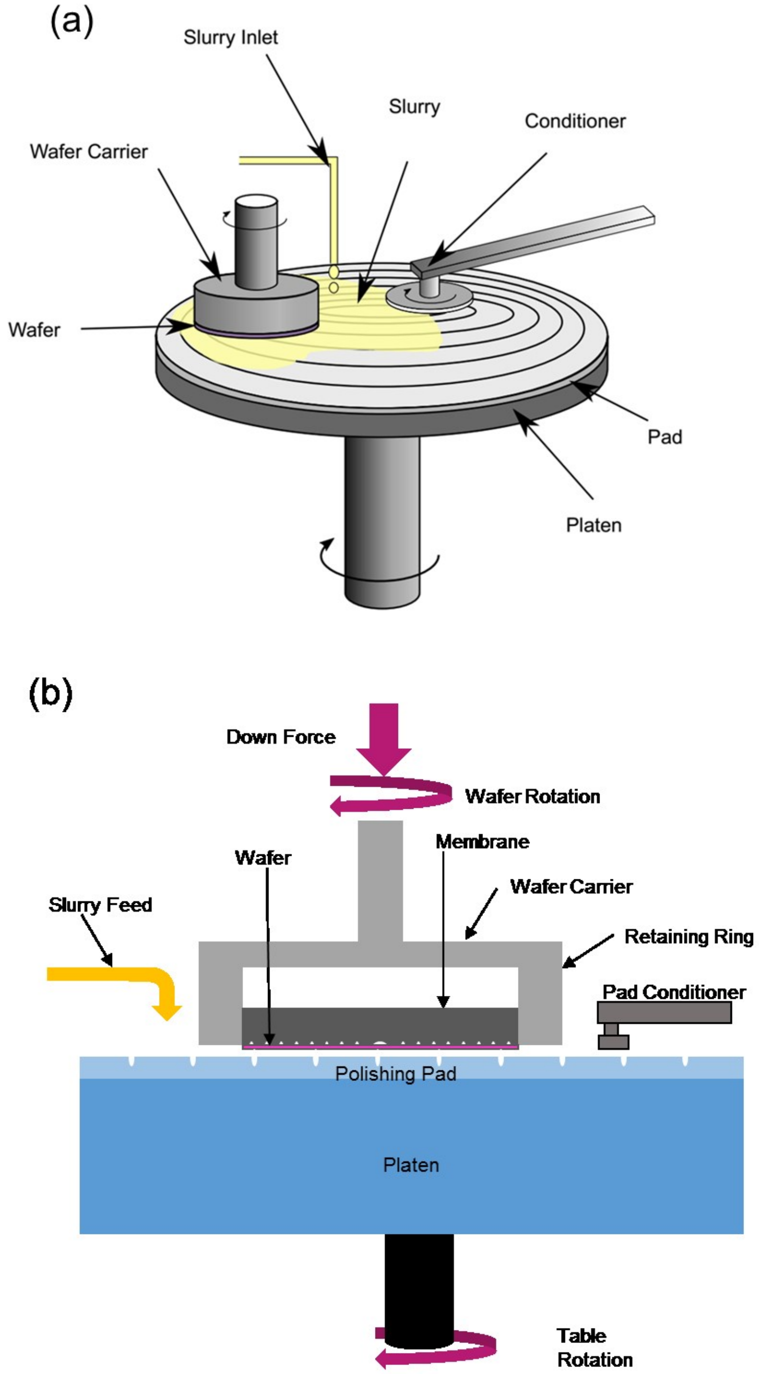

Figure 2-1 (a) Schematic diagram showing the polishing components and (b) cross-section through wafer carrier

In addition to removing material from the surface at rates of several hundred nanometers per minute, global planarization is also achieved.

From the literature [24], it is reported that the gap between the pad-wafer is approximately 40 µm. In the case of complete lubrication, the wafer is completely separated from the pad by the slurry flowing between them. CMP is a deceptively complex and multi-parameter process that should yield high material removal rates and global planarization with little to no surface defects [2,25]. In the case of isolation techniques, CMP should also provide high selectivity.

2.2 CMP Components

CMP systems consist of 3 main components: pad, wafer and slurry. These are considered to be "consumables" [26]. CMP processing cost are split between CMP equipment, cleaning equipment and consumable materials. The consumables account for about 70% of the total cost of the CMP process of which the slurry and pad are the most expensive and hence take a significant portion of the present billion dollar CMP market. The roles of each of these components are discussed below.

2.2.1 Surfaces to be polished

Initially, CMP was developed to polish crystal silicon wafer for interlayer dielectrics in the microelectronics industry. Since then it has been applied successfully to a wide range of surfaces such as: reflown glass, metals, metalloids, insulating materials for shallow trench isolation, ceramics and surfaces such as carbon nanotubes and zinc oxide [26]. A list of surfaces processed using CMP are given in Table 2.1.[26,27] When designing CMP processes for these materials, their structural, chemical and mechanical properties must be fully understood.

Different surfaces employ different CMP processes, for example the method used for metal surfaces such as Cu in the copper damascene process is different from insulating materials, such as SiO_2 and Si_3N_4 in shallow trench isolation. Typically, the metal or dielectric film is modified by the chemical properties of the polishing slurry and this modified top layer is abraded away by the abrasive particles. In the case where passivation agents are present in the slurry, a passivation layer is formed on the underlying barrier layer protecting it from chemical dissolution and erosion [28–30]. Continuous material removal from the top layer of the film occurs until the entire film surface is planar [28,29].

Table 2-1 A broad but not exhaustive list of surfaces processed using CMP[26,27]

Metal, Metalloids	**Dielectric**	**Others**
Al	SiO_2	ITO
Cu	Si_3N_4	Carbon nanotubes
Pt	Low-*k* dielectrics	Zinc Oxide
Au	Cu-alloys	Plastics, ceramics
Ti	Al -alloys	Aerogels
Ta	Polysilicon	Optoelectronic materials
TiN	Polymers	High *k* dielectrics
W	Tantalum Nitride	

2.2.2 Polishing Pad

Another consumable that influences the successful outcome of the CMP process is the polishing pad. Polishing pad properties such as compressibility, types of grooves, pad asperity, shear modulus, pad hardness and roughness are some of the variables that affect the efficiency of polishing. Polishing pads are polymeric and are typically made from cast polyurethane foam containing macroscopic porous regions or fibrous in their microstructure [26,27,31–33]. Filler material may also be added to the polyurethane to achieve desired mechanical properties such as pad hardness[31,32]. Depending on their application, polishing pads have different hardness, for example, softer pads are required for metal CMP such as copper while harder pads are typically used for SiO_2 polishing[34]. They are often grooved on the uppermost polishing surface and may also contain microscopic pores, asperities or peaks on the pad surface. The grooves facilitate slurry transportation on the surface, and establishes the lubrication system underneath the wafer. Grooving patterns range from radial and or concentric circular grooves, spirals, square grids and logarithmical "k" grooves [26,27]. A schematic representation of different groove patterns are shown below.

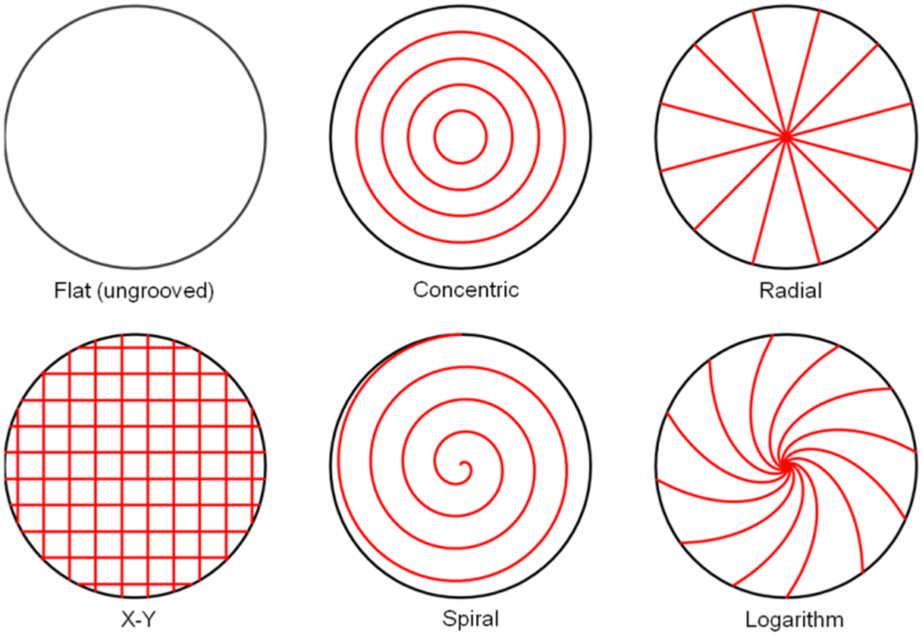

Figure 2-2 Pad grooving patterns [26]

The pad has several functions in the CMP process[26,27,34]: uniform slurry transport, the grooves transport slurry across the pad-wafer interface, from the centre of the pad towards the outer edge of the wafer. The pad executes polishing action as the pad asperities provide a point of contact for the abrasives with the wafer thus enabling polishing. Finally, residues produced during polishing are transported away by the grooves in the pad. Also, it plays a role in material removal uniformity and post polish surface quality [30], the pad provides uniform distribution of applied pressure across the wafer.

To maintain reproducible polishing conditions and uniform removal rates, CMP pads are usually conditioned using a rotating diamond grit disc pad conditioner between CMP runs [26,27] to prevent pad glazing that occurs after continuous use due to polish debris. Conditioning maintains the pad surface roughness thus extending the pad lifetime.

2.2.3 Slurry

CMP slurries are colloidal dispersions that consist of a combination of abrasive particles and chemical additives which are suspended in deionized water. CMP slurries consist mostly of water with the active components only making up a small percentage, typically 10% or less of the entire slurry volume [26,27]. Usually, polishing slurries contain between 1 wt% and 10 wt % solid abrasives. CMP slurries contain both chemical and mechanical active components. The abrasive particles vary in size between 5 nm and several microns and are responsible for the mechanical abrasion of the surface being polished [26,27,30]. The chemically active portion is brought about by additives to the slurry such as pH adjusters, buffers, oxidizers, corrosion inhibitors, chelating agents, and organic compounds such as dispersants, surfactants and passivation agents [26,27]. Chemical additives are used to soften/modify or oxidize the metal and/or dielectric film as well as slurry stabilization. Depending on the particular CMP application, additives are also chosen to optimize selectivity for selective removal of targeted materials.

Depending on the material to be polished, different types of chemical additives are added to the slurry. ILD CMP slurries used for polishing dielectric materials such as SiO_2 are composed of abrasives silica and/or ceria and dispersants among other additives to eliminate aggregates of the particles from the slurry as this will lead to scratching on the wafer surface. Slurries for STI CMP should produce high selectivity, that is, produce high oxide removal rates and able to stop on the silicon nitride layer. As a result, these slurries contain passivation agents/surfactants that will selectively adsorb on the nitride surface inhibiting polishing hence achieving oxide-to-nitride selectivity. On the other hand, metal slurries tend to be more chemically active than dielectric slurries which are less complex. Therefore, they contain a number of additives such as: hydrogen peroxide as an oxidizer to form a soft layer on the wafer surface for easy removal by mechanical abrasion, citric acid or glycine as chelating agents used to dissolve any polishing debris removed from the wafer surface and avoid scratching, and benzotriazole, or BTAH as corrosion inhibitors. They may also contain surfactants used to passivate the film as well as a pH adjuster [26,30].

Silica and alumina particles varying in size from several nanometers to several microns in diameter are typically used for polishing copper and tungsten while for polishing silicon oxide and nitride such as in shallow trench isolation, the abrasives are usually fumed or colloidal silica and/or ceria. It should also be noted that reactive abrasives such as ceria might contribute to the chemical active portion due to particle-substrate bonding [6,33]. Ceria is preferred over silica for the CMP of dielectric surfaces, especially for shallow trench isolation due to enhanced removal rate, selectivity and improved surface finish [5, 23].Composite particles or mixed abrasives have been fabricated and more recently used in oxide CMP [7–9,35,36] and is especially useful in STI CMP as it shows higher polish rates, better selectivity and low surface defects compared to single abrasives

Ideally, a CMP slurry should provide high material removal rates, within-wafer non-uniformity, global planarity and high selectivity with low surface defects. Slurry components such as abrasive type, shape and size, pH, concentration have significant influence on CMP performance and are also the cause of many surface defects.

2.2.3.1 Abrasives particles in CMP slurries.

Abrasive particles range in size from 5-500 nm and tend to be spherical in shape but larger particles may vary in shape such as cubes, platelets, ellipsoids, spheroids and flakes[26 30]. Slurries can either be single abrasive or mixed abrasives. As the name suggests, single abrasive slurries (SAS) consist of only one type of abrasive particle while mixed abrasive slurries (MAS) consists of a mixture of two abrasive particles usually chosen from alumina, ceria, silica, titanium dioxide, manganese oxide, zirconium dioxide among others. When two different types of abrasives are present, additional particle-particle electrostatic interactions occur which affects the stability of the slurry. Additionally, there is interaction between these composite particles and the film which might increase or decrease material removal rate. However they can be designed in a way to optimize material removal and selectivity.

For the rest of this section, we will limit our focus to silica and ceria abrasives for STI CMP.

Silica

Silica also known as silicon dioxide (SiO_2), found in nature as quartz sand, however, amorphous silica which we will be concentrating on is industrially manufactured and the two main forms are: (i) fumed and (ii) colloidal silica [37]. Amorphous silica is acidic and possess a small dielectric constant. It has a molecular weight of approximately 60.08 (g/mol), particle density[38] ~2.2 g/cm^3 and pH_{zpc} of ~ 2 [39]. Silica is the most commonly used abrasive in copper CMP and is also widely used in ILD and STI CMP.

Fumed silica is prepared by thermal pyrolysis of silicon tetrachloride according to the following equation [37]:

$$SiCl_4 + 2H_2 + O_2 \rightarrow SiO_2 + 4HCl \qquad (1)$$

Fumed silica has many advantages such as high purity and it is cheap and easy to prepare however, its main disadvantage is that it agglomerates easily in aqueous media [37] and leads to scratching on the wafer surface during polishing. As a result, colloidal silica has replaced fumed silica for polishing of film for high quality surface finish.

In contrast to fumed silica, colloidal silica is prepared in the liquid phase. Colloidal silica is typically spherical in shape and is usually very small ranging from 30-100 nm suspended in liquid. The Stober process can be used to synthesize precipitated colloidal silica particles by the precipitation of tetraethylorthosilicate with water and ammonia. Colloidal silica particles are made in such a manner that the desired particle size, uniform size distribution and particle porosity can all be controlled.

Ceria

Cerium is one of the most abundant rare earth metal in the lanthanide series in the earth's crust [40]. Ceria, otherwise called cerium oxide (CeO_2) is a rare earth metal oxide that has a MW of 172.115 g/mol, particle density of approximately 7.65 g/cm^3 and reported isoelectric point of ceria occurring between 6-9 [40–42]. Cerium oxide is ambiguous, containing multiple valences of which the most commonly used are: cerium (III) oxide, Ce_2O_3 otherwise called cerrous oxide and cerium (IV) oxide, CeO_2, otherwise called ceric oxide[41]. However, the most prevalent form in which cerium oxide exists is CeO_2 [43], which originally was said to enhance the chemical action on oxide surfaces[6], specifically silica. However, later investigations done suggest that $Ce^{3+}$is likely to be responsible for the high reactivity with silica [44] . CeO_2 possesses a fluorite crystal structure, having each cerium atom in the lattice structure surrounded by eight oxygen atoms[43]. Ceria has a lattice constant of 0.541 nm [43] and has a low aqueous solubility. Dahle et al [40] evaluated the solubility of ceria particles and found that it is soluble at low pH's , that is, at pH less than 5. However, they reported that Ce (III) has a higher aqueous solubility than Ce (IV).

Various methods have been reported for the commercial preparation of ceria nanoparticles such as precipitation reactions, hydrolysis methods and calcination among others not mentioned here[45,46]. It is postulated that the synthesis method of the ceria particles has an effect on the CMP process outcome[44,30]. The synthesis method determines the type of ceria abrasives, which has an effect on selectivity, surface defects and the overall colloidal properties. Smaller particles produced by calcination methods are known to agglomerate easily giving low oxide removal rates and high surface defects. Calcined ceria particles have proven to give higher removal rates than colloidal ceria [30,44].

The earliest use of cerium oxide was as a hydrocarbon catalyst during the high temperature cleaning process of self-cleaning ovens [47]. Ceria is extremely efficient as a glass polisher. Infact, cerium oxide slurries have been used for decades in glass and optical lens polishing. Other application of ceria include catalysis and heat resistant alloy coatings due to its ability to participate in redox reactions/cycles. Other commercial uses include UV adsorbent, solid oxide fuel cells. Ceria-based slurries have emerged as an important abrasive in CMP application such as shallow trench isolation, liquid crystal display and interlayer dielectric[42],[48–50].

Ceria abrasives are widely used for ILD and STI CMP due to its enhanced SiO_2 removal rate. Ceria based slurries show higher polish rates of SiO_2 films, high selectivity and improved surface finish compared to silica based slurries[48,50]. Different mechanisms have been proposed for the origin of the high selectivity of ceria slurry. The "chemical tooth" model, which will be explained in details later on, was proposed by Cook [6] and is said to be responsible for the enhanced oxide removal. A strong surface chemical bond forms between the ceria abrasives and the silica substrate during the polishing process as shown in equation 2 below. Silica is subsequently removed one molecule at a time, in the form of $Si(OH)_4$ into the solution.

$$Ce - OH + Si - O^- \leftrightarrow Si - O - Ce + OH^- \qquad [2]$$

Silica removal is dependent on the ceria slurry pH with maximum removal occurring near the isoelectric point [50]. Our group obtained similar results, analyzing the effect of pH on ceria-silica interaction for the subsequent removal of ceria abrasives from silica surfaces and found that adhesion of ceria particles to silica surfaces is pH dependent[41]. It is further proposed that Ce^{3+} species present on the ceria abrasive surface is chemically active and reacts with hydrated SiO_2 hence facilitating the breaking of the silicate lattice and is responsible for the enhanced oxide polishing[51,52].

2.3 Mixed Abrasive Slurries

Slurries containing more than one kind of abrasives usually chosen from alumina, ceria, silica, titania, manganese oxide or polymeric reins are known as mixed abrasive slurries, MAS. The particles that are formed are known as composite particles and commonly consist of a larger softer core coated with smaller, harder and more reactive particles. These particles usually have different isoelectric points and due to this difference, electrostatic attraction occurs through particle-particle interactions. MAS has an advantage over single abrasive slurry in that not only do they offer improved selectivity and planarization but it is also possible to take advantage of the mechanical properties of one material and at the same time, utilize the chemical properties of the other material[7]. Typically, the larger core serve as a carrier, increasing the contact of the smaller more reactive abrasives with the surface to be polished thus enhancing the polish rate. An example of these particles is shown schematically below along with a TEM image of ceria nanoparticles attached to the surface of silica particles.

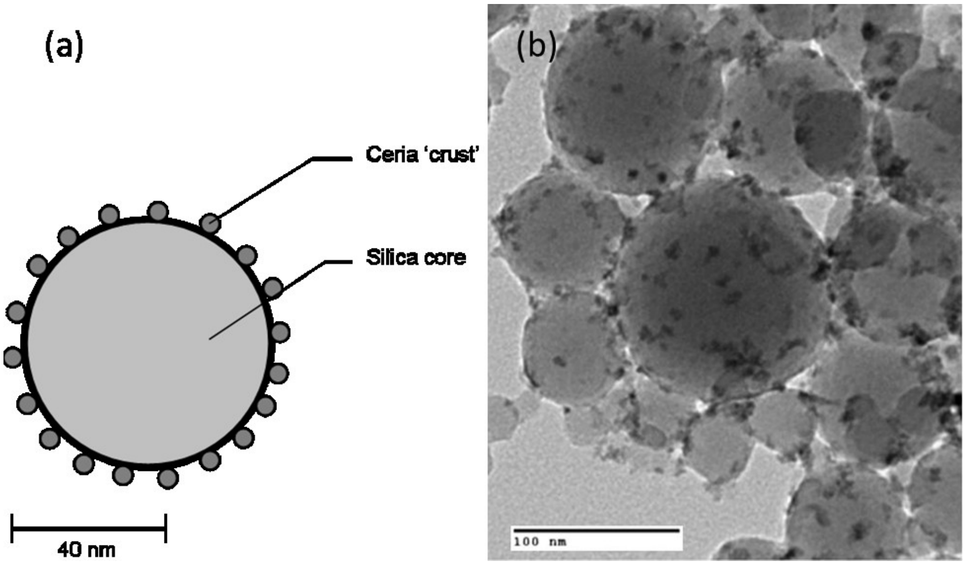

Figure 2-3 (a) Schematic diagram of silica core with ceria nanoparticle crusts and (b) TEM image of ceria nanoparticles attached to the surface of silica particles at pH 4 [7,26]

Mixed abrasives are commonly used in the CMP of dielectric films, especially in STI CMP. Jindal et al [8] performed CMP of metal and dielectric films using MAS of Al and Si particles at pH 4 and reported enhanced polish rates, improved surface finish of Ta and oxide films and more acceptable polish rate selectivity of Cu/Ta/oxide. Furthermore, Jindal et al [9]went on to report on the use of mixed abrasive slurries containing alumina and ceria abrasives at pH 4 for chemical mechanical planarization of silicon dioxide and silicon nitride films for shallow trench isolation application. They reported a polish rate selectivity between oxide and nitride films as high as 65 along with improved surface quality of the films. They presumed that the adsorption of smaller ceria particles onto larger alumina particles is responsible for these enhanced results when MAS are used.

Similarly, Seo et al [10] studied CMP of MAS containing manganese oxide within 1:10 diluted silica slurry. They achieved higher removal rates and low non-uniformity. They concluded that this improved CMP performance is due to the adsorption of smaller silica particles onto the manganese oxide surface through electrostatic interactions and polishing was dominated by the action of these new silica surrounded MnO_2 composite particles. Lu et al[36] and Lee et al [20] reported similar results of enhanced polish rates of oxide, low surface defects and good quality surface finish when MAS of ceria and silica were used compared to using single component slurries of silica or ceria. Ceria-coated silica slurries prepared by hydrothermal reaction of ceria and silica nanoparticles for oxide CMP demonstrated a significant increase in removal rates compared to using either slurries on their own[19]. Recent work by Lin et al [7]also demonstrated a twenty fold increase in oxide polish rates when using composite particles of a silica to ceria weight ratio of 0.1 (5 wt% silica particles and 0.5 wt% ceria particles), compared to polishing with either silica or ceria alone.

2.4 High Selectivity Slurries

Selectivity is a very important property in designing CMP slurries particularly those that will be used in STI and damascene fabrication. The selectivity of a slurry is its' ability to polish one material but not another or the polishing rate of the surface layer as compared with the underlying layer. In the case of STI CMP, selectivity is defined as the ratio of the material removal rate of silica to MRR of silicon nitride as seen below.

$$Selectivity = \frac{Material\ removal\ rate\ of\ silica}{Material\ removal\ rate\ of\ silicon\ nitride}$$

In the case of shallow trench isolation, the CMP slurry needs to completely remove the silicon dioxide layer and stop on the underlying silicon nitride layer while in the copper damascene process, the CMP slurry needs to selectively polish copper until the barrier layer Ta is exposed. In both cases, the underlying layers are then also removed. High selectivity slurries give a more effective endpoint detection due to the clear change in the tribological properties of the material being polished and the properties of the underlying layer [29]

Selectivity is achieved by shielding some of the layers of the film from polishing by forming a passivation layer that is generally achieved through the addition of additives such as surfactants and organic acids. In the case of STI CMP, surfactants and acids are carefully chosen to preferentially bind to the nitride surface forming a passivation layer that prevents it from being polished. Selective adsorption of the additive onto the surface can be achieved if there is an adequate difference in surface charges between them.

In STI CMP, there are three ways to improve selectivity: (i) increase oxide removal rate while decreasing nitride removal rate (ii) increase oxide removal rate and maintain the nitride removal rate at a minimum and (iii) maintain oxide removal rate and decrease the nitride removal rate to <1.

There is a wide selection of published and patent literature on high selectivity slurries employing different additives to enhance the oxide to nitride selectivity. These include ammonium polyacrylate (APA)[53] , glycine, proline, alanine, lysine, arginine [12], DL-aspartic acid, L-glutamic acid sodium [14] dodecyl sulfate (SDS)[15], glutamic acid [11], poly-acrylic acid[13] and amino acids [12] such as N-methyl, N,N-dimethyl glycine, 3-aminobutyric acid, picolinic acid[16],[18], iso-nicotinic acid [12,18] and cyclic amines such as pyridine HCL, piperazine and imidazole [17]. A broad but not exhaustive list of a combination of abrasives, additives employed, pH range in which high selectivity is reported and the corresponding selectivity values is provided in Table 1 of the review paper by Srinivasan et al [44].

The method of synthesis, type and size of the abrasive along with concentration of the additive, hydrogen bonding and pH of the slurry all play a crucial role in selectivity. Slurries exhibiting high selectivity are based on either silica or ceria abrasives[11–18,53]. The influence of pH is also critical in slurries that exhibit high selectivity. Some slurries exhibit high selectivity at a specific pH, some in a narrow pH range[12,14,44] while other slurries exhibit high selectivity in a wider pH range. America and Babu [12] suggested that pH is critical for the suppression of nitride removal rate. In their study of proline-ceria slurry for STI CMP, lowest nitride removal rate was reported at pH 9.7 which coincided with the point of zero charge for "oxide-free" silicon nitride surface and it is concluded that the minimal in nitride removal rate is related to the surface having zero net charge which leads to the optimization of interaction of proline with the nitride surface. Manivannan et al [14] reported that DL-aspartic acid-ceria slurries exhibit a high selectivity in the pH range of 4 to 5. In the case of surfactant concentration, Lee et al[13] suggested that there exists a "critical concentration" of surfactant which is dependent on the abrasive particle size for the minimal nitride removal. Manivannan et al[14] experimentally showed that increasing the concentration of the additive suppresses nitride removal rate but also silicon dioxide. America and Babu[12] investigated the effects of slurry additives on the suppression of silicon nitride removal during STI CMP and reported that high selectivity can be achieved by additives that contain an amino group in the alpha position (attached to the first carbon adjacent to the carboxylic acid). The amino group must possess atleast one hydrogen atom and hydrogen bonding was proposed to be responsible for suppressing nitride removal in CMP.

The hypothesis found in the literature for explaining high selectivity includes : (i) selective adsorption of the additive onto the nitride surface suppresses its' hydrolysis into silicon dioxide and hence the removal rate; (ii) the adsorption of the additive on chemically active sites on the abrasive, blocking the chemical interaction between the film and the abrasive and suppressing polishing[12,17,18]. Kim et al [54] suggested that high oxide to nitride selectivity is caused by the preferential adsorption of anionic polyelectrolytes onto nitride surfaces. Manivannan and Ramananthan [11] proposed that ceria abrasives contain two active sites, one that interacts with silica surfaces and the other with silicon nitride surfaces. Addition of additives modifies the different active sites and leads to changes in selectivity. They suggested that the interaction between the additive and the abrasive plays a major role in enhancing selectivity.

2.5 Effects of abrasive size, shape, pH and concentration.

The dynamic motion of the abrasive particles, rolling or sliding, plays a critical role in successful outcome of the CMP process[55]. However, this contact behavior of the abrasive particles is dependent on the shape, size, concentration, distribution, solubility, hardness and pH of the slurry particles. According to this mechanism, for the sliding motion of particles the polishing rate is directly proportional to solids loading and particle size while the polishing rate is inversely proportional to solids loading and particle size for the rolling motion of particles. Abrasive particle size plays a key role in material removal rate, surface defects and also surface roughness during CMP. Numerous studies have been done on the effect of abrasive particles on the CMP process, all with contradictory results stating that polish rate increases or decreases with particle size or in some cases, independent of the abrasive particle size.

In earlier works, it was implied that an increment in particle size and concentration results in an increase in oxide removal rates[56]. On the other hand, a decrease in polish rates with increasing particle size has been reported [57]. In their investigation on the effect of alumina abrasive particle size (0.1 to 10 µm) and solid loadings (2 to 15 wt %) on the polish rate of tungsten, Bielman et al[58] found that tungsten removal rate increased with decreasing particle size and increased solid loadings. It was concluded that the removal rate mechanism is related to the contact surface area between particles and polished surface and is not controlled by an indentation and scratching mechanism. Choi and Singh[59] reported similar results of an increase in polish rate with a decrease in particle size and an increase in solids loading and further proposed that polish rate increase with an increase in the contact area of the abrasive particles between wafer and pad. Mahajan et al [60] in their study of silica/silica polishing mechanism as a function of particle size and solids concentration reported that removal rate increased with increased solid loading for smaller particles, however, for larger particle sizes they observed a consistent decrease in the polishing rate as a function of the solid loadings. Furthermore, they went on to propose two different material removal mechanisms: contact-area-based mechanism is dominant for small particle sizes and indentation mechanism dominant for larger size abrasive particles where polishing rate increases with decreasing particle concentration and increasing particle size (via silica polishing experiments). Basim et al [61] reported increased material removal rates with larger size particles at high concentrations. Consequently, the surface damage occurring at these conditions was high. The surface damage increased with the increasing size and the concentration of the coarser size particles. Singh and Bajaj [62]proposed that material removal per particle may decrease with decreasing particle size due to lower stresses and the degree of surface scratching also decreases due to reduced indentation.

It is also implied that abrasive particles must be larger than a critical size to be effective for removal rates. Zhou et al [63]reported a critical abrasive particle size (80 nm) at which maximum material removal occurs and also gave the best surface finish. Simultaneously, they demonstrated that material removal rate increases with the increase of solid concentration from 0 wt% to 30 wt% of all 3 types of slurries studied containing 50 nm, 80 nm and 140 nm abrasives. Hence, polish rate increases with the increase in the number of particles in the slurry. As of yet, there is no consensus on the effect of slurry particle size on polishing performance.

The concentration of particles in the slurry also affects the polishing rate. Zantye et al [29] stated in their review that an increase in particle concentration should increase removal rates due to the increase in the number of active particles which will also increase indentations to the passivating film. Mahajan et al[60] reported that for smaller particles, removal rates increased as particle concentration increased, however, as particle sizes got larger, there is considerable decrease in removal rate with increase in particle concentration. Numerous studies have reported an increase in polish rate with increasing abrasive concentration [60,63,64] . Some of these reports indicated an increase in polish rate up to a critical concentration, beyond this point no further increase in polish rate is observed and polishing rate may decrease[58]. Cooper et al[64] also showed continuous reduction in surface roughness with increasing solid concentration. The increase in solid loadings/particle concentration leads to an increase in the number of particles interacting with the surface which results in an increase in friction force and higher removal rates. The effect of slurry particle shape on the removal rate has been studied in details by Zhenyu Lu et al[65].

pH has a strong effect on both dielectric and metal CMP. Recently our group studied the pH dependent attachment of ceria nanoparticles to silica[7,41] . Our results indicated that pH is not only important for material removal rate in dielectric CMP but also for the cleaning process in CMP. pH modification of the slurry is a useful strategy to enhance cleaning of the wafer. Jindal et al[66] studied the effect of pH on Cu/Ta polishing and suggested that a favorable Cu/Ta polish rate selectivity can be obtained by adjusting the pH of the slurry. They also observed that Cu removal rates decreased monotonically from pH 2 to pH 12 when using both silica and alumina abrasive particles. They suggested this decrease was as a result of the decrease in the hardness of Cu with decreasing pH while Ta surfaces showed high polish rates in alkaline region[66]. The pH also affects the slurry stability.

2.6 Slurry stability

The stability of a slurry can be defined as one in which the particles remain suspended in solution and particles are kept separated by electrostatic repulsion forces due to their surface charges. Usually, when colloidal particles are suspended in a liquid medium, they accumulate a surface charge and an electric double layer forms around each particle. This is a repulsive force that helps to stabilize the suspension. When two particles of the same charge approach each other, the overlap between the diffuse layers result in a high repulsive electrostatic interaction causing the double layer formation to increase and gives rise to stable suspensions. Screening caused by the addition of salts can reduce the electric double layer repulsion. If the screening is sufficient, particles will now have enough kinetic energy to overcome this repulsive energy barrier and Van der Waals attractive forces become dominant and promotes bonding/agglomeration of the particles which leads to a decrease in slurry stability. The tendency of particles to agglomerate depends on the slurry pH.

Not only does agglomeration reduces stability of the slurry but is also said to negatively affect the polishing capability of the particles due to the reduction in surface area and hence loss of active sites on the particle. These large groups of particles are undesirable for CMP as it introduces micro-scratches on the polished surface as a result of deep indentation decreasing device yield.

According to Choi et al[67], in the stable slurry regime material removal rate increases with an increase in ionic strength while in the unstable slurry conditions, material removal rate decreases with ionic strength. It was further stated that contact between larger agglomerated particles and the surface to be polished results in non-uniform distribution of pressure per particle leading to a decrease in removal rate. On the other hand, Lin et al[7] studied the colloidal stability of slurries via settling test and reported MAS with high colloidal instability (these slurries precipitated faster) showed higher oxide and nitride polish rate due to greater contact area between the particles and wafer surfaces. Chemical additives may affect slurry stability desirably or undesirably. They increase the ionic strength of the slurry and provide excellent slurry stability for CMP condition[68] but in some cases also cause the agglomeration of particles and tend to lubricate the surface to be polished preventing contact between particles and the surface hence decreasing polishing rate.

The zeta potential of colloidal slurry solutions is often used to determine the electrostatic interactions between particle-particle and particle-wafer and is also used as a method to gauge the solutions stability. Slurries with zeta potential greater than 30 ($\zeta > |30|$) are considered to be stable[69] , however, as abrasive particles approach their isoelectric point, slurries start to exhibit instability as at this point particles tend to agglomerate quickly. Once again, these agglomerated particles are undesirable for STI CMP as it causes micro-scratches, reduces device yield and functionality.

2.7 Material Removal

2.7.1 Mechanical Process

Earlier on, researchers assumed that material is removed from the polish surface in CMP when it is scratched away by the abrasive particles. However, the earliest model for the mechanical removal of material from the polished surface was proposed by Preston in 1927 to describe plate glass polishing[70]. He postulated that material removal from the surface in a given time was proportional to the work done on that surface. The work done is the product of the polishing pressure and velocity and is expressed mathematically as:

$$MRR = K_p \times PV \qquad [3]$$

where MRR is the material removal rate, P is the applied pressure and V relative velocity of the surfaces in contact and K_p is the Preston coefficient. The coefficient is experimentally determined and is a function of several parameters such as surface properties and reaction kinetics. This relationship between MRR and the product PV implies that polishing is independent of slurry characteristics and chemistry and does not hold for experimental results as there are quite a few process parameters apart from pressure and velocity that influence MRR today. Also, it implies that at a fixed pressure and velocity, the material removal rate should be constant which is also not feasible based on experimental data. Although the Preston equation is widely accepted, it does have many limitations. Numerous researches into proposing models attempting to overcome the limitations of the Prestons' equation and to describe the CMP mechanism have been done and can be found in the literature[71–75] .

2.7.2 "The Chemical Tooth"

Polishing of films is thought to be largely executed by mechanical abrasion, the M in CMP, however, in the early 1970's, an alternate theory to mechanical abrasion was developed by Cook[6]. The "chemical tooth" was proposed for glass polishing and is one of the first models used to explain the ceria-silica polishing mechanism. According to the chemical tooth, material removal takes place in a multi-step process. Initially, water penetrates the silica surface layer and forms $\equiv Si{-}OH$ bond, the chemical components of the slurry hydrolyze the surface of the abrasive particles and the wafer leading to a temporary bonding between the abrasive and the silicon atom [6]. The dissolved silica is released into the solution and is adsorbed onto the abrasive particle surface. Material removal occurs when the silica particles are bound by the abrasive and/or carried away in flowing slurry stream. However, the removed material at some point may re-deposit onto the wafer surface as an oxide[6].

Ceria slurries proved to be the most efficient when polishing glass or pure silica. To explain the ceria-silica mechanism, Cook examined the interactions between SiO_2 substrate and ceria abrasive. Cook proposed the abrasive particle-surface bonding is controlled by a hydrolysis reaction that is represented below [6,50]

$$\text{Si-O}^- + \text{Ce-OH} \rightarrow \text{Ce-O-Si} + \text{OH}^- \qquad [4]$$

Cerium oxide dispersed in solution forms Ce-OH groups which will react with Si-O^- present on the surface resulting in the formation of Ce-O-Si bonds and subsequent removal of silica as $Si(OH)_4$ one molecule at a time[6]. The chemical tooth model showed that material removal is related to interactions between surface functional groups on the substrate surface and the abrasive particle surface. The ceria-silica CMP polishing mechanism is expected to be a strong function of slurry pH [41,50].It should be noted that although the chemical tooth model is widely accepted, there is no experimental validation.

2.8 CMP Isolation Techniques

2.8.1 Local Oxidation of Silica (LOCOS)

Before the emergence of novel technologies such as shallow trench isolation, local oxidation of silicon, LOCOS, was the traditional method of choice for device isolation. In the LOCOS process, a thin layer of pad oxide is deposited onto the silicon substrate. Silicon nitride is then deposited onto the pad oxide, followed by chemical etching of regions of both layers where thermal oxide will be grown. The thermal oxide provides electrical isolation of the device by separating active regions. After the silicon substrate is thermally oxidized, the nitride layer that was used as a mask is stripped. LOCOS causes nonplanarity due to the undesirable “bird’s peak” structure that is produced during the process and therefore reduces device packing density[76], hence making this technique unacceptable for device line widths less than 250 nm[77].

2.8.2 Shallow Trench Isolation (STI)

Shallow Trench Isolation, also known as STI, is a novel isolation technology used for semiconductor devices with line widths less than 250 nm and high transistor packing densities. STI CMP is used to create dielectric isolation between transistors by the removal of the overburden dielectric fill in the shallow trench, hence separating adjacent active-areas of metal oxide semiconductor devices[27,78]. Although STI was invented in 1977[79] it wasn’t implemented in IC manufacturing until the 1990’s. As IC size shrinks continually, the traditional isolation technique, LOCOS, was no longer efficient because of the “bird’s peak” associated with the process and was replaced by the new STI technology. STI inhibited the undesirable “bird’s peak” by embedding field oxide into silicon providing a clear distinction between the oxide and the active-area regions[80] . Furthermore, STI provides an improved control over the geometry of the isolated area[81] which allows for denser and high speed devices to be fabricated.

A typical STI process starts with growing pad oxide onto a silicon substrate, then depositing a layer of nitride (used as a mask), after which a shallow trench is etched into the silicon substrate. PECVD silicon oxide is deposited to fill the trench. This is followed by CMP that is used to remove the silicon dioxide overburden and should stop on the silicon nitride masking layer which is stripped afterwards. A schematic representation of STI is shown in Figure 2-4.

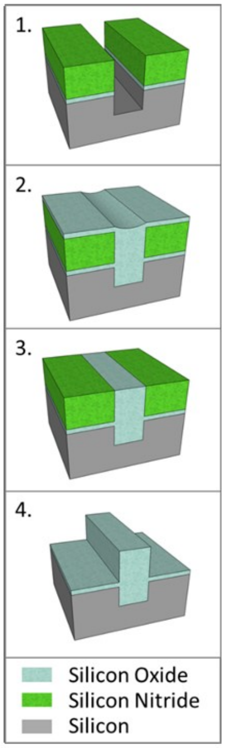

Figure 2-4 A schematic representation of STI process[27].

An ideal STI process should have a good oxide-polishing rate and stops at the nitride layer. Therefore, a high selectivity between oxide and nitride is desired for STI. The performance requirement for STI CMP is more stringent due to the smaller proximity between the transistor regions[78]. Therefore STI CMP slurries should not only have a high oxide-to-nitride removal rate selectivity but at the same time leave the surface defect-free with no scratches or particle residues. Polishing scratch is detrimental to device quality as it directly affects device yield. High selectivity slurries for STI CMP were discussed earlier in section 2.4.

2.8.2.1 Oxide Removal

Silica hydrolysis and dissolution are responsible for the chemically modified layer on silica surface as a result of siloxane bond breaking and hydration when silica reacts with water. The first step in SiO_2 removal involves water reacting with the siloxane bonds (Si-O-Si) present on the surface of silica and forming ≡Si-OH. This is usually represented by a hydrolysis reaction of silica shown below[82,26]:

$$\equiv Si - O - Si \equiv \; + H_2O \; \leftrightarrow 2 \equiv Si - OH \qquad [5]$$

Dissolution and hydration work together for the above reaction to take place. All four bridging oxygen bonds on the silica surface have to be hydrated inorder for dissolution of the silica to occur[6] . In this case, water diffuses into the silica surface, penetrating the siloxane bonds and forming the solute ≡Si-OH species.

Once the hydroxylated surface comes in contact with an abrasive particle in the slurry, one or more of the silica tetrahedral chemisorbs onto the abrasive particle and is lifted off the surface and taken away in the flowing slurry stream. Material removal occurs when the silica particle is bonded to the abrasive particle and be removed or it may enter the polishing slurry where re-deposition onto the wafer surface as an oxide may occur.

The rate of this reaction is controlled by slurry pH (dissolution of surface hydroxyls increases with increase in pH), water diffusion onto the silica surface and particle type and size (ceria particles is said to give higher polishing rates of silica surfaces when compared to other oxide particles)[6,26]. Different mechanisms/models are proposed in the literature about the interaction between ceria and silica during polishing. One of the earliest model on oxide polishing was provided by Cook[6] who proposed the chemical tooth effect of CeO_2 particles which helps in breaking the siloxane bonds on the silica surface and subsequently removing $Si(OH)_4$ into the solution one molecule at a time. Hoshino et al[83] presented another model where the siloxane bonds react with CeO_2 particles forming Si-O-Ce bonds which leads to the oxide removal as a lump instead of one molecule at a time which was proposed by Cook. Kelsall[84] and Dandu et al[51] also provided an alternative model where they proposed that Ce^{3+} (and not Ce^{4+} as proposed by Cook) present on the ceria surface is chemically active and is responsible for the enhanced oxide removal.

2.8.2.2 Nitride Removal

Hydrolysis is also responsible for the removal mechanism for silicon nitride[85] . Silicon nitride polishing occurs in two steps[44,85]. The first step entails the hydrolysis of nitride where silicon nitride surface reacts with water/air and oxidizes to silicon dioxide. This hydrolysis/oxidation reaction is represented below[85]:

$$Si_3N_4 + 6H_2O \rightarrow 3SiO_2 + 4NH_3 \qquad [6]$$

$$Si_3N_4 + 3O_2 \rightarrow 3SiO_2 + 2N_2 \qquad [7]$$

In the second step, the top layer of silicon dioxide is removed by CMP which leaves the underlying nitride layer susceptible to the aqueous slurry and repetition of the first step may occur.

Hu et al[85] proposed the following sequence of hydrolysis reactions for nitride CMP process:

$$Si_3N + H_2O \rightarrow Si_2NH + Si-OH \qquad [8]$$

$$Si_2NH + H_2O \rightarrow SiNH_2 + Si-OH \qquad [9]$$

$$SiNH_2 + Si-OH \rightarrow \equiv Si-O-Si \equiv + NH_3 \qquad [10]$$

$$Si_2NH + H_2O \rightarrow \equiv Si-O-Si \equiv + NH_3 \qquad [11]$$

The hydrolyzed surface layer can be further hydrated in the presence of water during CMP according to the following hydration reaction[85] [Hu et al]:

$$\equiv Si-O-Si \equiv + H_2O \rightarrow Si(OH)_4 \qquad [12]$$

This reaction is the same as in oxide polishing. It was suggested that both nitride hydrolysis and oxide hydration reactions resulted in a mechanically weak oxide surface layer which can easily be removed by mechanical wear by the slurry abrasives.

Therefore, additives can be chosen in such a way that inhibits the first step by preferentially adsorbing on the silicon nitride surface preventing the conversion of silicon nitride to oxide and hence suppressing the nitride removal. The suppression of silicon nitride removal is critical for a successful STI CMP process.

2.9 Challenges of CMP

Compared to other planarization techniques, CMP has many advantages, however, on the other hand it does come with a few challenges. Despite the wide acceptance of CMP in semiconductor manufacturing, the exact mechanism of the process is still not clear, and therefore it is unable to produce accurate control over the polishing results. Therefore a better understanding of the fundamental principles of the CMP process is required. CMP is a multi-variable process and a thorough understanding of each of these variables and their interactions must be reached for a successful outcome of the process and for its future applicability in device manufacture.

With the emergence of technology such as STI that has more stringent requirements of the CMP process, there is increased need for high selectivity STI CMP slurries which means the development of novel slurries containing new abrasive particles or mixed abrasive particles along with additives. The use of new abrasive particles and mixed abrasive particles to achieve selectivity in polishing requires further investigation. As dimension size gets smaller, Within-Die gets tighter and tighter and there is need for improvement in CMP performance to facilitate this. Other major challenges include reduction in surface defects including micro-scratches, particle contamination, WIW and WID non-uniformity and improvement in end point detection.

The International Technology Roadmap for Semiconductors (ITRS) have identified future challenges for CMP which include[27,86]:

- Increasing within-wafer removal rate uniformity and decreasing dishing for shallow-trench isolation
- Reduction surface defects
- Scaling to 450mm wafers

CMP is a costly process which includes the cost of the equipment, maintenance and consumables and also the additional process of post-CMP cleaning. One way to reduce CMP cost is by developing slurries designed to minimize the use of expensive materials and designed for recyclability.

Chapter 3 : Experimental Procedures

This work involves the use of colloidal abrasive particles for the polishing of silicon dioxide and silicon nitride surfaces. Analysis of the mechanisms of oxide and nitride polishing using mixed abrasive slurries is conducted through both polishing experiments and friction measurements using a system that can measure the carrier motor current is discussed. The colloidal stability of slurries is an important factor in STI CMP because it affects material removal rate as well as causes defects. Therefore, the colloidal stability of ceria-silica MAS at different weight ratios is studied via settling tests. Due to the small scale of the abrasives in the slurry used in CMP, surface effects dominate the behavior of the particles. As a result of this, particle size and surface charge influence slurry stability and CMP performance. The surface charge of the abrasive in the slurry is determined using zeta potential measurements at different slurry pHs. Particle size measurements are made to determine the degree of agglomeration of the particles in the slurry. A light scattering technique used to measure both the particle size and zeta potential are reported. The effect of the slurry chemistry on the polished surface using x-ray photoelectron spectroscopy, scanning electron microscopy and auger electron spectroscopy are presented.

3.1 Wafer, Slurry Preparation and Polishing

All polishing experiments were performed on a Strasbaugh 6EC Polisher in our lab at the University of Alberta as seen in Figure 3-1. This polisher came equipped with a ViPRR 8”wafer carrier and a high-grade aluminum polishing table of ~ 22-in. diameter with chuck and platen rotational speeds of up to 185 rpm, and a maximum down force of 10 psi for 200 mm-diameter wafers . In this work, the polishing time for all substrates lasted between 1- 1.5 minutes using table and carrier rotational speeds of up to 60 rpm and down force of up to 8 psi. The back pressure was always kept at one-third of the down force value to avoid blowing the wafer off the carrier during a polish cycle. During the polish cycle, the slurry was constantly mixed at 350 rpm using an IKA EUROSTAR digital stirrer while it was pumped onto the pad using a peristaltic pump at a rate of 200 ml/ min to 250 ml/min. The recipe used for polishing both oxide and nitride substrates unless otherwise stated is shown in Figure 3-2.

Figure 3-1 Strasbaugh 6ec Polisher

The pads used in this work were NexPlanar E7450-30S and E7070-30S which are both radially and concentrically grooved. The pad was conditioned with a powered diamond-grit pad conditioner. This is carried out continuously during polishing. The powered pad conditioner has a brushless servo motor mounted to the end of the conditioning arm that applies a downward force while sweeping a rotating conditioning device across the polishing pad.

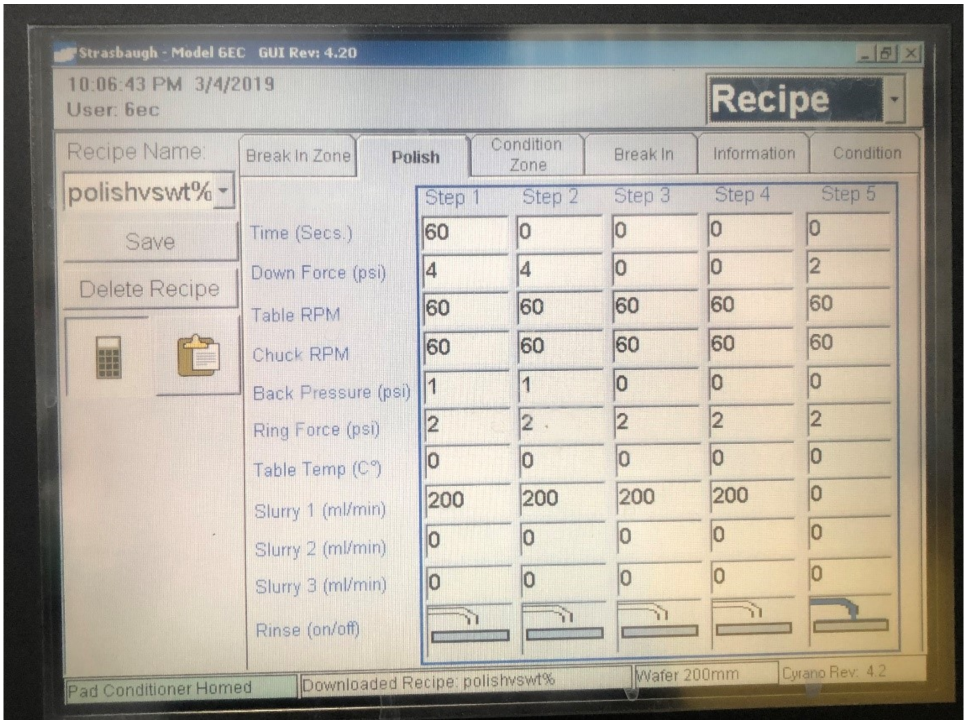

10:06:43 PM 3/4/2019
User: 6ec

Recipe Name: polishvswt%

	Step 1	Step 2	Step 3	Step 4	Step 5
Time (Secs.)	60	0	0	0	0
Down Force (psi)	4	4	0	0	2
Table RPM	60	60	60	60	60
Chuck RPM	60	60	60	60	60
Back Pressure (psi)	1	1	0	0	0
Ring Force (psi)	2	2	2	2	2
Table Temp (C°)	0	0	0	0	0
Slurry 1 (ml/min)	200	200	200	200	0
Slurry 2 (ml/min)	0	0	0	0	0
Slurry 3 (ml/min)	0	0	0	0	0
Rinse (on/off)					

Pad Conditioner Homed
Downloaded Recipe: polishvswt%
Wafer 200mm
Cyrano Rev: 4.2

Figure 3-2 Screen shot of the recipe for chemical mechanical polishing of both oxide and nitride surfaces.

Table 3-1 Process parameters used in the chemical mechanical polishing of oxide and nitride surfaces.

Polishing Time (s)	60
Down Force (psi)	4
Table RPM	60
Chuck RPM	60
Back Pressure (psi)	1
Slurry Flow Rate (ml/min)	200

3.1.1 Sample Preparation

All polishing was carried out on 8” (200mm) diameter silicon wafers with PECVD oxide or nitride deposited on one side. PECVD silicon dioxide, grown at 300-400ºC with initial film thickness of 1000 nm were obtained from WRS Materials Company. Other conditions for the deposition were not disclosed to us by the vendor. Plasma enhanced chemical vapor deposition (PECVD) was used to deposit nitride layers of thickness around 100 nm – 200 nm. Deposition was carried out at a temperature of 300^0C using a Trion PECVD system in the NanoFab at the University of Alberta. PECVD silicon nitride was prepared according to the following reaction:

$$3SiH_4 + 4NH_3 \xrightarrow{plasma} Si_3N_4 + 12H_2 \qquad [13]$$

The removal rate of each wafer was calculated from the difference in film thickness before and after polishing, measured using a Filmetrics F50-UV (shown in Figure 3-3) located in the NanoFab at the University of Alberta. This system measures the film thickness via specular reflectance, with an automated stage to enable efficient collection of thickness uniformity maps. The thickness of oxide or nitride on each wafer was mapped at 13 locations across the wafer surface, however, only the wafer center measurement was taken into consideration. An edge exclusion of 5mm from the edge of the wafer was used. Polishing rates were calculated by dividing the change in film thickness by the polishing time. The polishing results shown are an average of the removals rates from three different wafers. The standard deviation in the removal rate was determined from the removal rates of these three wafers.

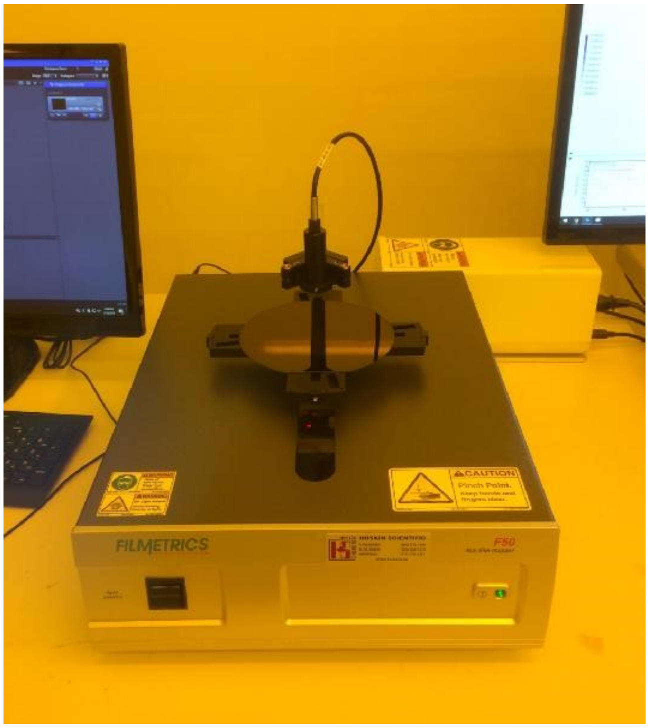

Figure 3-3 Filmetrics F50-UV in the NanoFab at the University of Alberta.

3.1.2 Slurry Preparation

Two kinds of silica slurry obtained from AkzoNobel, namely Bindzil EB6080 (EB6080) and Bindzil EB6040 (EB6040), and one kind of ceria slurry supplied by Nyacol Nano Technologies (named CEO2 (AC)) were utilized for this work. The concentration of the particles in suspension are 35.48 wt%, 38.98 wt%, and 20 wt% respectively. The mean diameter measured for the ceria particles in the dispersion was approximately 5 nm while the mean diameter measured for both EB6080 and EB 6040 was approximately 125 nm and 80 nm respectively. The colloidal ceria particles and silica particles appear almost spherical in shape. Transmission electron microscopy images of these particles are shown in Figure 9 of Reference 7 and are not repeated here. De-ionized water from a Milli-Q UV PLUS system, referred to as Milli-Q water, was used for slurry dilution. Citric acid powder obtained from Acros Organics and potassium hydroxide pellets obtained from Fisher Scientific Inc. were used to adjust the pH of suspensions to the desired value. The pH of the suspensions was measured by an Accumet Basic AB 15 pH meter, which was calibrated each time prior to use. All the additives, L-proline, nicotinic acid, sodium dodecyl sulfate and glycine were used at low weight concentrations between 0.1-2 wt %. L-Proline was obtained from Sigma Aldrich, nicotinic acid from Acros Organics while both glycine and SDS were obtained from Fisher Scientific Inc.

All the slurries used in polishing experiments, settling experiments, zeta potential measurements and particles size measurements were prepared as mentioned above. Mixed abrasive slurries were prepared by simply mixing one kind of the diluted silica slurry with the diluted ceria slurry. All polishing slurries were mixed from their constituents no more than 24 hours before use.

3.2 Friction Measurement

Frictional forces exists between the pad and the wafer surface during the polishing process. Friction force is strongly dependent on the contact area between the pad and wafer and on interfacial electrostatic interactions and also surface conditions of the wafer being polished.

Friction measurements using motor current signals provides useful information about endpoint detection and material removal rate during STI chemical mechanical polishing.

In polishing tools such as the Strasbaugh 6ec, friction can be measured indirectly by the measurement of either the table/platen or wafer carrier motor current. Xie and Boning[87] presented a model of the macroscopic frictional force based on surface topography to determine CMP endpoint to be used for STI and found the platen motor current during polishing to be directly proportional to the frictional force generated during polishing. In this work, friction force was monitored from the motor current of the platen. According to other works within the group done on measuring friction using similar procedure (monitoring the wafer carrier/chuck motor current)[88,89], when the pad and wafer carrier are in contact (engaged) during polishing, frictional forces promote/assist wafer rotation thereby reducing the motor power required to rotate the carrier at a set speed compared to the power required by the motor to rotate the wafer carrier when not in contact with the pad (disengaged) at the same set speed. The difference between the motor power supply to rotate the wafer carrier when carrier and pad are engaged and when disengaged can be related to friction using the following relationships:

$$P = Vi = T\omega \qquad [14]$$

Where P is the power of the motor for the wafer carrier, V is motor voltage, I is the motor current measured when the pad and wafer are engaged or disengaged, T is the torque produced and ω is the set carrier rotational speed.

The Strasbaugh 6ec polisher is capable of measuring both table and chuck (quill) load during the polishing process. Feedback from the motor current can be monitored directly on the GUI touch screen in auto mode. The quill motor is driven by its own motor speed controller operated by the MYSTIC 200 CPU.

3.3 Particle Characterization

3.3.1 Zeta Potential Measurements

Colloids or small particles when immersed in a liquid develop positive or negative surface charge. They are surrounded by counter ions and undergo thermal/Brownian motion. When an electric field is applied to the solution, the particles move in the potential direction opposite to their charge with a velocity that is proportional to the magnitude of the electric field. When the solution is irradiated with light, the scattered light from the moving particles causes a phase shift. Zeta potential is the potential at the shear plane/slipping plane and is measured by the magnitude of the frequency shift or phase shift caused by the moving particles.

In order to measure the surface charge of the particles in the slurry and on the wafer surface, the zeta potentials of ceria and silicon dioxide particles were measured as a function of slurry pH using a Nano ZS Zetasizer from Malvern Inc. The zeta potential of silicon nitride is shown in Figure 2 of Reference 7 and is not repeated here. Zeta- potential measurements of the MASs of ceria and silica particles at different weight ratios maintained at pH 4 were also carried out. It should be mentioned that no instrument is capable of directly measuring zeta potential. Instead, the Malvern Nano ZS Zetasizer measures the electrophoretic mobility. The electrophoretic mobility is the velocity of a charged species in an applied electric field. In this method, particles suspended in a liquid are irradiated with laser light and an electric field is applied. Once the electric field is applied, the electrophoretic mobility is measured by the frequency or phase shift due to the particles motion and the following equation is formed:

$$\mu_e = \frac{v}{E} \qquad [15]$$

where v is particle motion velocity, E is the electric field applied, and μ_e is the electrophoretic mobility. The mobility is then related to the zeta potential at the interface using the Smoluchowski equation:

$$\mu_e = \frac{\varepsilon_0 \varepsilon_r \zeta}{\eta} \qquad [16]$$

where ε_r is the solvent dielectric constant, ε_0 is the permittivity of free space, ζ is the zeta potential of the particle and η is the solvent viscosity.

The suspensions used for zeta potential measurements were prepared by dilution of the original slurries to approximately 1 wt % for ceria, and 0.5 wt % for silica using Milli-Q water. The pH of the suspensions was adjusted using citric acid and potassium hydroxide. The refractive indices used were 1.457, 1.33and 2.1 for silica, water and ceria respectively, while the absorptivity was set at 0.01 for silica and 0.05 for ceria. All measurements were done at room temperature (25°C). The viscosity was set at 8.872 x10^{-4} Pa.s. The zeta potential measurement recorded was an average of three consecutive measurements for each sample.

For the zeta potential measurements of the mixed abrasive slurries, silica was maintained at a concentration of 0.5 wt % while ceria was varied between 0.015-0.075 wt %. The refractive index of silica was used (1.457) based on the assumption that the concentration of ceria was very low.

3.3.2 Particle Size Distribution

The Malvern Nano ZS Zetasizer which was previously used for the zeta potential measurements was also used to measure the particle size and size distribution of all 3 abrasives utilized. This instrument utilizes dynamic light scattering for measuring the size of particles. When the particles inside the suspension are illuminated with a laser light, the light scattered by the moving particles is proportional to the particle velocity due to the Brownian motion. The larger the particle the slower the Brownian motion and the smaller the particle the faster and more active the Brownian motion is. Based on the theory of Brownian motion, light scattered from the particles causes a pattern change or fluctuation signal resulting from the particle motion. This pattern change is quantified as a diffusion coefficient. The particle size can be calculated from the diffusion coefficient using the Stokes-Einstein equation:

$$R = \frac{kT}{6\pi\eta D} \qquad [17]$$

where R is particle radius, k is the Boltzmann constant, T is absolute temperature, η is the viscosity of the liquid and D is diffusion coefficient.

The ceria and silica suspensions used for particle size measurements were prepared by dilution of the original slurries to 0.5 wt % using Milli-Q water and the pH was adjusted to approximately 4 ± 0.03. A small disposable cuvette was used to hold the suspension. All measurements were done at room temperature, 23 °C. The refractive index was set at 2.1, 1.457 and 1.33 for ceria, silica and water respectively. Again, the final measurement recorded was an average of three consecutive measurements.

3.4 Settling Tests

Settling tests of the slurry containing silica and ceria colloidal particles are conducted at various ceria-to-silica weight ratios. Silica, namely Bindzil EB6080 and Bindzil 6040 was simply mixed with ceria slurry. The weight concentration of silica was kept constant at 5 wt%, while the weight concentration of ceria was varied (see Table 3-2). The pH of the mixed slurries was adjusted to 4 unless otherwise stated. The mixtures were shaken well before the first set of photos was taken. Photographs of all samples were taken using a Samsung SL605 camera over a period of several days and weeks. The photographs were not edited except for cropping and proportional resizing.

Table 3-2 Weight ratios of the MAS used for settling tests.

Ce:Si ratio	**0.04**	**0.05**	**0.06**	**0.07**	**0.08**	**0.09**	**0.1**	**0.15**	**0.2**	**0.25**	**0.3**
Si wt%	5	5	5	5	5	5	5	5	5	5	5
Ce wt%	0.2	0.25	0.3	0.35	0.4	0.45	0.5	0.75	1	1.25	1.5

3.5 Characterization Techniques

3.5.1 X-ray Photoelectron Spectroscopy

XPS is a surface analysis tool that provides a combination of quantitative elemental composition and chemical information. XPS is surface sensitive (sampling between 3–10 nm)[90] , therefore, it is ideally suited to quantify the particles on the surface of the wafers before and after polishing and also determine the nature of chemical bonds present on the upper 3nm of the wafer. XPS also provides an excellent means to characterize the silica and ceria nanoparticles. XPS involves the removal of a single core electron of binding energy *BE*, by a x-ray photon of energy *hv*. Auger electrons are produced in XPS along with photoelectrons. The emitted photoelectrons have a kinetic energy KE which is measured by the electron spectrometer and is given by:

$$\mathrm{KE} = hv - BE - W \qquad [18]$$

where $BE < hv$ and W is the work function of the spectrometer.

All XPS measurements (except pH 12 survey spectrum) were completed using a Kratos Axis Ultra spectrometer equipped with a monochromatic Al Kα (hv = 1486.7 eV) radiation source. The spectrometer was operated at 144 W with a hybrid lens and a spot size of 700 µm x 400 µm. The samples were prepared by mounting the sample wafers onto a sample holder with the use of copper strips and transferred to the analysis chamber where a pressure of $\sim 10^{-9}$ Torr was maintained. Samples were not sputter-cleaned and were found to be non-conducting.

To determine the surface composition of the different wafers after slurry treatment, survey spectra of all three samples (pH 6, 9, and 12) were acquired using the following parameters:

(a) For pH 6, and 9: binding energy (BE) range = 0 – 1100 eV, pass energy = 80 eV, step size = 0.4 eV, and dwell time = 0.1 s.

(b) For pH 12, a Mg Kα source (1253.7 eV operated at 120 W) was used with the following parameters: BE range = 0 – 1100 eV, pass energy = 80 eV, step size = 0.4 eV, and dwell time = 0.1 s.

To determine the chemical composition of Ce on the wafer surface, the component analysis of high resolution Ce 3d spectra were also collected, where applicable, based on the survey spectra, with the following parameters: BE range = 877 – 921 eV, pass energy = 20 eV, step size = 0.12 eV, and dwell time = 0.2 s.

The software CASAXPS was used to perform offline processing of the collected spectra. It should be noted that alignment was necessary. All spectra were calibrated to the C 1s core-line at 284.8 eV arising from the C–C/C–H bonds in adventitious carbon. To calibrate high resolution peaks using C 1s at 284.8 eV, means that each element in the spectrum will shift by 1.2 eV to the right. Core-lines were fitted to a pseudo-Voight lineshape (70% Gaussian, 30% Lorentzian) to account for peak broadening after the background was removed using a Shirley function. The precision of the binding energies is estimated at ±0.1 eV and the precision of the compositional analysis is estimated at ±0.1%.

3.5.2 Scanning Electron Microscopy and Auger Electron Spectroscopy

Scanning electron microscopy (SEM) produces a highly magnified image of the material surface using electrons to form the image. Secondary electrons and backscattered electrons are commonly used for imaging samples. In the Auger process, the surface to be analyzed is irradiated with a beam of electrons of sufficient energy, typically in the range 2-10 keV, to ionize one or more core levels in the surface. Auger energy is a function of atomic energies and as a result, knowing that no two elements have the same set of atomic binding energies, elemental identification can be provided by an analysis of Auger energies[91].

To investigate the particle-wafer interaction and the extent of particle contamination, SEM and Auger electron spectroscopy (AES) were used to image the surfaces and perform chemical analysis using a JAMP-9500F Auger microprobe (JEOL) shown in Figure 3-4, at the Alberta Centre for Surface Engineering and Science, University of Alberta.

Non-metals are made conductive by covering the sample with a thin layer of conductive material; in this case graphite was used. A Schottky field emitter was used to produce electron probe diameter of approximately 3 to 8 nm at the sample surface. The SEM and Auger imaging were done using high accelerating voltage and low beam emission current of 15 kV and 8 nA, respectively. AES spectra at different points on the sample surface were acquired by tilting the sample at an angle of 30^0 to face the electron energy analyzer. AES has auto tracking as in SEM the image is moving. Auger spectroscopy and imaging was carried out with a M5 lens with 0.6% energy resolution. AES line profiles and AES mapping was acquired. This data was then quantified and processed.

Figure 3-4 The Auger Microprobe JAMP9500F (JEOL)

3.5.3 Inductively coupled plasma mass spectrometry (ICP-MS)

ICP-MS is an analytical technique that has been used for detecting/determining elements at very low concentrations. As the name suggests, ICP-MS combines a high temperature inductively coupled plasma source with a mass spectrometer. Atoms in the sample are converted to ions by the ICP source which are then separated and detected by the mass spectrometer. Instrument detection limits are as low as or below one part per trillion (ppt) level for different elements in the periodic table. To determine the elements that are present in the clear liquid after 30 days of settling of the MAS of ceria and silica at pH 4, ICP-MS measurements were carried out. Only 4 solutions were used for ICP-MS measurements at the following weight ratios: 0.04, 0.05, 0.07 and 0.1.

This experiment was carried out in the mass spectrometry lab in the Department of Earth and Atmospheric Sciences at the University of Alberta. A Thermo Scientific iCAP Q ICP-MS instrument was used. Typical count rates for 1 ppb In are above 220,000 cps; measurement units are counts per second (cps). 4 point calibration curves are used (0, 50, 100, 200 ppb for Si; 0, 1, 2, 4 ppb for Ce). Bi, Sc and In are used as internal standards. The experiment was done taking 0.1 ml of sample solution and adding 0.1 ml HNO_3, 0.1 ml internal standards (In, Bi and Sc) and 9.7 ml DI water. The mixture was shaken well prior to analysis.

Chapter 4 : Fundamentals of ceria removal from silica surfaces.

This chapter is based on the K. Dawkins, R.W. Rudyk, Z. Xu and K. Cadien paper published in Applied Surface Science[41] .

The ceria slurry pH influences not only the silica surface dissolution leading to its removal but also the surface finish, particulate contamination, defects on the film surface, ceria abrasive size due to agglomeration, ceria slurry stability, friction force, and even the electrostatic interactions between abrasive particles and silica substrate[50]. In the same way, the surface chemistry of the ceria particles is not only influenced by the slurry pH but is also affected by the particle size, zeta-potential and slurry stability. We also know that material removal and the post-cleaning of the wafer surface is controlled by the interaction between ceria abrasive-silica surface functional groups. However, this interaction is very unclear as some research describe it as being a chemical interaction and in other cases a ceria-silica bonding has also been suggested. Therefore to better understand the ceria-silica interaction, the adhesion and removal of ceria particles to a silica surface was studied with the use of X-ray photoelectron spectroscopy (XPS), scanning electron microscopy (SEM) and auger electron spectroscopy (AES) measurements. XPS is an effective technique for surface analysis and has been used extensively in many areas of surface and materials analysis due to the exceptional combination of compositional and chemical information that it provides. SEM, along with Auger emission spectroscopy (AES) imaging and point analysis, was applied to obtain information about wafer surface topography and composition of the multi-elemental sample, at various pH levels (pH 6, 9, and 12) chosen based on the results of the zeta-potential determination. The experimental analysis of the effect of pH on ceria-silica interaction for the subsequent removal of ceria abrasives from silica surfaces will be useful to obtain clean silica film surfaces and to design slurries that limit contact between abrasive and substrate during the CMP process. To the best of our knowledge, there are no other studies which employ these surface characterization techniques to understand the mechanism of residual CeO_2 contamination and removal. In the end, a model will be presented based on electrophoretic mobility measurements of ceria slurry and silica particles at different pHs

4.1 Sample Preparation

The ceria slurry used in this study, namely CeO_2, from Nyacol Nano Technologies, had a 20 wt% ceria concentration and Milli-Q water was used for slurry dilution to 5 wt% concentration. The pH of solutions/suspensions was measured by an Accumet Basic AB15 pH meter, which was calibrated each time prior to use. Citric acid and potassium hydroxide were used to adjust the pH of suspensions. A silicon oxide wafer which was cleaved into three 1 cm x 1 cm pieces was used as the substrate for this experiment**.** The substrate was dipped into the ceria suspension for one minute at a stirring speed of 286 revolutions/min. It was then rinsed in Milli-Q water for one minute at a flow rate of 250 mL/min and dried in air.

Experimental procedures for particle size distributions, zeta potential measurements and XPS, SEM, AES analysis of the samples can be found in Chapter 3 of this work. Colloidal silica abrasives namely EB6080 obtained from AkzoNobel with weight concentration of 35.48 wt% was employed to perform both particle size distribution and zeta potential measurements. Although, the silica slurry, EB6040 was not employed for this experiment, particle size distribution of this silica slurry was measured and this data will be used later on in this work. The original silica slurry, EB6040 had a 38.98 wt % silica concentration.

4.2 Particle Size Distribution

Figure 4-1 shows ceria particle size to be consistent with the value provided by the slurry supplier of ~ 5 nm. At pH 4, the particles were mono-dispersed and therefore show little or no agglomeration. Silica Bindzil EB6080 had the largest particle size of ~ 125 nm while Bindzil EB6040 had the smallest particle size of 81 nm. Both silica abrasives were mono-dispersed at pH 4.

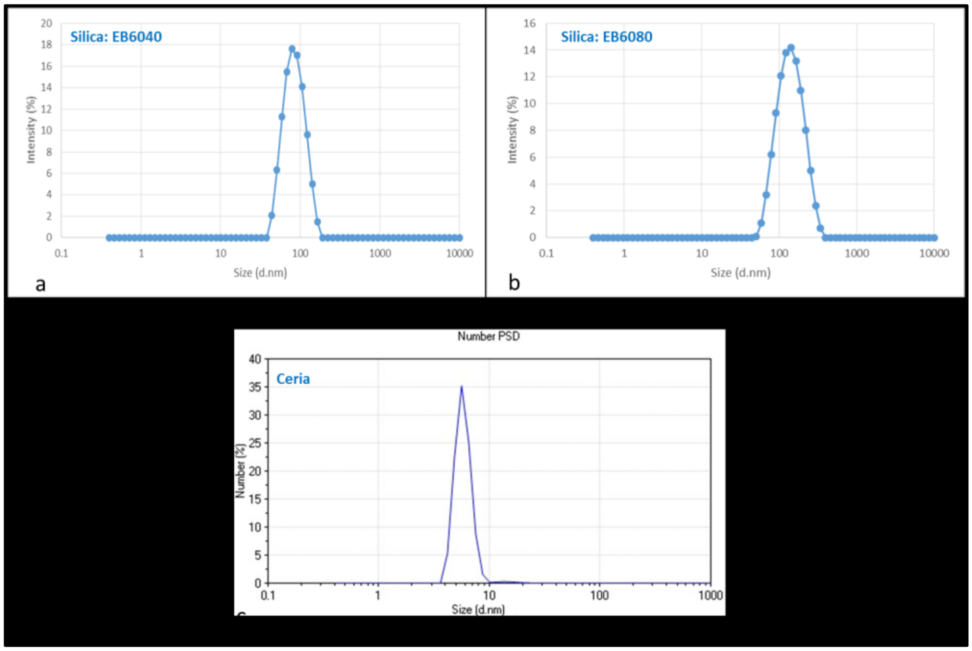

Figure 4-1 Particle size distributions by intensity (%) at pH 4 for (a) Silica EB6040, (b) Silica EB6080 and (c) screenshot of ceria size distribution by Number (%)

4.3 Ceria and Silica Zeta Potential Measurements

Particles attach to surfaces due to coulombic interactions which states that same surface charges repel while opposite charges attract. When particles adhere to surfaces, it results in particle contamination of the surface. The electrostatic interactions between ceria and silica particles were studied via electrophoretic measurements. These measurements were used to determine the surface charge of ceria particles in the slurry and of silica surfaces. The zeta potential of both ceria and silica particles were measured over a wide pH range (3-13) as shown in Figure 4-2.

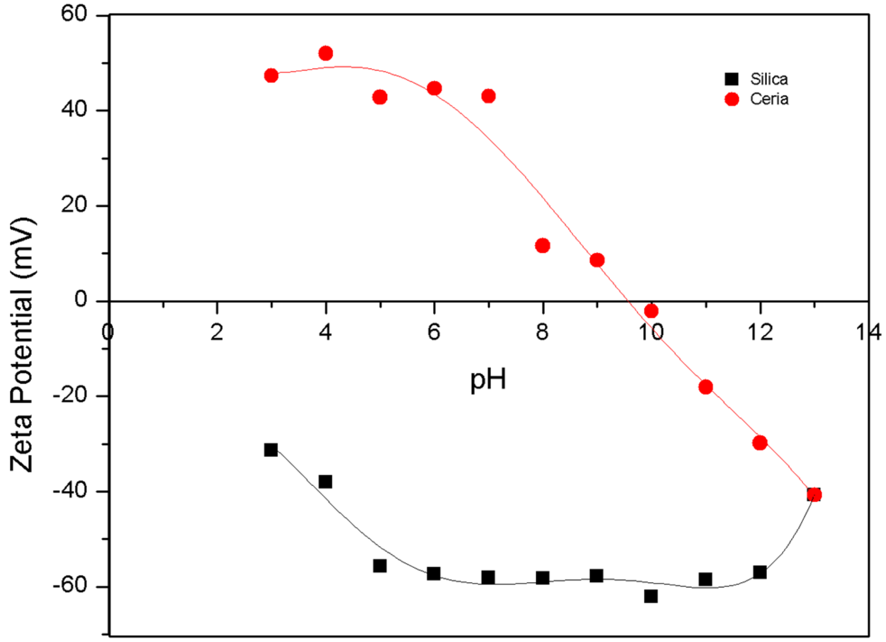

Figure 4-2 Zeta potential measurements of silica and ceria, from pH 3 to 13[41] .

Silica has a negative zeta-potential over the entire pH range (3-13) studied and this negative surface charge is said to be due to the deprotonation of silanol (SiOH) groups on silica surfaces[50] according to the following equation:

$$\text{Si-OH} \leftrightarrow \text{Si-O}^- + \text{H}^+ \quad [19]$$

On the other hand, the isoelectric point of ceria was found to be approximately 9.6 which is consistent with the values for IEP of ceria found in the literature[7]; the ceria zeta potential is positive for pH<9.6 and negative for pH>9.6. Over the pH range of 3-9.6, positively charged ceria particles are expected to be attracted to negatively charged silicon dioxide surface due to electrostatic attraction as illustrated in Figure 4-3 (a). In contrast, for pH>9.6 repulsion of the ceria particles is expected by similarly charged silica surface as represented in Figure 4-3 (b).

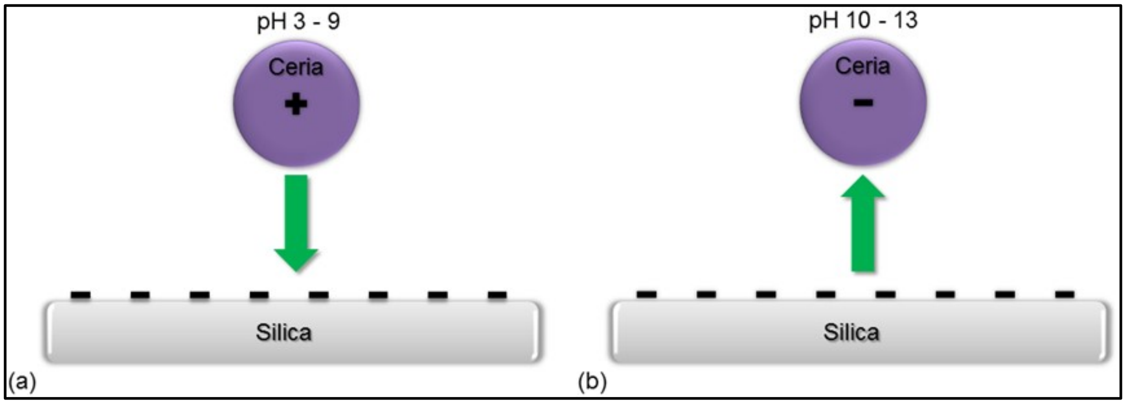

Figure 4-3 Schematic representation of (a) electrostatic attraction between positively charged ceria particle and negatively charged silica surface and (b) repulsive force between negatively charged ceria particle and silica surface[41].

Based on the above zeta potential measurements, three pH values were selected for the ceria slurry which are 6, 9 and 12, representative of acidic, neutral and basic pHs accordingly.

These pHs were chosen because at acidic pH values, the ceria-silica interactions should be completely attractive due to different surface charges on ceria and silica particles while in very basic media, a predominantly repulsive interaction is expected since both surfaces are negatively charged according to the zeta-potential measurements. pH 9 was selected as it was found to be close to the isoelectric point of ceria particles, at this point, particles tend to aggregate faster and will also be attracted to the silica surface. According to the studies done on this topic[50,92] , it is postulated that at ceria slurry pH's close to its IEP, particles tend to aggregate faster resulting in bigger abrasive size particles and an increase in slurry instability, both of which provide the most favorable condition for silica polishing, however, for cleaning this is the opposite. Also, these bigger agglomerated particles are known to cause micro-scratches on the wafer surface. Therefore, to minimize ceria particulate contamination on the silica substrate, a high pH is required so both surfaces are negatively charged and a repulsive electrostatic force exists.

4.4 XPS Analysis

XPS is a surface sensitive technique (sampling between 3–10 nm), therefore, it is ideally suited to quantify the ceria remaining on the Si wafers; however, because the average particle size of the ceria (~5 nm, as determined from the particle size distribution diagram shown in Figure 4-1) is well below the maximum sampling depth, XPS also provides an excellent means to characterize the ceria nanoparticles. Thus, it was important to examine both survey spectra, and high resolution Ce 3d spectra. The surface composition was determined for samples 1 to 3 (pH 6, 9, and 12, respectively). Survey spectra obtained are shown in Figure 4-4.

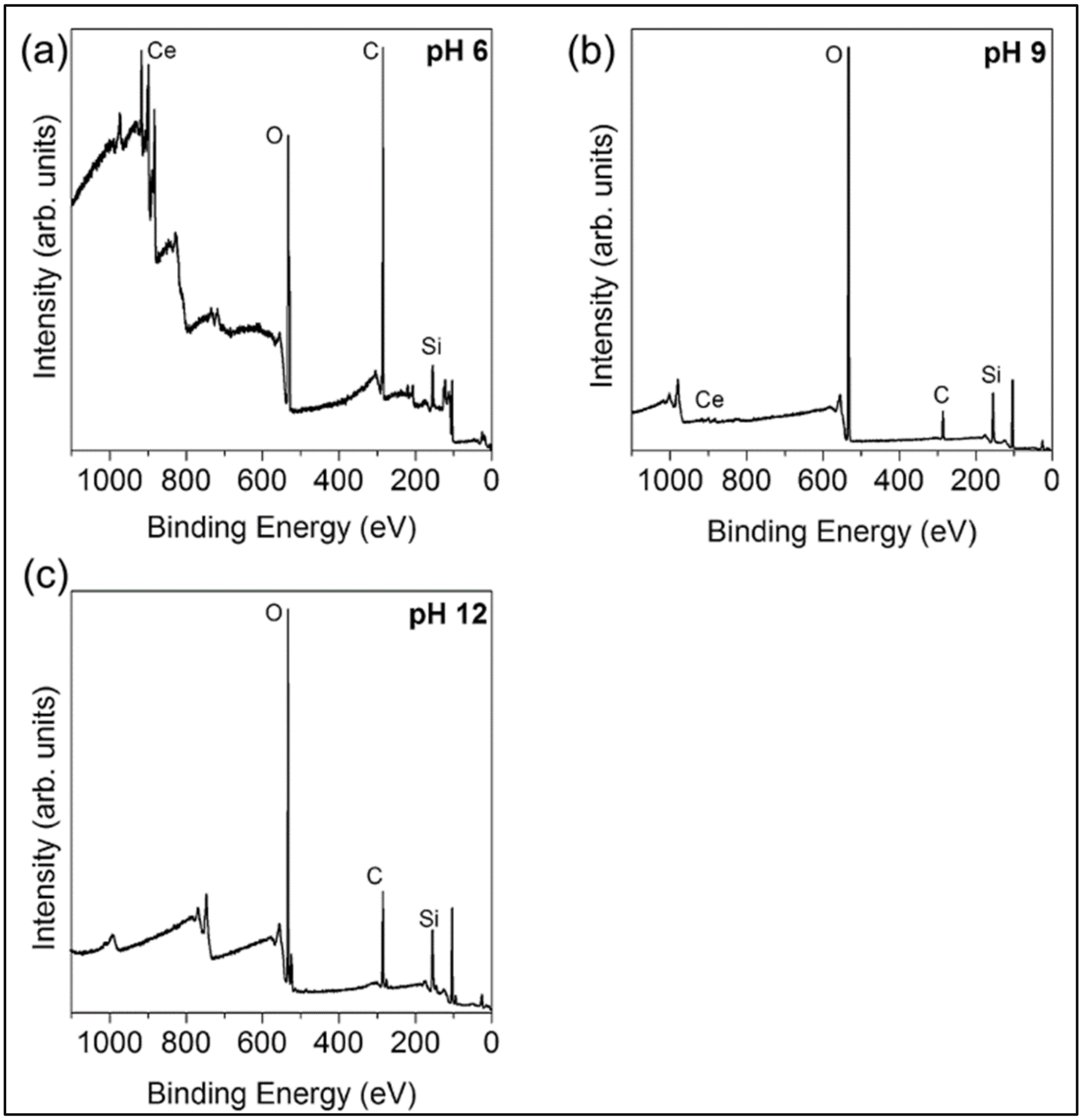

Figure 4-4 XPS survey spectra of samples prepared in (a) pH 6, (b) pH 9, and (c) pH 12 slurries. The most intense core-lines (Ce 4f, O 1s, C 1s, and Si 2p) are labelled for each element present. Ce was not observed in (c)[41].

Analysis of the as-received surfaces confirmed the presence of C, O, and Si (identified with C 1s, O 1s, and Si 2s core-lines), as expected, on all samples. C 1s peak at 284.6 can be used to correct peak shifting due to charging. Ce was detected (identified with Ce 3d core-line) on silica samples that were dipped into the ceria slurry at pH 6 and 9, with the greater amount present on the silica surface at pH 6. It should be noted that Ce 3d peaks are broader than C, O and Si photoelectron peaks. A slight excess of O was observed in the pH 6 sample, this is primarily attributed to surface hydration and oxidation as a result of exposure to atmosphere. Ce was not detected in the pH 12 sample (Figure 4-4(c)).

The effect of slurry pH on the % Ce surface concentration is shown in Figure 4-5. The composition of the Ce found on the surface was at the highest with 2.6% for the pH 6 slurry, while only a trace of Ce was detected on the pH 9 slurry sample (< 1 % atomic concentration). As expected, there is an electrostatic attraction between positively charged ceria and negatively charged silica surface at pH 6 which accounts for the higher atomic concentration of ceria on sample 1. Unlike the ceria particles in sample 1 (pH 6), which are electrostatically bound to the Si surface, those in sample 2 (pH 9) adhere in a different way. The adhesion in sample 2 (pH 9) is believed to be weak since the ceria particles are not electrostatically attached to the silica surface. On preparation of the pH 9 ceria slurry, rapid settling was observed. This is generally attributed to the formation of agglomerates of unstable CeO_2 nanoparticles close to the IEP of ceria, which are held together by relatively weak electrostatic interactions[7,93]. The ceria particles will agglomerate on the surface and when rinsed with water, will be washed away. The few ceria nanoparticles that remain on the surface are probably remnants dislodged from agglomerates after the wafer was rinsed with DI water. Another possible reason for this is that ceria and silica may have formed a Ce-O-Si bond at pH 9, but this could not be confirmed from the XPS data. The absence of cerium on the pH 12 slurry sample validated our theory of electrostatic repulsion between same charge surfaces.

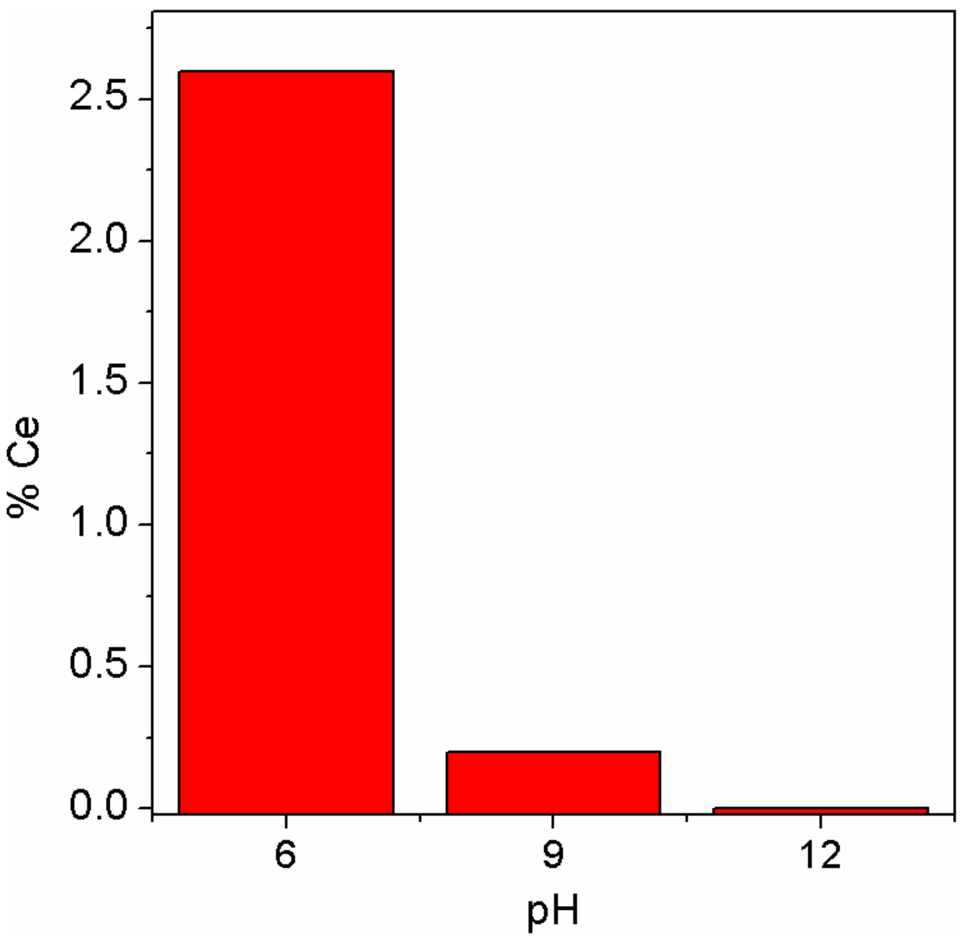

Figure 4-5 % Ce remaining on the silica surface after exposure to different pH ceria slurries[41]

High resolution Ce 3d spectra (Figure 4-6) show significant fine structure, induced by a multitude of shakedown satellite features, and are difficult to interpret. The complexity of Ce 3d spectra is well documented [94,95,104,96–103], and the overall lineshape shown in Figure 4-6 is consistent with systems of mixed Ce valence[95]. The envelope comprises ten different peaks that can be further categorized into five spin-orbit split, $3d_{5/2}$ and $3d_{3/2}$, core-hole pairs. In keeping with the most common labelling scheme, we denote all spin-up (j = 5/2) final states as v, and all spin-down (j =3/2) as u [94]. The pairs, v/u, v''/u'', and v'''/u''', are attributed to the various Ce(IV) final states (Ce $3d^9 4f^2$ O $2p^4$, Ce $3d^9 4f^1$ O $2p^5$, and Ce $3d^9 4f^0$ O $2p^6$, respectively), while v_0/u_0, and v'/u', are associated with Ce(III) final states, Ce $3d^9 4f^2$ O $2p^5$ and Ce $3d^9 4f^1$ O $2p^6$. [94,95]

Because of the incredible complexity in a Ce 3d spectrum, the presence of the u''' peak is often considered a fingerprint for the existence of Ce(IV) [95,101]. The spin-orbit splitting is approximately 18.3 eV which is consistent with literature values [95,101]. The peak positions and compositional data are tabulated in Table 4-1.

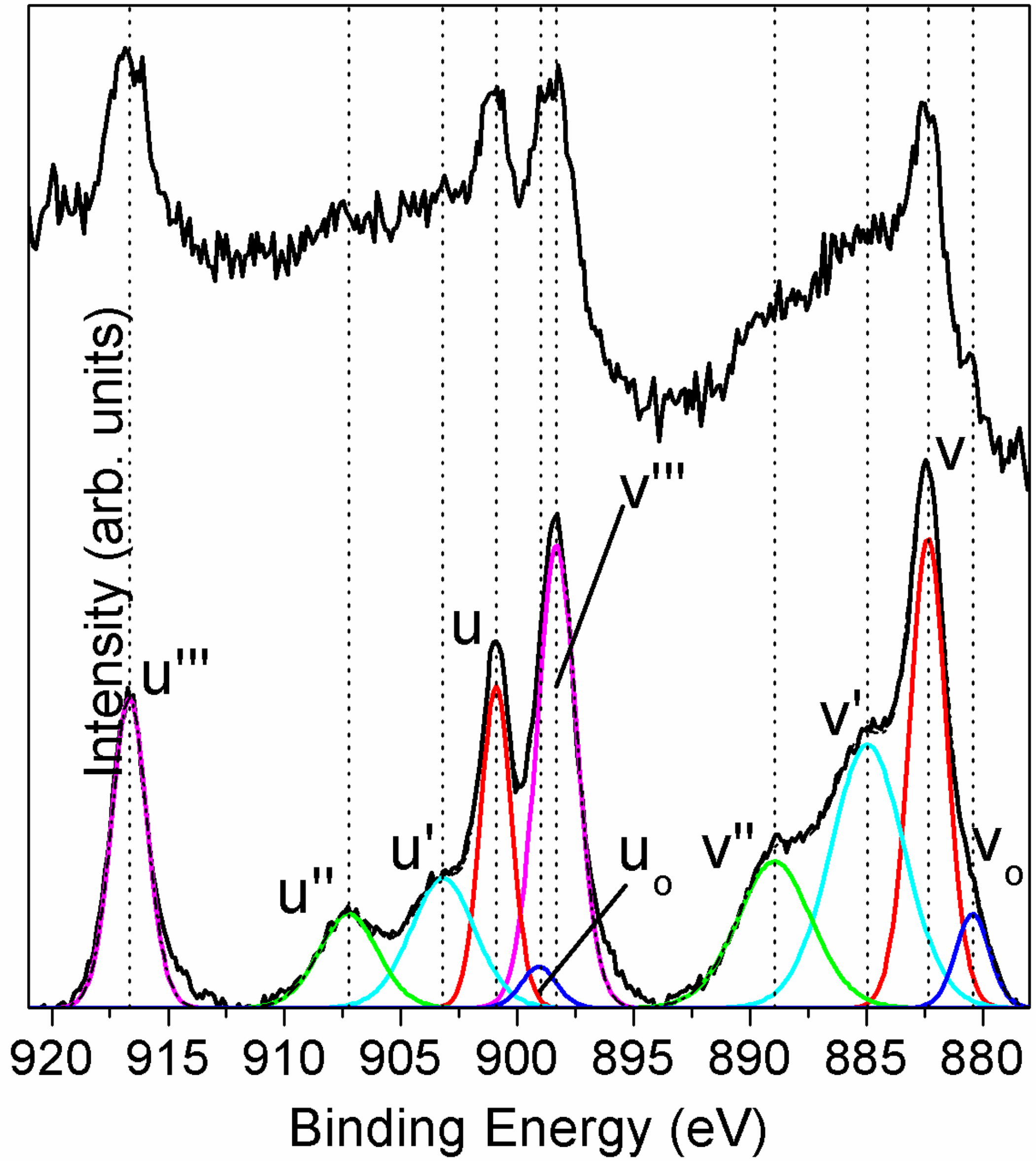

Figure 4-6 High resolution Ce 3d XPS spectra for samples treated at pH 6 and 9. pH 6 (baseline) component peaks are labelled as v/u (spin-up/spin-down) core-hole pairs. The vertical dashed lines mark the peak positions for comparison with the pH 9 sample (raised)[41].

By adding the component peaks, in accordance with the literature[102,103], associated with both Ce(III) ($v_0 + u_0 + v' + u'$) and Ce(IV) ($v + v'' + v''' + u + u'' + u'''$), the Ce(III)/Ce(IV) composition was determined to be 30.8%/69.3%. It is clear from the Ce 3d spectrum collected at pH 6 that the Ce remaining on the surface is mostly Ce (IV). The Ce 3d spectrum stacked above the deconvoluted spectrum in Figure 4-6 resulted from the sample treated with the pH 9 slurry. All features discussed previously with the pH 6 sample persist in the pH 9 sample, as highlighted by the vertical dashed lines, however the significantly decreased concentration of particles remaining on the surface resulted in a poorer signal to noise ratio which precluded any significant quantification. Interactions between silicon-based substrates and deposited thin films are documented and varied. Some cases (e.g. TiO_2 on SiO_2)[105] report temperature-dependent Si diffusion from the substrate into the target film, while other cases suggest interfacial reaction as in the formation of cerium silicate species in heat treated CeO_2/Si films[102,104]. The amount of Ce(III) present in this work (~31%) is consistent with that reported in the previously mentioned thin-film studies[102,104] where it is largely attributed to the reduction of CeO_2 to $Ce_2Si_2O_7$ and various cerium sub-oxides (Ce_2O_3, and Ce_7O_{12}). The extent to which the silicate formation applies to the non-heated nanoparticles presented here is unclear. The use of nanoparticles will decrease the overall interfacial surface area as compared to a thin film, but it will increase the surface area available for surface hydration and sub-oxide formation. It is likely that the true picture is a mixture of both scenarios.

Table 4-1 XPS results for high-resolution Ce 3d core-line

Ce $3d_{5/2,3/2}$ label	**Source**	**Final state electronic configuration**	**Position (eV)**	**Atomic Conc. (%)**
v_0	Ce (III)	Ce $3d^9 4f^2$ O $2p^5$	880.4	3.0
u_0			899.1	1.4
v	Ce (IV)	Ce $3d^9 4f^2$ O $2p^4$	882.4	16.5
u			900.9	9.4
v′	Ce (III)	Ce $3d^9 4f^1$ O $2p^6$	885.0	18.5
u′			903.2	7.9
v″	Ce (IV)	Ce $3d^9 4f^1$ O $2p^5$	889.0	10.4
u″			907.3	5.3
v‴	Ce (IV)	Ce $3d^9 4f^0$ O $2p^6$	898.3	17.3
u‴			916.7	10.4

4.5 SEM and AES Analysis

Scanning electron microscopy (SEM) along with auger electron spectroscopy were used to image the surface of all 3 samples. SEM of the sample surfaces (Figure 4-7) clearly showed that particle contamination/particle adhesion on the surface was highest at pH 6 since the electrostatic attraction between the particle and the film surface would be greater at this pH. At pH 9, particle adhesion is still observed but there are fewer number of particles than sample 1. No ceria particles was imaged on sample 3. This result is in agreement with the XPS data and the electrostatic model.

Ceria is an insulator and appears as small white dots due to charging. Figure 4-7(a) shows uniform ceria particle distribution on the silica surface which confirms particle contamination when both surfaces are oppositely charged. Since the ceria particles have the same charge, they tend to distribute uniformly when they electrostatically attach to silica. However, at pH 9, a non-uniform particle distribution on the substrate is observed as shown in Figure 4-7(b). It was also observed that the number of ceria particles that can be seen on the substrate is significantly less than at pH 6 and the ceria particles appear to be larger in contrast to the particles at pH 6 which tend to be more individual which affirms particle agglomeration at pH 9. This is in agreement with previous studies, which showed that over a pH range of 7-10.5, ceria particles tend to agglomerate quickly due to particle-particle bonding of unstable ceria particles[93]. The SEM of the pH 12 sample, shown in Figure 4-7(c), serves as a visual confirmation of the absence of ceria particles noted from the XPS data.

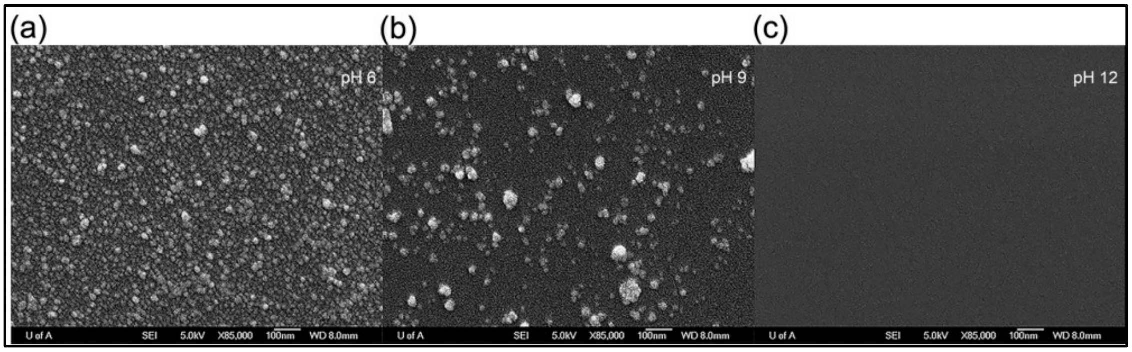

Figure 4-7 SEM images of the adhesion of ceria particles to silica surfaces when ceria slurry was used at (a) pH 6 (b) pH 9 and (c) pH 12.[41]

Auger electron spectroscopy mapping was done on both the pH 6 and pH 9 samples to confirm the presence of ceria. Two different points were measured per sample; the results are shown in Figure 4-8. The images, Figures 4-8(a), and 4-8(d), for pH 6 and 9 respectively, show similar results to the previously discussed SEM images in Figure 4-7. The particles deposited on the wafer at pH 6 are generally much smaller (largely invisible due to the much larger scale bar when compared to the SEM), with less overall agglomeration than with the pH 9 sample. The Auger spectra (shown in Figures 4-8(b), (c), (e), and (f) as the signal derivative) all show the presence of Ce, O, and Si, in agreement with the XPS results. Carbon was detected in both points of the pH 9 sample but not in the pH 6 sample (carbon was detected in all XPS survey spectra). This discrepancy is likely the result of a slightly longer exposure to atmosphere for the pH 9 sample resulting in a buildup of dust and adventitious carbon. We consider the points measured to be representative of sample surfaces.

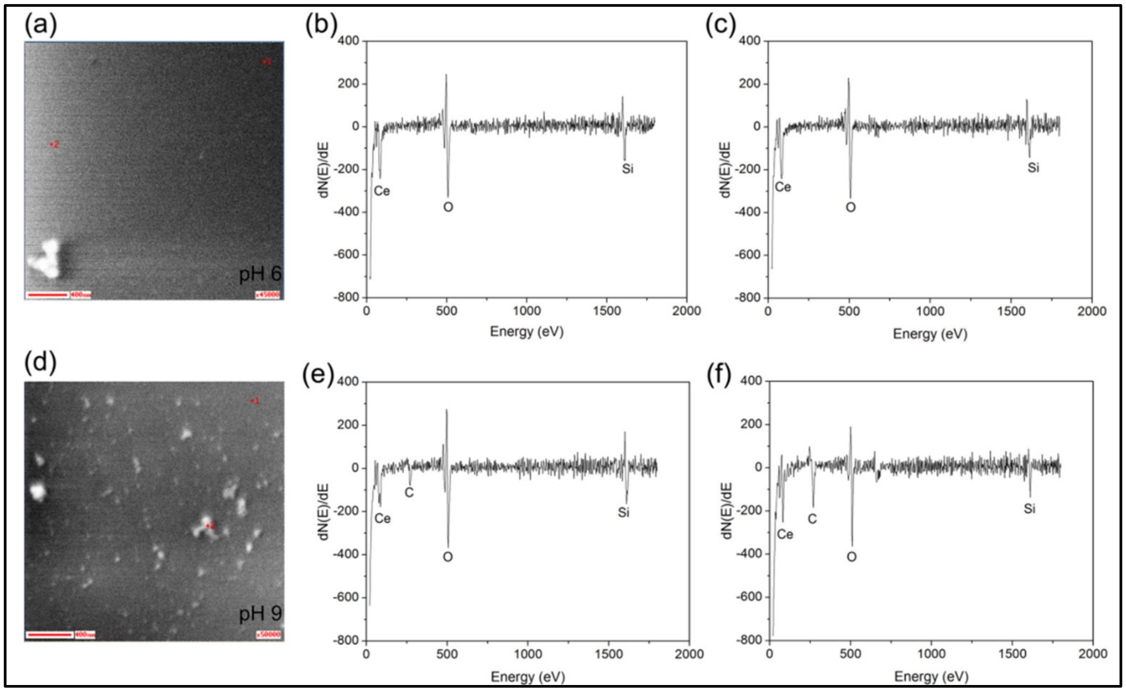

Figure 4-8 Images of (a) pH 6 sample, and (d) pH 9 sample accompanied by AES point analysis at (b) pH 6 – point 1, (c) pH 6 – point 2, (e) pH 9 – point 1, and (f) pH 9 – point 2.[41]

4.6 Conclusions

The removal of ceria abrasives from silica surfaces has been evaluated using XPS, SEM, and AES. The zeta potential of ceria showed a positive surface charge in the pH range of 3 to 9.6 with an IEP at approximately pH 9.6 and a negative surface charge for pH > 9.6 while silica maintained a negative surface charge in the pH range of 3-13. Based on the zeta potential measurements, it was suggested that a high pH (>9) is required to prevent ceria particles from interacting with silica surface due to electrostatic repulsion. This was explained using coulombic interactions and was confirmed by the experimental findings (XPS, SEM and AES). Of the tested samples, the adhesion of ceria particles to the silica substrate was greatest at pH 6 and decreased through pH 9, where only limited adhesion was observed, to pH 12, for which the silica wafer was devoid of ceria. Ceria present on the surface at pH 6 was shown, through high-resolution Ce 3d XPS analysis, to be composed of a ~31%:69% ratio of Ce(III):Ce(IV). The pH 9 sample showed similar lineshape, and, likely, a similar Ce(III):Ce(IV) ratio, however the decrease magnitude prevented any meaningful quantitative analysis. Based on XPS, SEM and AES analyses, it is clear that an interaction exists between the ceria and silica surfaces, however, the nature of this interaction was not studied in detail.

Chapter 5 : Colloidal Stability of Mixed Abrasive Slurries and their effect on Silicon Dioxide and Silicon Nitride Removal Rate for STI CMP.

Colloidal stability is an important factor in the chemical mechanical polishing process as it affects material removal rate, defects on the surface of thin films which can be seen through micro-scratches on the wafer due to the agglomeration of particles. In a previous study of colloidal stability of CMP slurries containing silica and ceria nanoparticles by Lin et al[7], they found a correlation between slurry stability and increased CMP efficiency on oxide surfaces at pH 4. Lin et al observed that MAS with ceria to silica weight ratio at approximately 0.05 to 0.15 precipitated faster and had higher viscosities than mixed slurries with higher or lower weight ratio and as a result exhibited high colloidal instability. These slurries showed higher oxide and nitride polish rate due to greater contact area between the composite particles and wafer surfaces. Since the colloidal stability of slurries affects the overall polishing performance, stability of these slurries was studied via settling tests. In this chapter, the settling/precipitation of mixed abrasive slurries consisting of two different abrasives namely ceria and silica controlled by mixing ratio in order to optimize the CMP removal rate was studied over a period of time. Polishing of both silicon dioxide and silicon nitride films were also carried out using the slurry weight ratios that were used for the settling tests in order to study the influence of slurry stability on material removal.

All the materials and the experimental methods used in this chapter are described in Chapter 3 of this work and the CMP parameters listed in Table 3-1.

5.1 MAS Zeta potential Measurements

The zeta potential of the composite particles was measured at various ceria to silica weight ratio in the range of 0.03-0.15 at pH 4 and shown in Figure 5-1. The zeta potential measurements show that at low ceria to silica weight ratio of ≤ 0.03, the MAS zeta potential value is approximately the same as the zeta potential of silica at pH 4 that was presented in Chapter 4 and reference 40. The composite particle at this point will possess a negative surface charge and the MAS is expected to behave as a stable single component silica slurry. A general guideline is that particles with zeta- potentials greater than ± 20-30 mV are usually stable[69]. In relation to material removal, slurries of this composition are expected to have low oxide removal rate due to electrostatic repulsion by similarly charged oxide surface but will be attracted to positively charged nitride surfaces. At a ceria to silica weight ratio of approximately 0.068, the zeta potential of the composite particles is zero and the overall net surface charge is zero. This agrees well with the value of IEP calculated by Lin et al[7] and correlates with their experimental data and the proposed model on zero net surface charge. A transition of the zeta potential of the MAS occurred in the range of ceria to silica weight ratio 0.05 to 0.1 (known as the transition range). Within this range, composite particles should settle quickly as particles tend to agglomerate close to or at the IEP forming unstable suspensions. When the ceria to silica weight ratio exceeds 0.1, the MAS zeta potential is slightly lower than that of the ceria zeta potential at pH 4 which was approximately 40 mV (Figure 4-2). The composites particles are believed to now have a positive surface charge due to the higher concentration of ceria where ceria nanoparticles are now covering the entire silica core and will once again form stable slurries due to mutual repulsion among same charged particles. The positively charged composite particles are now expected to be attracted by oppositely charged oxide surfaces and repelled by similarly charged nitride surface. Based on the above zeta-potential measurements, the surface charge on the composite particles shifted from that of pure silica to that of pure ceria by increasing the concentration of ceria particles within the silica slurry at a given pH.

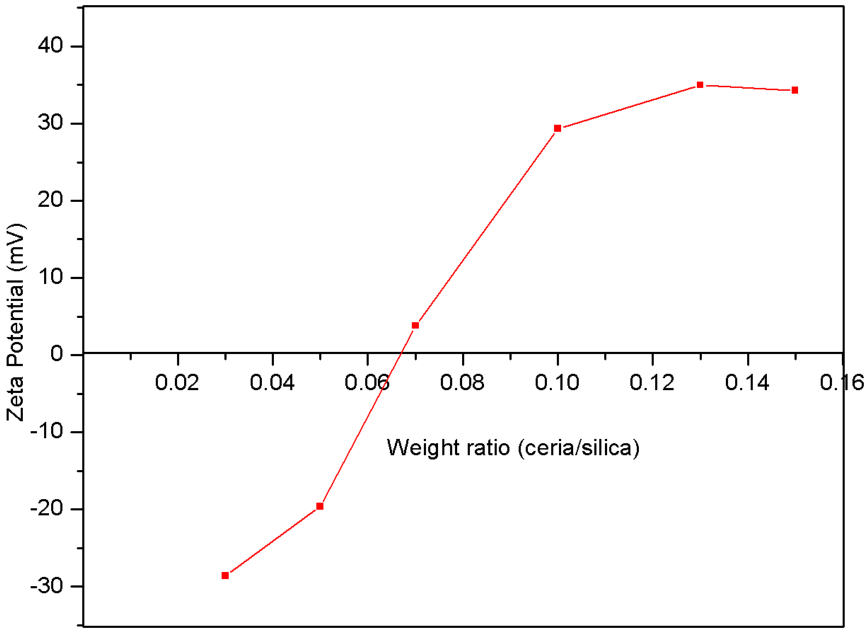

Figure 5-1 Zeta potential of MAS (silica EB6080 and ceria) as a function of weight ratio at pH 4.

5.2 Settling Tests

Once the individual slurries are mixed together, ceria-silica interactions will occur. Positively charged ceria nanoparticles attaches to negatively charged silica nanoparticles almost immediately at pH 4 due to electrostatic attractions. The attachment of smaller, harder ceria particles unto larger softer core silica particles, forming a sheath around the silica particles results in changes in the surface charge of the composite particles and hence the stability of these mixed abrasive slurries. Numerous investigators have shown that smaller ceria particles form a sheath around the larger silica core with the use of TEM images[30,8,9,7] . Slurry stability of these MAS was studied via settling tests over a period of time shown in Figures 5-2 and 5-3. The effect of slurry stability on polishing rate of both oxide and nitride films was also studied using the mixed abrasive slurries in order to determine the best weight ratio of MAS to optimize selectivity. The first set of settling tests was done over a wide range of weight ratios (0.02 -0.3) and settling was observed to happen quickly between 0.05-0.1 weight ratios. A more defined set of settling tests was done between weight ratios 0.04-0.1 which is represented in Figure 5-3. This was done to identify the exact weight ratio at which settling occurs the fastest, as this point should correspond to the isoelectric point of the composite particles. The number at the bottom of each bottle shows the ceria to silica weight percent ratio.

It was observed that at a very low ceria to silica weight ratio (0.02) the MAS is partially stable, that settles after a prolonged period of time (see Figure 5-2). The ceria concentration here is very low and the SiO_2 particles are not fully covered by the smaller CeO_2 particles which results in an overall negative net surface charge of the composite particle which falls below the isoelectric point of these composite particles. High repulsive electrostatic interactions exist between negatively charged composite particles forming stable suspensions that take a longer time to settle.

As the ceria concentration increases, more ceria particles are now available to cover the silica surface and the composite particle becomes neutral and reaches an overall net surface charge of zero known as the isoelectric point (IEP). MAS close to or at the isoelectric point settled quickly (within 1 hour of mixing) due to poor stability mostly due to particle agglomeration. This is observed in slurries of weight ratios between 0.05-0.08 where the IEP of these composite particles were measured to be 0.068 (Figure 5-1). MAS with weight ratios in the range of 0.08-0.1 started to settle after 8 hours, these slurries settled completely within 48 hours and can also be classified as unstable.

Once the ceria concentration is increased beyond the isoelectric point, there is an excess of ceria and silica particles are now completely covered with ceria nanoparticles forming composite particles with an overall net positive charge. The absolute magnitude of the zeta potential is much larger and once again high repulsive forces exist between these particles which allow it to form stable colloidal suspensions. However, these particles settle out over a longer period of time. This is due to the gravitational settling forces of these nanoparticles irregardles of the conditions that exist in these solutions. A schematic representation of the settling pattern/zones is shown in Figure 5-5.

The settling of 5 wt% silica slurry was also studied over a long period of time (represented in Figure 5-4) and was found to be very stable due to the mutual repulsion of the silanol (SiOH) surface groups at high negative zeta potential at pH 4. Allen et al[106] proposed that the stability of silica at low pHs (2-4) can be attributed to particle hydration as the silanol groups are highly hydrophilic resulting in hydrogen bonding with water. It is suggested that upon hydrogen bonding with water, formed water structures at the silica surface prevents particle-particle interactions and also prevents agglomeration by Van der Waals forces [15].

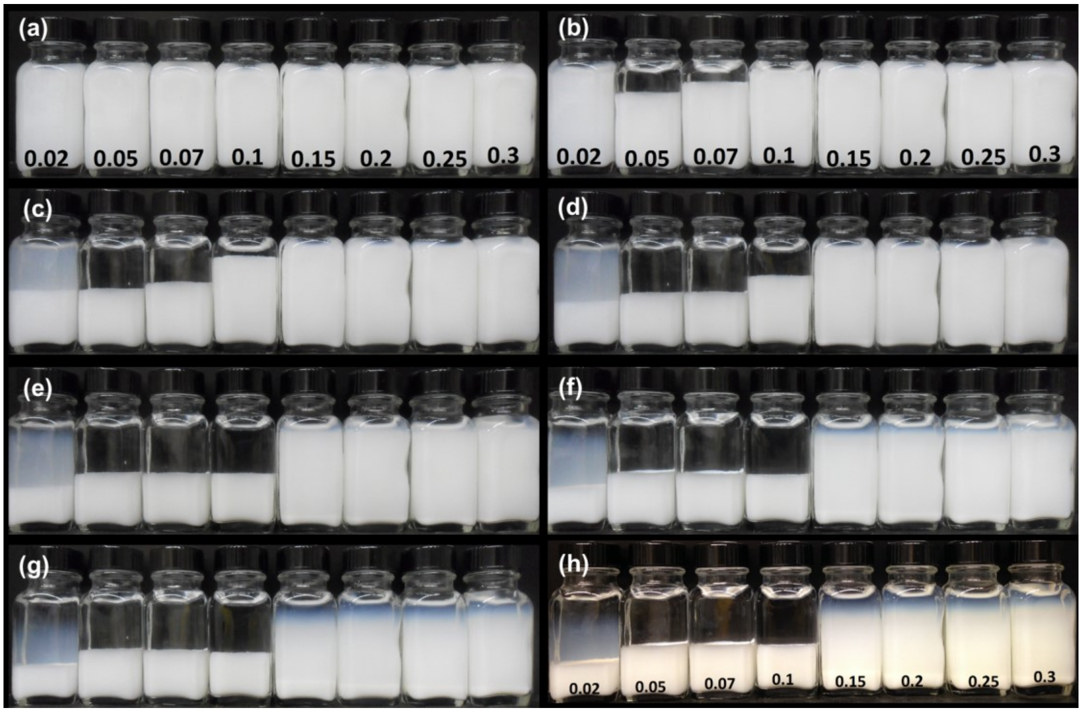

Figure 5-2 Settling of 0.02-0.3 weight ratio CeO_2:SiO_2 at pH 4 over (a) 0 hour (b) 2 hours (c) 8 hours (d) 24 hours (e) 48 hours (f) 1 week (g) 2 weeks and (h) 1 month.

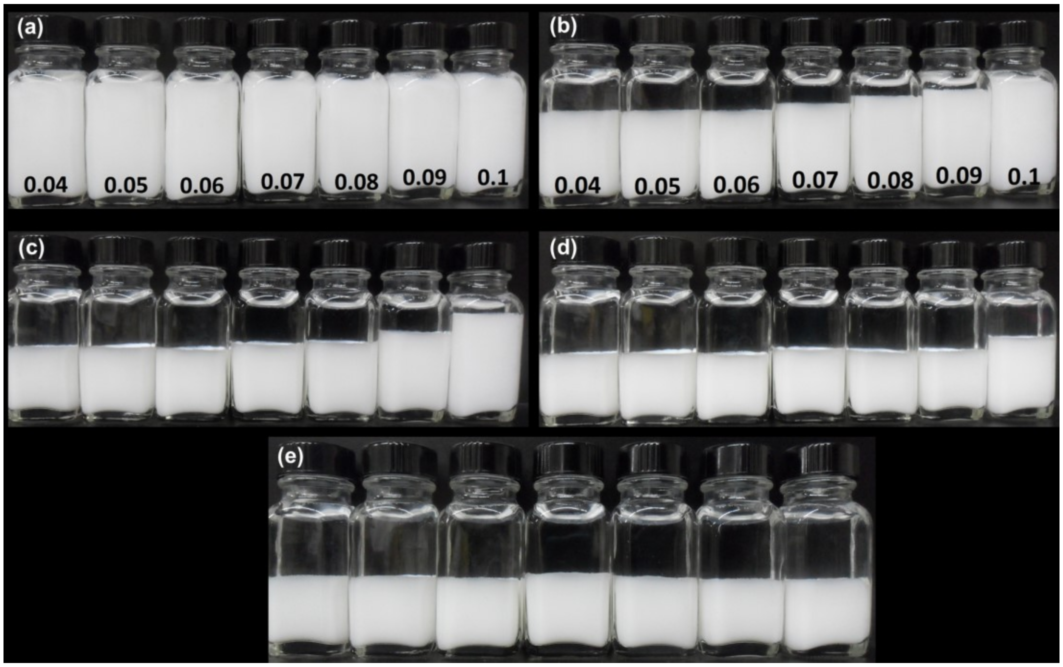

Figure 5-3 Settling of 0.04-0.1 weight ratio CeO_2:SiO_2 at pH 4 over (a) 0 hour (b) 2 hours (c) 8 hours (d) 24 hours and (e) 48 hours

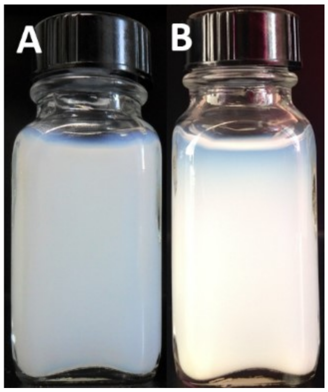

Figure 5-4 Settling of 5 wt % SiO_2 slurry at pH 4 over (A) 2 hours and (B) 1 month

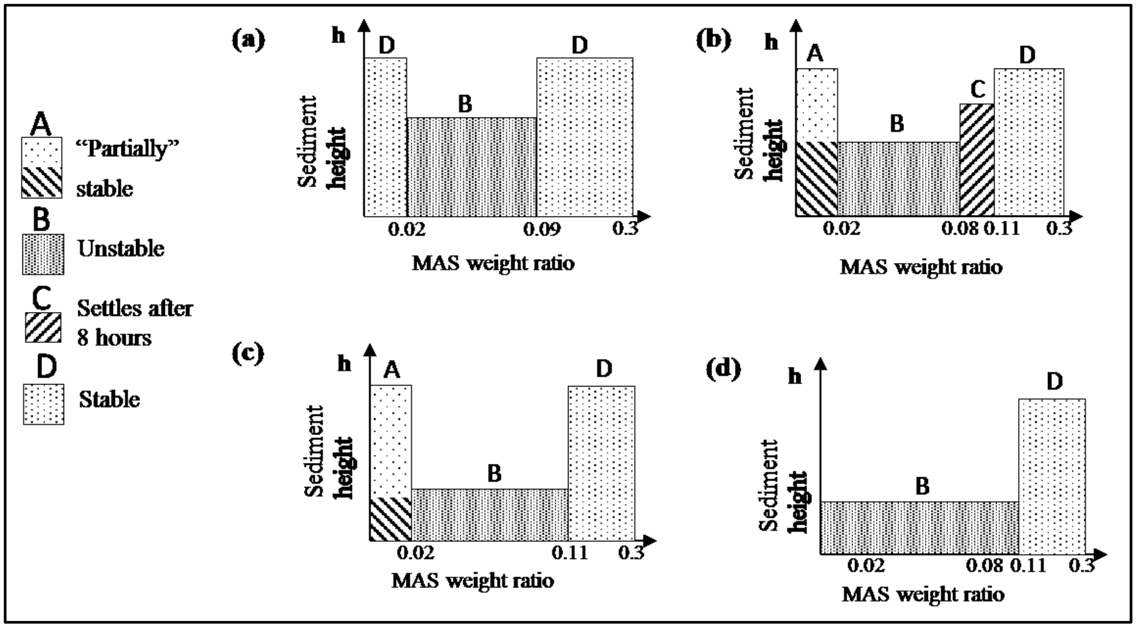

Figure 5-5 Schematic presentation of the MAS stability at (a) 2 hours, (b) 8 hours, (c) 48 hours and, (d) 1 month.

One of the aims of our earlier investigation[41] was to determine if ceria particles were chemically bonded to silica particles using XPS, however, we were not able to determine this. There still exists the question if the particles attach, can they be unattached by changing the pH. To determine if this was possible, settling tests were carried out with 0.05 weight ratio Ce:Si at pH 4 and this same solution was shaken and its' pH increased to10. The results are shown in Figures 5-6 and 5-7.

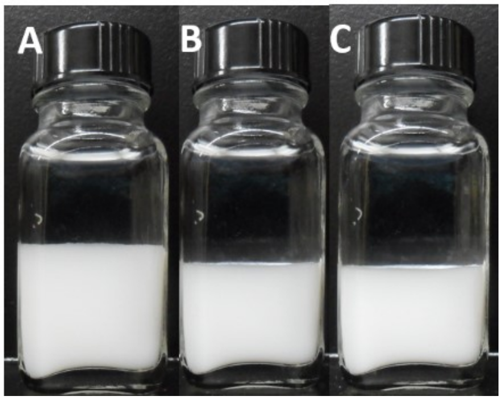

Figure 5-6 Settling of 0.05 weight ratio CeO_2:SiO_2 at pH 4 over (A) 2 hours (B) 24 hours and (C) 7 days

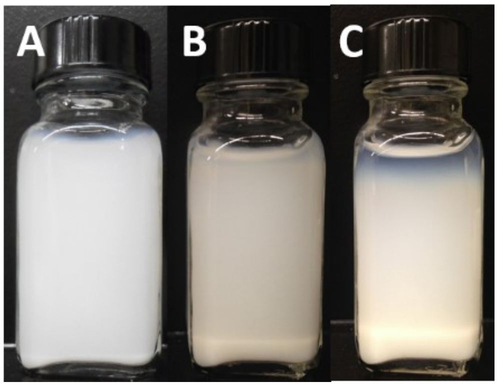

Figure 5-7 Settling of 0.05 weight ratio CeO_2:SiO_2 at pH 10 over (A) 2 hours (B) 24 hours and (C) 7 days

Based on the settling data, we can conclude that that the particles are not strongly chemically bonded as a higher pH causes the particle to separate forming a stable solution at pH 10.

5.3 Settling vs pH

As discussed before in our previous study and numerous investigations on particle-particle interactions of binary systems[7,41,50], pH has a significant effect on ceria-silica interaction. We found that the adhesion of ceria particles to silica surfaces and subsequent removal is pH dependent. For this experiment, two different MAS slurry weight ratios were chosen, 0.1 and 0.2, and their pHs' were varied. The number at the bottom of each bottle represents the pH.

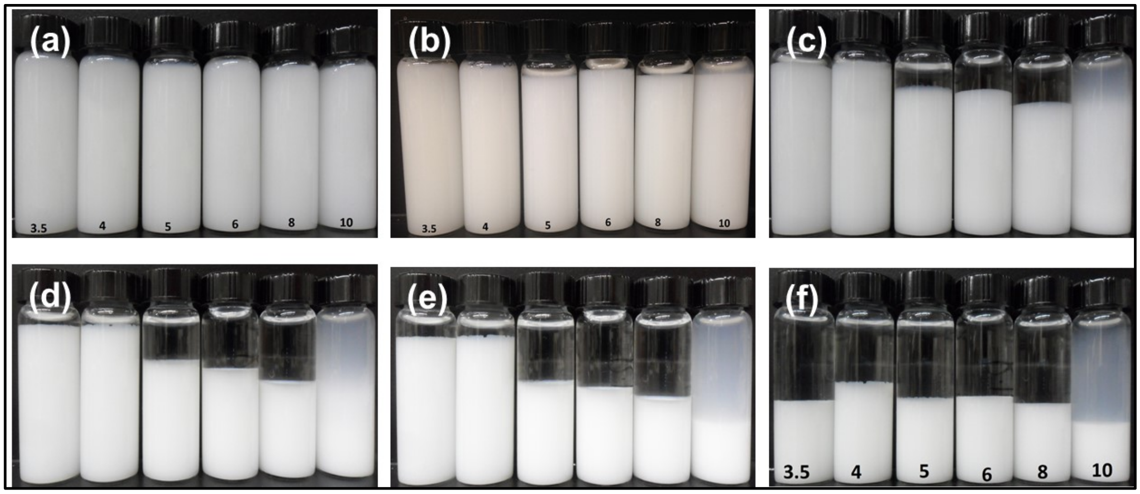

Figure 5-8 Settling of MAS of 0.1 weight ratio ceria-to-silica vs pH at (a) 0 hour (b) 5 mins (c) 1 hour (d) 2 hours (e) 4 hours and (f) 24 hours.

It was observed that for the weight ratio of 0.1 ceria/silica MAS, the slurries with pH from 4 to 8 have very poor colloidal stability as settling was observed immediately after mixing. This is expected as the absolute value of zeta potential of pure silica increases from pH 3-10 (i.e silica zeta potential got more negative) while the zeta potential of ceria decreases to zero around pH 9. This suggests that between pH 3-9, strong electrostatic attraction exist between silica and ceria forming composite particles that will settle. These newly formed composite particles at 0.1 weight ratio, have a positive zeta potential at pH 4 as seen in Figure 5-1, however, as pH increased from 4 to 10, the zeta potential of the composite particles shifts from positive values to negative values where at pH 10 both silica and ceria particles possess negative surface charges and electrostatic repulsion dominates among the particles keeping them suspended within the solution leading to dispersion stability. MAS of 0.1 weight ratio ceria/silica are unstable between pH 3.5-9, however when the pH exceed 10, it begins to regain stability.

While, at a weight ratio of 0.2 ceria/silica, slurries with pHs 6-10 started settling almost immediately after mixing. After 24 hours, slurries at pH 5, 6, 8 and 10 settled completely while pHs 3.5 and 4 did not precipitate. Unlike slurries at 0.1 wt ratio that gained stability by increasing the pH, slurries at 0.2 weight ratio became unstable when pH was increased.

Lin et al[7] measured the zeta potential distributions of MAS of silica and ceria over a wide weight ratio range between 0.02-0.4 (ceria/silica) at both pH 4 and 10 (Figure 7 of Reference 7). All weight ratios showed negative zeta- potentials at pH 10. At pH 10, there is little to no ceria to silica attachments due to same surface charge on both nanoparticles resulting in stable slurries, however, 0.2 ceria to silica weight ratio slurry at pH 4 is very stable and has a zeta potential measurement similar to that of pure ceria at pH of +40 mV. The composite particles at this weight ratio will behave as single component ceria slurries and will have an IEP between pH 9-10. Therefore between pH 9-10, very weak repulsive forces exist between the composite particles and agglomeration occurs leading to settling. As discussed before, it is believed that the agglomeration of the particles are loose due to these weak repulsive forces and will be easily separated during polishing as a result of high shear force. It is stated[7] that unstable slurries i.e slurries that precipitate quickly, produces the highest polishing rates of silicon dioxide. Using these settling results, polishing tests were carried out at the different weight ratios keeping the pH constant and then varying the pH at weight ratios 0.1 and 0.2 ceria-to-silica.

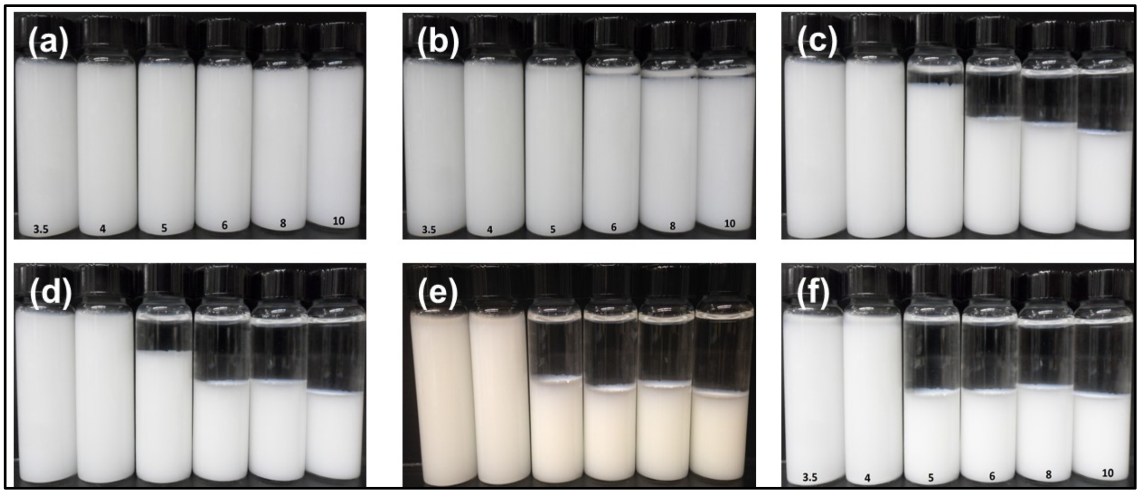

Figure 5-9 Settling of MAS of 0.2 weight ratio ceria-to-silica vs pH at (a) 0 hour (b) 5 mins (c) 1 hour (d) 2 hours (e) 4 hours and (f) 24 hours

5.4 Chemical Mechanical Polishing of PECVD Oxide and Nitride

The effect of slurry weight ratio on material removal is shown in Figure 5-10. The error bars indicate standard deviation in the experimentally measured polish rates. The data shown is that obtained while polishing under conditions described in Experimental using the CMP parameters in Table 3-1. The SiO_2 concentration was kept at 5 wt % while ceria concentration was varied. The pH of all the slurries used was kept constant at pH 4 ± 0.6.

It is apparent that at very low ceria concentration compared to silica (0.1:5), mechanical abrasion by the composites particles of both silicon dioxide and silicon nitride is low with polish rates of 125.97 nm/min and 23.13 nm/min respectively. The composite particle at this weight ratio has a negative surface charge with a zeta-potential value close to that of silica and will behave as a single silica particle and we also know that the silicon dioxide surface is negatively charged. Both particle and wafer now have the same polarity and will repel each other which will result in low oxide polish rates due to limited particles reaching the wafer surface. Also, particle-

particle interactions are responsible for this low oxide polish rates as repulsive interactions among the negatively charged composite particles push them further apart from each other resulting in less particles reaching the wafer surface.

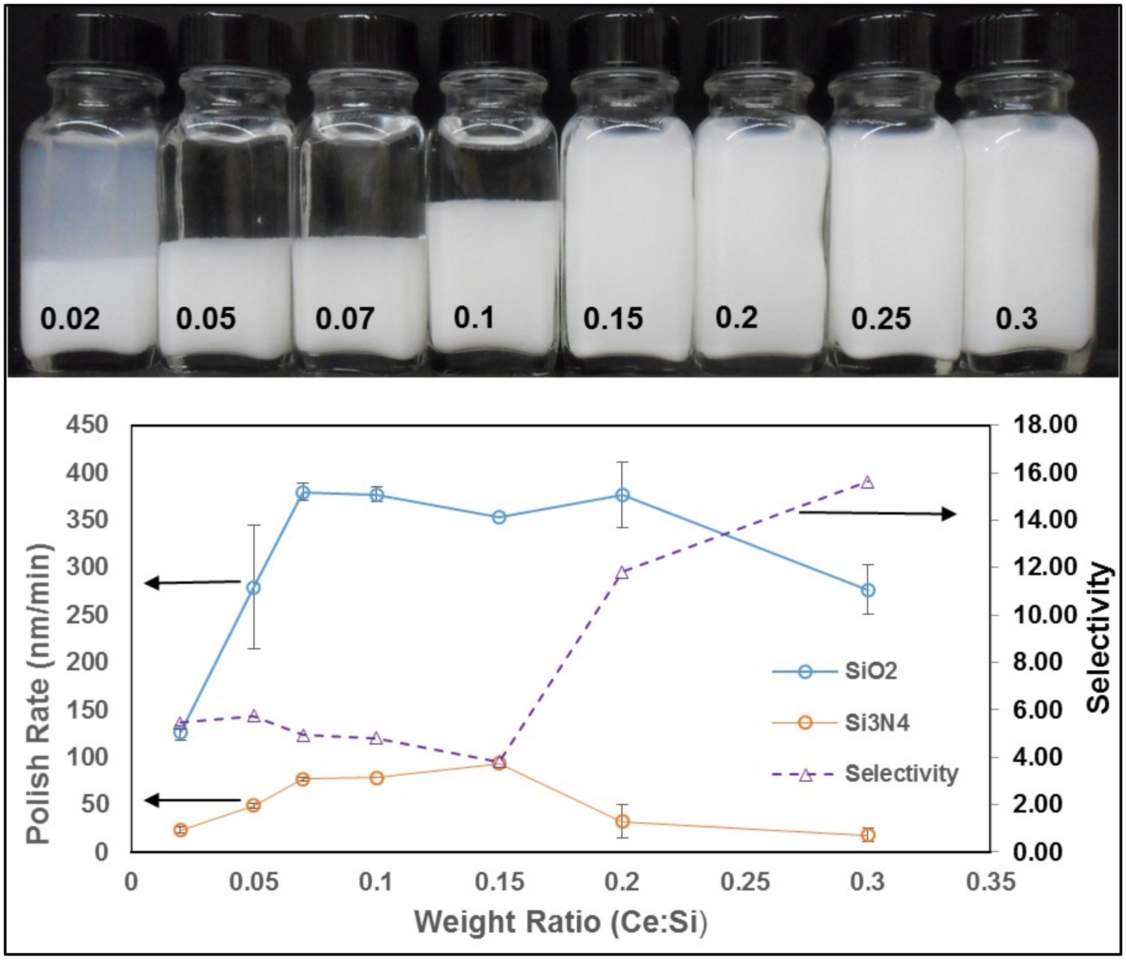

Figure 5-10 Polishing rate of silicon dioxide and nitride vs slurry weight ratio at pH 4. The corresponding settling data for each weight ratio is shown above at 24 hours (All slurries used in this experiment were used within 24 hours of making)

The silicon dioxide removal mechanism proposed in the literature and in the literature review of this work refers to the hydrolysis and dissolution of silica as fundamental to its removal[82]. Cook [6] proposed that chemical interactions between particle and the substrate is the key to material removal during polishing .He went on to propose that ceria followed by zirconia particles are best for polishing oxides due to their chemical activity[6]. It was shown that higher polish rates directly relates to increasing particle surface activity represented by their valence as Ce^{4+} is at the top of the "chemical tooth" followed by Zr^{4+}, SiO_2 is at the very end which suggests that silica is slow to polish silicon dioxide surfaces [6].

In our work, the removal rate achieved using MAS of ceria and silica at 0.02 weight ratio is an order of magnitude 13 times greater than that obtained when using silica abrasive particles on its' own at the same concentration and pH to polish silicon dioxide, which showed a removal rate of just 9.71 nm/min. Similarly, the silicon nitride removal rate was 2 times as high when MAS were used. This suggests that small amounts of ceria in conjunction with silica results in a faster silicon dioxide dissolution when compared to using silica slurries alone.

It is apparent that increasing the concentration of ceria increases the material removal rate of both oxide and nitride surface up to a maximum value. Beyond this maximum value the removal rate reaches a plateau where the addition of more ceria doesn't result in an increase in removal rates. There is a steep increase in oxide polish rates from 0.02 weight ratio to 0.07 weight ratio reaching a maximum polish rate of approximately 380 nm/min. This weight ratio correspond to the IEP of the composite particle reported above in Figure 5-1. At this weight ratio, composite particles become neutralized, agglomeration occurs resulting in quick settling of the slurry which increases the number of particles trapped between the pad and wafer hence increasing the number of particles that come in contact with the silicon dioxide surface enhancing material removal.

Between weight ratios 0.07-0.1 ceria-to-silica, oxide polish rate remains constant with just a difference of 2.6 nm/min between the 2 points. This concurs with the work of Lin et al[107] which states that unstable slurries produce high oxide polish rates. However a decrease in oxide polish rate is observed between 0.1-0.15 weight ratios. Between these weight ratios, the slurry regains stability. This transition is probably responsible for the decrease. At this point more ceria particles are present in the slurry and all the silica particles present are expected to be fully covered with ceria particles changing the surface charge to positive. There will exist repulsive electrostatic forces between the composite particles, limiting the amount of ceria particles that come in contact with the oxide surface, slightly decreasing the polish rate.

However, as the slurry got more stable and the concentration of ceria increases at 0.2 weight ratio, the oxide removal rate reached a new maximum of 381 nm/min. The now positively charged composite particles that have zeta-potential value close to that of pure ceria, will be attracted to the negatively charged oxide surface which is advantageous for polishing.

Increasing the ceria concentration beyond 0.2 weight ratio causes oxide polish rate to decrease. At 0.3 weight ratio, 1.5 wt % ceria is present in the solution leading to saturation at higher ceria abrasive concentrations. An excess of ceria particles exists within the MAS and a higher electrostatic repulsive force among positively charged composite particles and also among composite particles and the extra ceria particles suspended in the slurry which limits the amount of particles reaching the wafer surface especially particles further away from the surface. Also the extra ceria particles that are suspended in the slurry do not reach the wafer surface due to their small sizes and are limited to the pores of the pad. However, at 0.3 weight ratio, oxide removal rate is still relatively high due to the “chemical tooth” of the ceria particles that do reach the surface.

In relation to nitride removal, there is a linear increase from weight ratio 0.02 to 0.07. Polishing rate remains more or less constant between 0.07-0.1 weight ratio ceria to silica and reaches a peak maximum polish rate of 93 nm/min at 0.15 weight ratio from which polish rate starts to decrease steadily to a minimum of approximately 10 nm/min at 0.3 weight ratio. Over the entire weight ratio range, the Si_3N_4 polish rate was much lower than the oxide polish rate. Based on zeta-potential measurements[7], ceria and silicon nitride have IEP at pH 9 and 7.5 respectively while silica has negative zeta-potentials over the pH range 3-13. Therefore, at pH 4, ceria particles should be attracted to oxide surfaces but repulsed by the same charged silicon nitride surfaces. As the concentration of ceria increases in the slurry, the composite particles will possess a positive charge and act as a shield for the silicon nitride surface that is similarly charged hence suppressing the silicon nitride polish rate. We can conclude that removal rate of nitride increases with unstable slurries, however, the more stable the slurry, the nitride polish rate decreases significantly.

Despite the existence of electrostatic repulsion between particle and the silicon nitride surface, the nitride film is being polished. Hu et al[85] proposed that nitride hydrolysis and further hydration in the presence of water results in a chemically modified nitride surface layer of $Si(OH)_4$ which is assumed to be mechanically weaker than slurry particles such as CeO_2 which are able to remove this layer during polishing due to the "chemical tooth" effect. He further postulated that this mechanically weak surface layer can be dissolved in the slurry. However, several researchers proposed the suppression of nitride removal rates through the use of additives to modulate hydrolysis and hydration reactions that will hinder the formation of silicon dioxide which were discussed earlier in the Literature Review of this work.

A detailed schematic representation of the polishing mechanism of both oxide and nitride surfaces by the composite particles at different surface charges is shown in Figure 5-11.

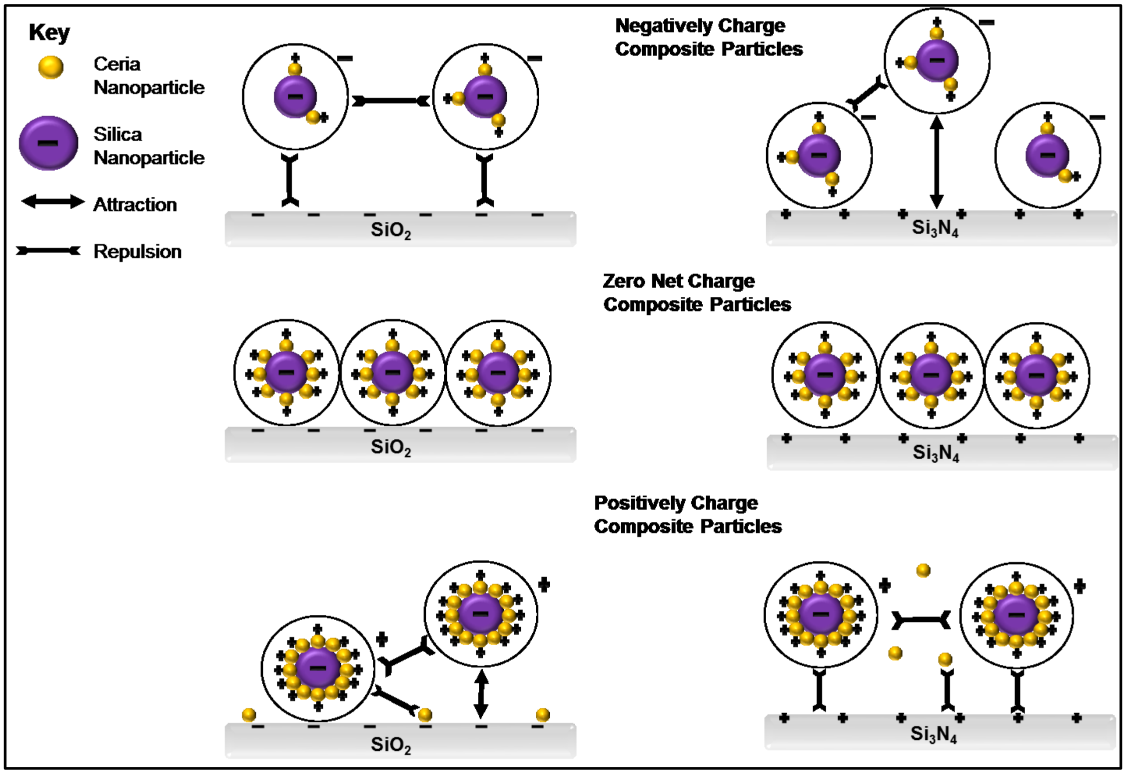

Figure 5-11 Schematic presentation of the polishing mechanism of mixed abrasive slurries at different surface charges on silicon dioxide and silicon nitride surfaces.

The effect of pH of the composite particles on polishing rate of both oxide and nitride surfaces was studied at ceria to silica weight ratios of 0.1 and 0.2 and shown in Figure 5-12 (a) and (b) respectively. For both weight ratios, we saw oxide and nitride removal rates initially increasing to a maximum and then decreasing steadily with an increase in pH. It was suggested that a high pH (>9) is required to prevent ceria particles from interacting with silica[41]. Based on the settling results above and previous zeta potential measurements, we know that increasing the pH from 4 to 10 changes the surface charge on the particles from positive to negative, hence, it is expected that mixed abrasive slurries at pHs ≥ 9 will result in lower oxide and nitride polish rates. However, while we expect very low polishing rates of silicon dioxide, SiO_2 material removal was observed to be up to 200 nm/min at pH 10. This is probable due to the quick hydrolysis of the silicon dioxide surface layer at higher pHs.

Based on zeta potential measurements, we expected high selectivity between pH 3-7, however, selectivity was highest at pH 10 for both MAS weight ratios 0.1 and 0.2 at 15 and 28 respectively. This is mainly due to the very low nitride polishing rates at pH 10. A selectivity of approximately 26 was also observed when 0.2 weight ratio MAS was used at pH 3.5 due to a drop in the nitride polish rate. Despite reaching a maximum oxide polishing rate of 420 nm/min at pH 6 when polishing with slurries at weight ratio of 0.2, selectivity was only about 8 as nitride polish rate was also at a maximum of 55 nm/min. For effective application in STI CMP, a much higher selectivity is required.

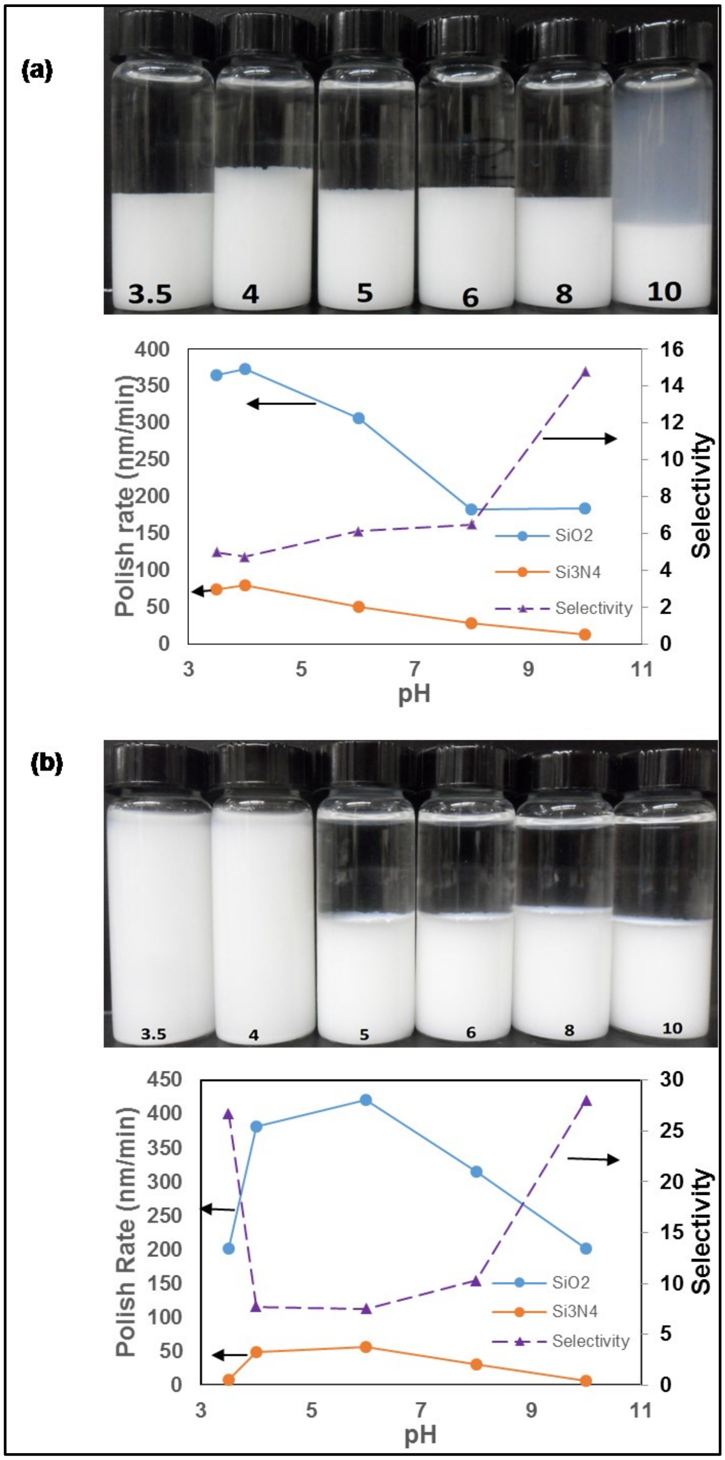

Figure 5-12 Silicon dioxide and nitride removal rates vs pH using MAS of cera-to-silica at (a) 0.1 wt ratio and (b) 0.2 wt ratio. Settling test of corresponding pHs are shown above at 24 hours.

5.5 Polish Rate as a Synergistic Effect of the Interactions of Mixed Abrasive Particles.

The interaction of colloidal ceria and silica abrasive particles in CMP is synergistic in nature. Colloidal silica particles, namely EB6080 when used alone at 5 wt % and pH 4 did not polish oxide appreciably, generating an oxide polish rate of just 9.71 nm/min and nitride polish rate of 12.39 nm/min, while silicon oxide and nitride polish rates using ceria alone at 1 wt% and pH 4 were 169.05 nm/min and 5.3 nm/min respectively. Combining ceria and silica lead to oxide polish rates that are much higher than the sum of the polishing rates of the particles in isolation. When ceria and silica were added to each other at weight ratio of 0.2 (1 wt% ceria and 5 wt% silica) oxide polish rates were as high as 381 nm/min at pH 4. Nitride polish rate also increased using MAS at pH 4. Higher oxide and nitride polish rates are likely due to the synergistic combination of the "chemical tooth effect" of the ceria particles and mechanical force of larger silica particles. The low polish rates using silica alone at pH 4 is due to the fact that at low pH, silica is not chemically active and as reported by Cook, silica has little polishing ability except when used at very high pHs ≥11[6]. Also, at low pH values, dissociation of the silanol groups on the silica film surface does not occur, this approaches 100 % only in very alkaline solutions. Another reason for low oxide polish rates, is that at pH 4, both silica particle and silica surface have a net negative surface charge exhibiting repulsive behavior.

Using ceria alone to polish oxide surfaces did not produce very high polishing rates. This is mainly due to the small size of the ceria particles used in this study which was measured to be about 5 nm in diameter. Due to their small sizes, they are mostly confined to open pores in the pad resulting in a small contact area between particle and wafer surface. The larger silica particles acts as a carrier for the smaller ceria particles bringing them closer to the wafer surface hence increasing the contact of the abrasives with the surface being polished.

Lee et al[19] performed polishing on SiO_2 films using silica core coated with ceria nanoparticles and reported that while polish rate was significantly increased compared to using pure ceria alone, polish rate was independent on the concentration and pH of the coated particles. It is suggested that both the effect of the increased surface area of the abrasives and indentation mechanism were in play. In our study, both abrasive concentration and pH had an effect on the polishing process. The ceria particles in this work were not permanently bonded to the silica core, however, based on our experimental data, it is believed that the attachment of the smaller ceria particles to the larger silica core resulted in a higher indentation of the particles into the SiO_2 film surface and higher contact area per overall composite particle.

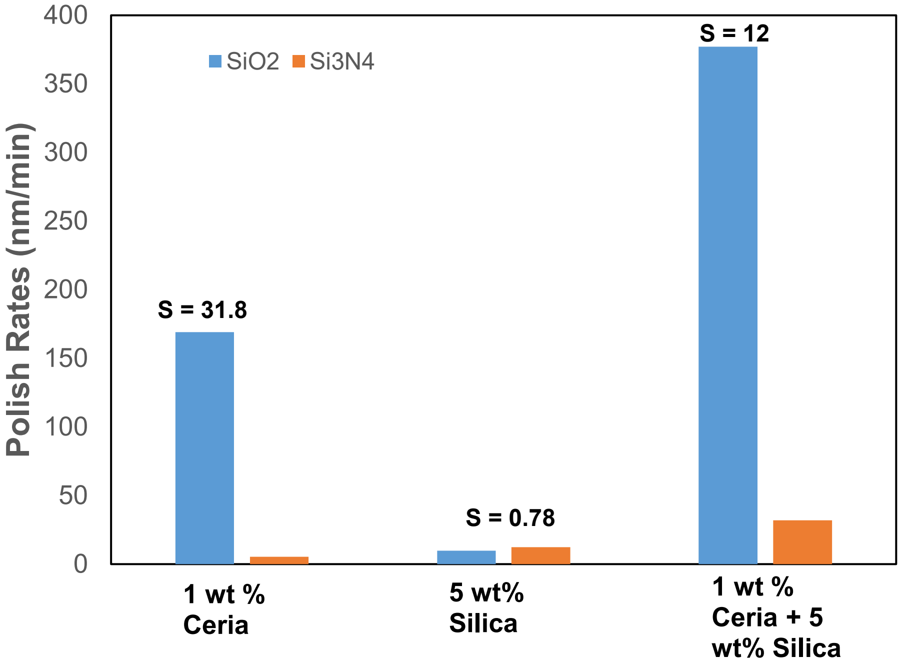

Figure 5-13 Polish rates of silicon dioxide and nitride films using single and mixed abrasives of ceria and silica at pH 4. (S is the selectivity)

5.6 MAS Selectivity

In our study, we were able to produce high oxide polish rates of up to 420 nm/min when using 0.2 weight ratio MAS of ceria to silica at pH 6, however, these mixed abrasive slurries also produced higher than expected silicon nitride polish rates of up to 93 nm/min when using 0.15 weight ratio MAS at pH 4. Based on Figure 5-10, the highest selectivity of about 16 was achieved using MAS ceria to silica at 0.3 weight ratio. Based on Figure 5-12, we know that increasing the pH of the slurries significantly decreased nitride polish rates, however, oxide polish rates were also decreased. The highest selectivity reported for this study was 28 using 0.2 weight ratio MAS ceria/silica at pH 10.

5.7 Inductively Coupled Plasma Mass Spectrometry (ICP-MS) Measurements

ICP-MS measurements were performed using four samples at ceria to silica weight ratios of 0.04, 0.05, 0.07 and 0.1 at pH 4. The clear liquid was analyzed after settling occurred. Silica was not detected in all four samples and it can be assumed that all the silica particles were attached to ceria particles and settled due to gravitational forces on the larger composite particles. The silica particles used are much larger in size (125 nm) compared to the ceria particles (5 nm). Silica on its' own shows great stability, at pH=4 silica slurries are very stable. However, upon addition of CeO_2, settling occurs at weight ratios < 0.2. We can conclude that ceria particles affect the stability of silica particles.

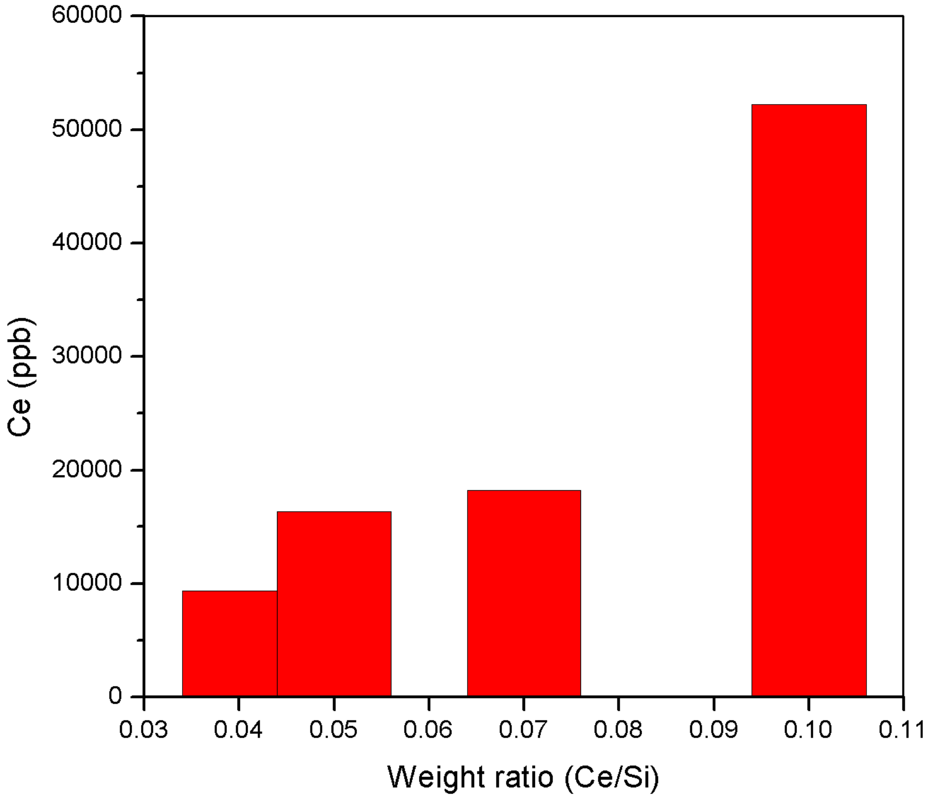

Figure 5-14 Amount of Ce present (ppb) in clear liquid after settling vs weight ratio of the MAS (ceria and silica)

The results plotted in Figure 5-14 show that as the concentration of ceria increased, the concentration of ceria detected in the clear liquid after sedimentation also increased. In regards, to the concentration of cerium found in the clear liquid compared to the original concentration of ceria that was used in the preparation of each sample, only a minute concentration of Ce was found in these clear liquid samples with the highest amount of 1.04% of the original concentration when ceria was added at 0.5 wt% (0.1 weight ratio MAS). This corresponds to positive zeta potential measurements of the composite particles. This result corroborates our theory that once the IEP of the composite particles is passed, all silica particles are fully covered with ceria particles and the composite particles are now behaving as positive ceria particles. There is also an excess of ceria particles present in the suspension. Large repulsive electrostatic interactions exist between these nanoparticles which keep them suspended in the liquid. Other possible reasons for the extra ceria includes:

- Agglomeration of silica nanoparticles may occur which means less surface area for adsorption of ceria particles.
- Ceria particles are expected to attach to silica particles immediately upon mixing of both solutions at pH 4, however a case of maximum coverage of some silica particles may exist at a faster pace than some, changing the overall surface charge of the composite particle to positive while other particles partially covered remain with a negative surface charge. These particles will bind together and settle.

All the other weight ratios (0.04, 0.05 and 0.07) were found to be less than 1% of the original concentration.

5.8 Conclusions

Zeta potential measurements clearly showed the surface charge present on the composite particle changing from that of pure silica to that of pure ceria as ceria concentration increases. Mixed abrasive slurries with weight ratios close to or at the IEP of the composite particles proved to be unstable and settled quickly (or within 24 hours). These slurries produced high oxide and nitride polish rates which is not advantageous for selectivity. Increasing the ceria concentration beyond the IEP cause slurries to regain stability. Silicon dioxide polish rates remained high up to a maximum weight ratio of 0.2, beyond which it started to decrease. At higher MAS weight ratios (≥ 0.2) where slurries got more stable, nitride polish rates decreased significantly. pH of mixed abrasive slurries also has an effect on the polish rates. Increasing slurry pH causes the nitride polish rates to decrease significantly which increased selectivity, however, oxide polish rates were also decreased. Our experimental data clearly showed that using mixed abrasives of colloidal ceria and silica abrasive particles significantly increased oxide removal rates compared to using pure ceria or silica alone. We propose the use of MAS consisting of colloidal ceria and silica between weight ratio of 0.2-0.3 for STI CMP as these slurries produced high oxide polish rates and low nitride removal. The process can be further optimized by using additives to lower nitride removal rates. Finally, our proposed MAS can cut cost in regards to slurry consumption and production as both ceria and silica were used in low concentrations resulting in low weight ratios and production of the composite particles was as simple as mixing the two particles together formed through electrostatic interactions. In addition, optimizing selectivity for STI CMP can be achieved by controlling the surface charge of the particles.

Chapter 6 : Maximizing Selectivity in STI CMP

In this chapter, the results obtained in Chapter 5 will be optimized to produce higher selectivity for STI CMP. This chapter will focus on increasing selectivity of the MASs for STI CMP through the use of additives, varying slurry pH and the size of the core particle. The main objective is to suppress the nitride polish rate. As mentioned earlier, there are three ways to improve selectivity: (i) increase oxide removal rate while decreasing nitride removal rate (ii) increase oxide removal rate and maintain the nitride removal rate at a minimum and (iii) maintain oxide removal rate and decrease the nitride removal rate to <1 nm/min. Our approach is to utilize step (iii). Our first model for selectivity utilized electrostatic interactions where particle-particle interactions, which deal with the stability of the slurries, and particle-film interactions, which include the adhesion of abrasive particles to the film surface, were studied. A comprehensive study of these interactions was done and used to produce optimum conditions for chemical mechanical planarization. Using mixed abrasive slurries between pH 4-6, we were able to achieve high SiO_2 removal rates of up to 420 nm/min, however, these slurries also produced higher than expected silicon nitride removal rates. Therefore, it was necessary to employ additives that are expected to passivate the silicon nitride layer inhibiting its polish rate without significantly changing the oxide polish rate.

The literature has a plethora of information and patents about additives that are used in the polishing process to inhibit nitride polishing hence increasing selectivity for STI CMP that were discussed earlier in the literature review, Chapter 2. It is proposed that the adsorption of the additives on the film surface plays a key role in modifying the polish rate.

The proposed hypothesis of the silicon nitride removal is said to occur in a two-step mechanism[85]. In the first step, the silicon nitride surface is hydrolyzed when in contact with water, subsequently forming silicon dioxide which is removed by polishing in the second step[85]. It is suggested that the additive selectively adsorbs onto the silicon nitride surface but not on the silicon dioxide surface and inhibits the hydrolysis of the nitride to silicon dioxide in the first step which is not easily removed by the abrasive and hence suppresses the nitride removal rate, while the oxide surface remains unaffected by the additive leading to high oxide-to-nitride polish rate selectivity[11–15,18,51].

America and Babu[12] presented the effect of proline and other amino acids with ceria abrasives on STI CMP and proposed that proline suppresses the nitride polish rate to very low values ~ 1 nm/min by adsorbing on the nitride surface and stopping the hydrolysis of the silicon nitride to silicon dioxide, thereby suppressing the nitride polishing. It was reported that while carboxylic acid groups are necessary to suppress hydrolysis, the additive must contain an amino group in the alpha position and hydrogen bonding was responsible for the adsorption of proline on the silicon nitride film. On the other hand, Prasad and Ramanathan[108] studied the role of adsorption of L-proline and L-arginine on silicon dioxide and silicon nitride surfaces and proposed that both amino acids adsorbed on both silicon dioxide and silicon nitride surfaces to similar extent, however, while proline only suppresses the nitride polish rate, arginine on the other hand suppresses both the oxide and nitride polish rate. Therefore, it was suggested that adsorption alone may not be responsible for oxide to nitride selectivity but modification of the chemical mechanism of removal may also play a key role in achieving high oxide-to-nitride removal.

The adsorption of several amino acids in ceria dispersions on oxide and nitride surfaces was reported by Penta et al.[18]. Polishing results suggested that additives containing protonated amino groups, when available in sufficient amounts, can suppress the nitride polish rate. Again, hydrogen bonding is stated to be responsible for the adsorption of the amino acids on the oxide and nitride surfaces. It is said that protonated amines form strong hydrogen bonds with the nitride surface while the corresponding bond on oxide surface is weak. The stronger hydrogen bond inhibits nitride hydrolysis and effectively suppresses the nitride removal rate.

Another approach is the use of anionic surfactants that will attach to the silicon nitride surfaces but not to the silicon dioxide surface. Silica has a negative zeta- potential over a wide pH range with a point of zero charge at nearly pH 2 while isoelectric point of silicon nitride is around pH 7. However, ceria also has an isoelectric point at around pH 9. Selective adsorption of the additive can occur if there is adequate difference in the surface charge of the film surfaces being polished. At a pH range of 3-7, the nitride surface will be positively charged while the oxide surface has a negative charge. Hence, it is expected that an anionic surfactant would be attracted to the nitride surface but not the oxide surface. Bu and Moudgil[15] reported a ten-fold increase in oxide to nitride selectivity by the addition of an anionic surfactant, sodium dodecyl sulfate (SDS), to a colloidal silica dispersion at pH 2 over conventional colloidal slurry. SDS adsorption was said to be significantly higher on silicon nitride surfaces than silica due to electrostatic interactions and it was concluded that the preferential adsorption of SDS on the nitride surface resulted in the formation of a passivation layer leading to oxide-to-nitride selectivity.

Based on these observations, amino acids containing carboxylic groups namely, L-proline, glycine and nicotinic acid along with an anionic surfactant, SDS, were chosen as additives with the goal of suppressing the nitride removal. These additives have been reported to adsorb onto the silicon nitride surface, inhibiting the hydrolysis reaction. Most of the literature reports of the use of additives enhancing selectivity were based on using either ceria or silica abrasives on its own but not as mixed abrasives.

6.1 CMP Using L-Proline as an Additive to the MAS

The variation of material removal during CMP of silicon dioxide and silicon nitride, and the resulting selectivity with and without L-proline addition, as a function of MAS (Ce/Si) weight ratio is shown in Figure 6-1. The data obtained for polishing rates of both oxide and nitride using MAS without any additive was reported and discussed earlier in the previous chapter and is repeated here for comparison with the presence of additive L-proline to the MAS. The data shown is for polishing conditions described in the Experimental section. The SiO_2 concentration was kept at 5 wt % while the ceria concentration was varied and 0.5 wt % of L-proline was added. The pH of all the slurries used was kept constant at pH 4 ± 0.6. The error bars indicate standard deviation in the experimentally measured polish rates. It is observed in Figure 6-1 that the error bars overlap for the measured CMP removal rates for silicon dioxide with and without the addition of L-proline. Our results suggest that the addition of 0.5 wt % of the amino acid L-proline has little to no effect on SiO_2 removal since the oxide polish rate is unchanged over the entire weight ratio range. In contrast, the nitride polish rates were suppressed at MAS weight ratios greater than 0.07, which corresponds to positively charge composite particles. Between weight ratios 0.07-0.1 selectivity increased slightly, at both 0.15 and 0.2 weight ratios selectivity was increased by >3 times and at a weight ratio of 0.3 the selectivity was increased 2 fold with a nitride removal rate ~8 nm/min. However, at weight ratios < 0.07, selectivity was either the same or lower when compared to MAS without L-proline.

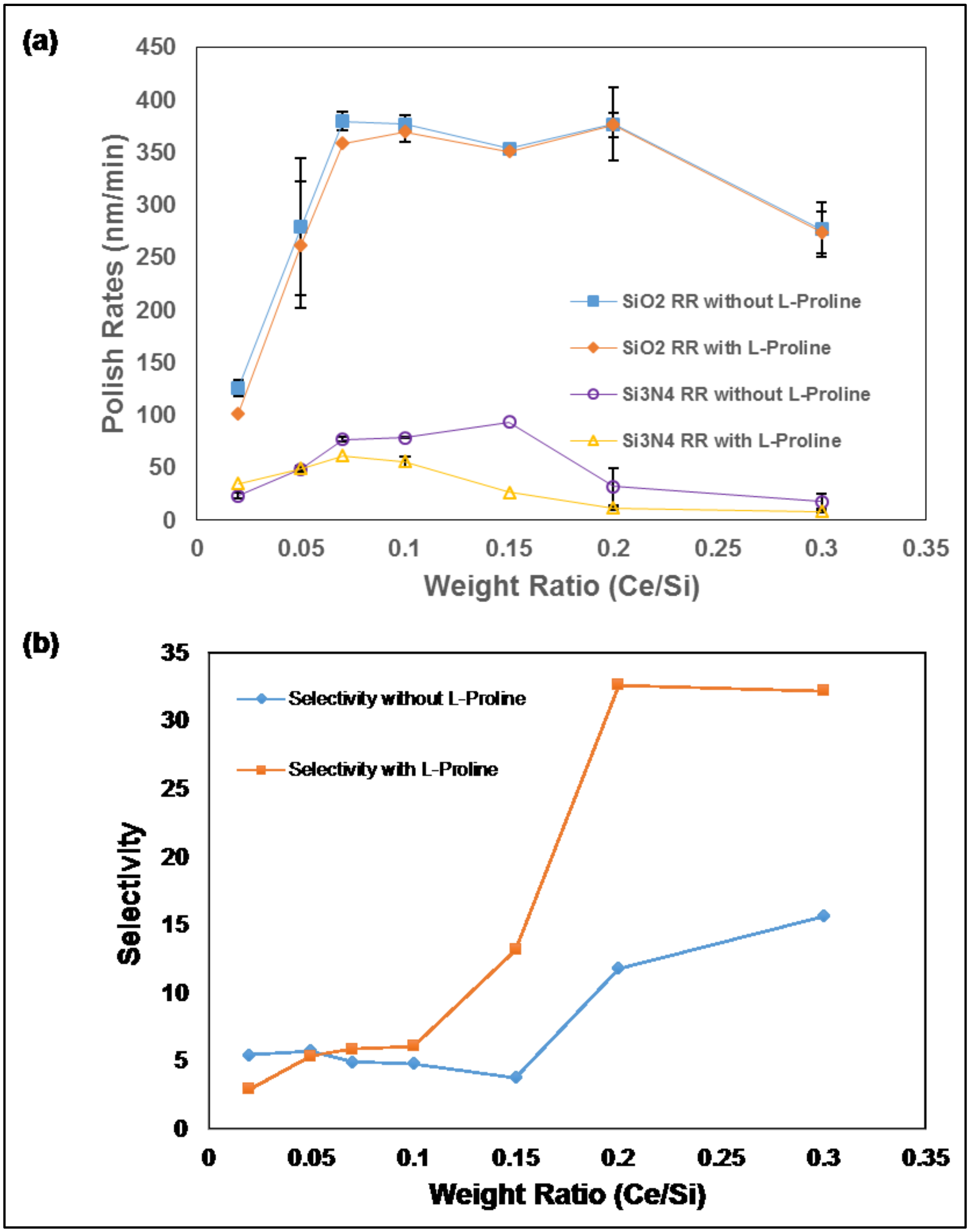

Figure 6-1 (a) Variation of material removal rate for both silicon dioxide and silicon nitride as a function of slurry weight ratio with and without 0.5 wt% L-proline. (b) Accompanying selectivity of the slurry with and without L-proline.

As discussed in our previous work, slurries below 0.07 weight ratio have low ceria concentrations and zeta potentials close to that of silica. It is interesting to note that when the MAS slurry surface charge resembles that of pure silica (low ceria concentrations), suppression of the nitride film does not occur in the presence of L- proline but as the ceria concentration increases and the MAS surface charge resembles that of a pure ceria slurry, the addition of L-proline inhibits the nitride polish rate. Manivannan[11] et al reported similar results using glutamic acid as an additive in ceria and silica based single abrasive slurries. It was observed that the addition of glutamic acid suppressed the nitride polish rates only for ceria slurries and not for silica slurries. He further proposed that the adsorption of amino acid onto the nitride surface is not the key mechanism of polish rate inhibition but that ceria abrasives may possess different types of active sites, one type that bonds with silicon dioxide and another type that bonds with silicon nitride. Addition of the additives to the abrasives would modify these active sites on the ceria abrasive resulting in changes in selectivity. According to adsorption studies, it was suggested that the proposed hypothesis of the adsorption of amino acids on the silicon nitride wafer surface alone does not account for the overall change in the oxide-to-nitride polish rate selectivity[108]. Hence, in another study by Manivannan et al, they proposed that the adsorption of the additive onto the active sites of the abrasive particle hinders the chemical interaction between the abrasive particle and the surface being polished[14].

The explanation of Manivannan et al[14] appears to explain the MAS polish data seen here. If L-proline adsorbs onto the silicon nitride surface and suppresses the polish rate, then it should apply also to when the film surface is being polished with MAS at weight ratios below 0.07. If adsorption of the additive alone explains the change in oxide-to nitride polish rate selectivity then it should inhibit nitride polish rate over the entire weight ratio studied of the MAS at a constant pH. The surface charge of the composite particles also seem to affect the selectivity when the amino acid is added (Figure 5-1 in Chapter 5, we know that below a weight ratio of 0.07 ceria to silica, the composite particles possess a negative surface charge and above this value possess a positive surface charge). A possible explanation for the decrease in nitride polish rates with addition of L-proline in slurries with weight ratios > 0.07 may be due to the additive interacting with the positively charged composite particle blocking active sites that interact with the nitride surfaces. Based on Figure 6-1(a), while there was not a significant difference in oxide polish rates, it is obvious that there is a lower oxide polish rate using L-proline with the composite particles at weight ratios between 0.02-0.07 compared to ceria/silica weight ratio between 0.1-0.3 which appeared to be essentially the same as that of the graph without addition of the amino acid.

The highest selectivity obtained using L-proline was ~33 when L-proline was used as an additive to MAS weight ratio 0.2 ceria to silica at pH 4, an increase of three fold when compared to the MAS without L-proline. With the addition of L-proline to the 0.2 weight ratio ceria/silica MAS, we were able to suppress the nitride polish rate to ~11 nm/min from 32 nm/min at pH 4. However, the nitride polish rate with the addition of L-proline went as low as 8 nm/min at 0.3 weight ratio ceria/silica from 18 nm/min without L-proline resulting in a two-fold increase in selectivity from approximately 15 to 32 with the addition of L-proline. For the data obtained in Figure 6-1, the addition of L-proline to the MAS occurred after both ceria and silica were mixed together and pH adjusted. A different approach of the addition of L-proline to the MAS was tried to optimize selectivity, this time around, L-proline was added to the ceria slurry first before mixing it with the silica slurry and pH adjusted to 4. Table 6-1 summarizes the results of the oxide and nitride polish rates at different MAS weight ratios without L-proline, with the addition of L-proline to the MAS and with the addition of L-proline to the ceria slurry before mixing with the silica abrasives.

Table 6-1 . A comparison of oxide and nitride surfaces RR using MAS at different weight ratios at pH 4 with and without the addition of L-proline

MAS Weight Ratio (Ceria/silica)	Without L-proline		With 0.5 wt% L-proline added to MAS		With 0.5 wt% L-proline added to the ceria slurry first before mixing with silica.	
	Oxide RR (nm/min)	Nitride RR (nm/min)	Oxide RR (nm/min)	Nitride RR (nm/min)	Oxide RR (nm/min)	Nitride RR (nm/min)
0.02	125.97	23.13	101.75	34.84	63.55	26.53
0.1	377.17	78.46	370.00	55.68	304.53	69.67
0.2	377.06	31.92	376.34	11.50	401.57	47.50
0.3	276.73	17.70	274.97	8.51	258.41	14.59

When L-proline was added to the ceria slurry first before mixing it with silica to form MAS and used to polish both silicon dioxide and silicon nitride wafers, interestingly, silicon dioxide polish rates for all the weight ratios studied were much lower than that of the case where proline was absent in the MAS, with the exception of 0.2 weight ratio MAS which increased slightly. The decrease in silicon dioxide removal rate is probably due to the presence of proline changing the ceria-silica particle interaction when it was added to the ceria slurry first, then mixed with the silica abrasives. The nitride polish rates were similar to polish rates without the addition of the amino acid. This result suggests that the additive does interact with the abrasive particles and modify them as postulated above.

Penta et al[18] reported that protonation of the amino group is important and the additive (L-proline) has to be available in sufficient amounts to suppress the nitride removal rate. They proposed that L-proline is protonated between pH 4-10 and proline concentration as high as 2 wt % is required to sufficiently suppress the nitride removal rate. Polishing experiments were carried out at 0.2 slurry weight ratio using 2 wt% L-proline at both pH 4 and 5. The results are shown in Figure 6-2. Silicon dioxide removal rates were not performed since, at this MAS weight ratio, L-proline has little to no effect on the oxide polish rate. Silicon nitride removal rates with the addition of 2 wt% L-proline at both pH 4 and 5 were approximately the same at approximately 21 nm/min. However, using L-proline at a lower weight concentration of 0.05 wt% proved to be more effective in suppressing the silicon nitride removal rate. It should be noted also that a significant increase in silicon nitride removal rate occurred polishing with MAS without L-proline at pH 5 compared to pH 4. Figure 5-9 showed that slurries of this MAS weight ratio at pH 4 were very stable over a long period of time, however, unstable slurries were formed at pH 5. The higher nitride removal rates may be due to larger agglomerated particles at or near the IEP coming into contact with the work surface at pH 5.

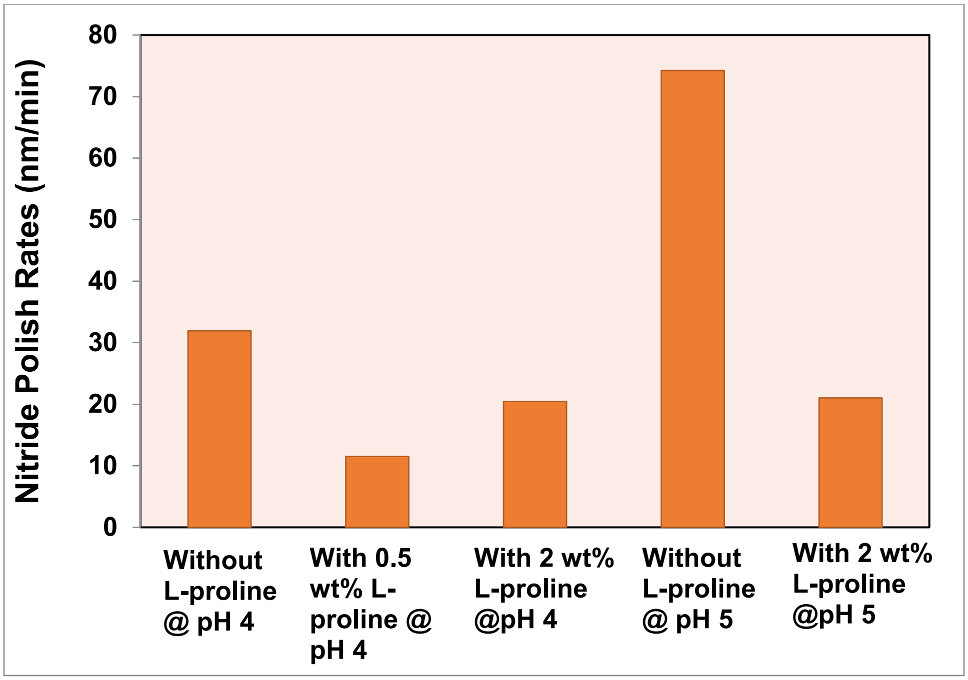

Figure 6-2 A comparison of silicon nitride polish rates using 0.2 weight ratio (Ce/Si) MAS at pH 4 and 5 with and without the addition of L-proline.

L-proline has a positive surface charge in the alkaline pH range of 9-11[108]. In this pH range, both oxide and nitride surfaces will be negatively charged; therefore, based on columbic interactions, L-proline is expected to be attracted to both surfaces. It is suggested that even though the amino acid is adsorbed onto the silicon dioxide surface, the interaction is weak and will not affect the oxide polish rate, however, a stronger hydrogen bond is said to exist between L-proline and the nitride surface that hinders it from being polished[108]. Using 0.3 weight ratio ceria/silica MAS, polishing experiments were performed at pH 9 and 9.6 first without L-proline and repeated with the addition of L-proline. The stability of these slurries was also observed. The results are reported in Figure 6-3.

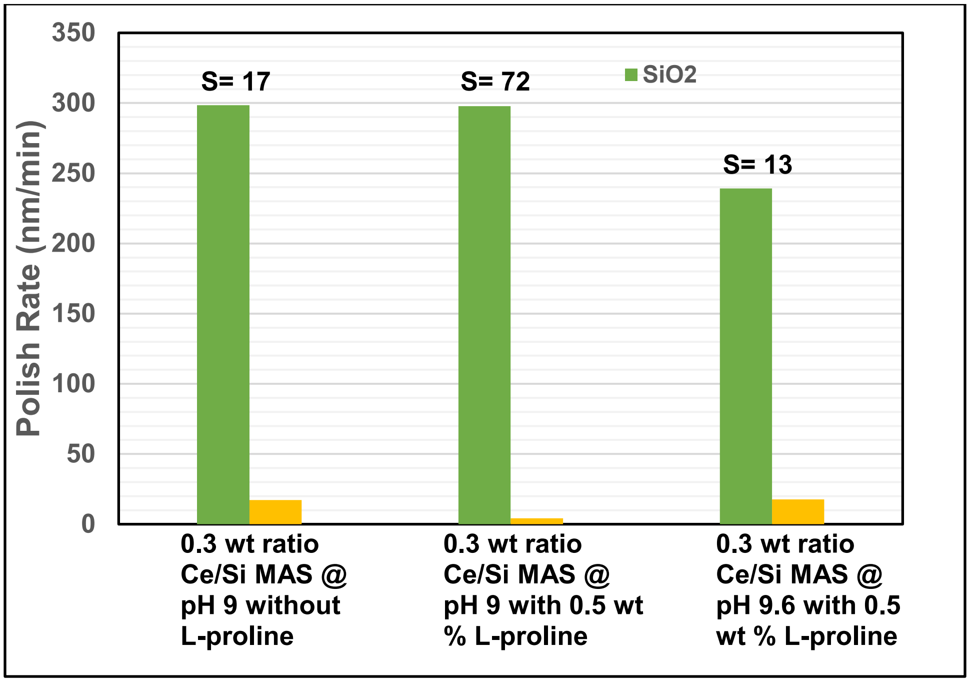

Figure 6-3 Polish rates of silicon dioxide and silicon nitride films using 0.3 weight ratio (Ce/Si) MAS at pH 9 and 9.6 with and without the addition of L-proline (S signifies selectivity).

Figure 6-4 Settling tests of 0.3 weight ratio (Ce/Si) MAS at pH 9 and 9.6 with the addition of L-proline after 10 minutes (approximate time at which the slurries were used for polishing after preparation).

Silicon dioxide polish rates remained essentially the same when L-proline was added at pH 9, however, the silicon nitride removal rate was suppressed from 17.24 nm/min to ~4 nm/min resulting in a selectivity of approximately 72. As the pH increases further, the silicon nitride removal rate increases by nearly 4 times at pH 9.6 with selectivity dropping to approximately 14. A steady decrease in oxide polish rates was also observed with the increase in pH. Zeta-potential measurements were performed, using 0.3 ceria-to-silica weight ratio MAS, with varying pH to understand this polish rate data. The zeta-potential results are shown in Figure 6-5.

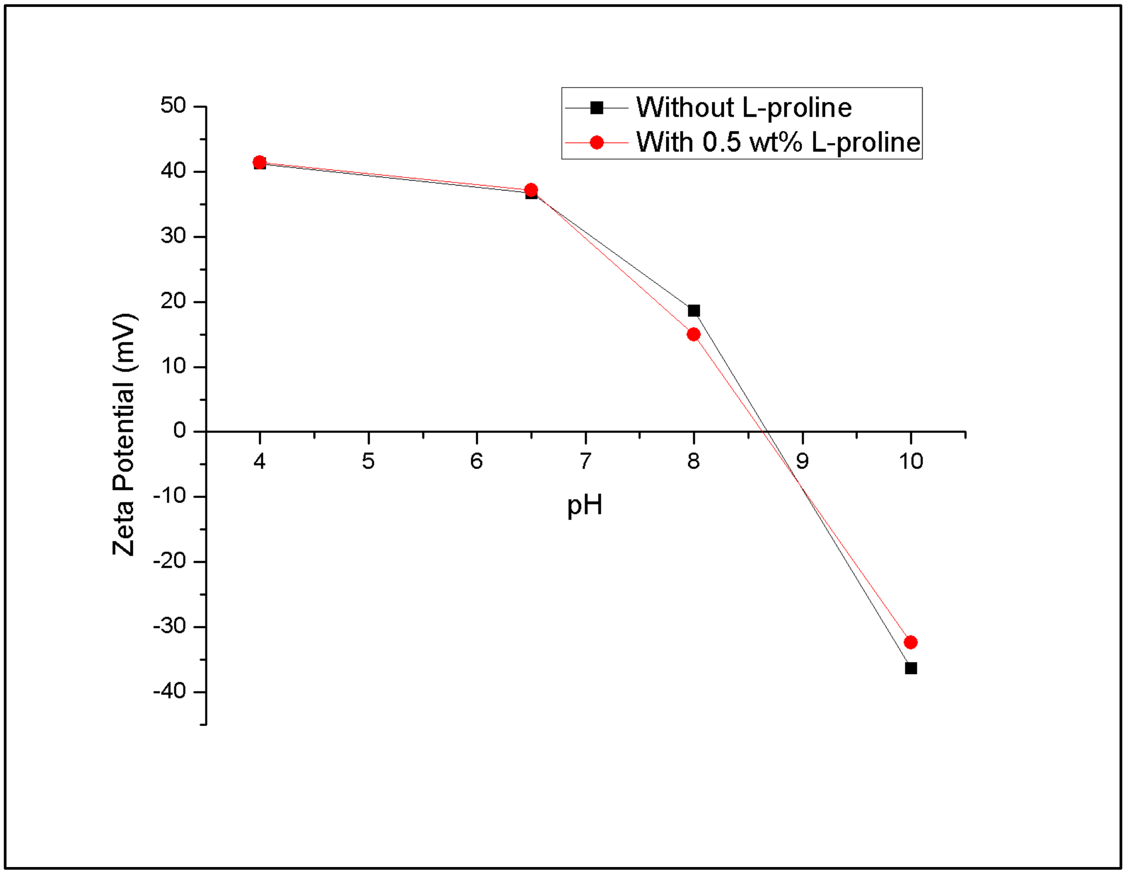

Figure 6-5 Zeta- potential vs pH using 0.3 ceria-to-silica weight ratio MAS with and without the addition of L-proline.

When the pH of the MAS is increased from pH 4 to 9, the slurry stability changes from being stable at pH 4 to unstable at pH ≥9, and settling was observed almost immediately upon mixing at pH 9 (see Figure 6-4) which signifies a change in the surface charge of the composite particles from positively charged at pH 4 (> +40 mV) to a slightly negative charge at pH 9 (~ -8 mV). The isoelectric point of the 0.3 weight ratio composite particle occurs at pH 8.7. Since pH 9 is relatively close to the isoelectric point of the particle, rapid settling was observed because the repulsion between the particles was not large enough to prevent agglomeration and nitride polish rate using L-proline was at its' lowest. As pH increases further, there is a steep decrease in zeta-potential reaching almost -40 mV at pH 10 and the silicon nitride removal rate increases by over 4 times at pH 9.6. America et al[12] observed minimum silicon nitride removal using L-proline at pH 9.7 which corresponded with the isoelectric point of "oxide-free" silicon nitride surface. They explained this behavior through the surface charge present on the nitride surface when free of an oxide layer and presumed optimal interaction of proline with the nitride surface when it's at zero net charge. However, it is clear from the results above (Figure 6-5) that while the addition of L-proline does not alter the surface charge of the composite particles, there is some interaction with the abrasive particles that presumably blocks "nitride-affinity" [11] active sites on the ceria abrasive, which prevents the ceria-silicon nitride interaction and this presumably occurs when the L-proline has a positive charge and the abrasive particle is at or near the point of zero net charge.

The decrease of silicon nitride polishing rate using L-proline in our study could be attributed to both the adsorption of L-proline onto the nitride surface coupled with the modification of active sites on the abrasive by L-proline. Another explanation for the suppression of the nitride polish rate occurring at higher weight ratios may be due to the additive attaching to the extra ceria particles that exists within the suspension and limits the amount of ceria that reaches the wafer surface.

6.2 Other Additives.

Several other additives, namely Nicotinic acid (NA), a cyclic and non-α amino acid, glycine and SDS, an anionic surfactant, were evaluated as potential suppressants of the nitride removal rate and the results are tabulated in Table 6-2.

Table 6-2 . Silicon dioxide and silicon nitride removal rates with their corresponding selectivity using additives with MASs.

Slurry Composition	pH	Silicon Oxide RR (nm/min)	Silicon Nitride RR (nm/min)	Selectivity	Selectivity without additives
0.3 weight ratio Ceria/Silica with 0.1 wt % nicotinic acid	4	253.26	13.80	19	**16**
0.1 weight ratio Ceria/Silica with 1 wt % nicotinic acid	4	320.73	79.84	4	**5**
0.2 weight ratio Ceria/Silica with 1 wt % nicotinic acid	4	293.84	36.62	8	**12**
0.3 weight ratio Ceria/Silica with 1 wt % nicotinic acid	4	295.90	18.20	16	**16**
0.2 weight ratio Ceria/Silica with 0.5 wt % glycine	4	361.20	31.37	12	**12**
0.07 weight ratio Ceria/Silica with 10mmol SDS	4	277.89	69.56	4	**5**

When 1 wt% of NA was used as an additive to the MAS, the silicon dioxide removal rates were decreased at all MAS weight ratios studied with the exception of 0.3 ceria-to-silica weight ratio while the nitride removal rates were unaffected when compared to MRR without the use of nicotinic acid. As the highest selectivity using 1 wt% nicotinic acid was observed at 0.3 ceria-to-silica weight ratio, polishing was carried out using a lower amino acid concentration of 0.1 wt % added to the MAS at 0.3 weight ratio and both silicon dioxide and silicon nitride results were slightly decreased. This result contrasts that of Penta et al[18] that showed suppression of the nitride removal rates down to 1 nm/min while the oxide removal rates remained unaffected. They further postulated that the amine need not be attached to the alpha carbon to suppress the nitride removal rate as previously suggested such as in the case of proline. However, in our study, while L-proline did suppress the nitride polish rates at certain weight ratios, nicotinic acid did not hinder the MRR of silicon nitride. Therefore, it can be postulated that the additive should contain an amino group in the alpha position (eg. L-proline) to suppress the nitride removal rates while not affecting the silicon dioxide removal rates when using MAS. Also, a lower additive concentration in the case of nicotinic acid proved to be more effective in suppressing the nitride polish rate.

A similar result was obtained in the presence of 0.5 wt % glycine when added to 0.2 weight ratio MAS at pH 4, the nitride removal rate remained unaffected, while there was a slight decrease in oxide MRR. It is proposed that glycine in the form of zwitterions adsorbs onto the silica surface and the formation of a monolayer through hydrogen bonding is said to be responsible for the suppression of material removal rate[18, 109]. It is clear from our result that glycine does interact with the silica work surface and possibly forms a passivation layer which slightly lowered the silicon dioxide removal rate, however, at 0.5 wt %, it had no effect on the nitride removal rate. It is suggested that if present in higher concentrations surface-induced precipitation ensues which hinders the suppression of silicon nitride[18,109]

With the addition of SDS to the MAS, material removal of both silicon dioxide and silicon nitride was lower for the weight ratio investigated. Ceria-to-silica weight ratio of 0.07 was chosen to perform polishing due to the fact that this weight ratio was close to the IEP of the composite particle and was expected to have little to no interaction with the negatively charged polar head of the surfactant. SDS was chosen as a surfactant to selectively adsorb on the positively charged nitride surface at pH 4 forming a passivation layer preventing it from being polished, and it was expected to be repelled from similar charge silicon dioxide surface. Instead, it significantly lowered the MRR of silicon dioxide and slightly lowered the nitride MRR. Bu and Moudgil[15] showed that there is a preferential higher adsorption of SDS on silicon nitride surface as compared to silica. Preferential adsorption of SDS on silicon nitride was postulated to be as a result of the high electrostatic attraction between the work surface and the anionic surfactant, which resulted in differential lubrication and hence lower MRR of the silicon nitride compared to silicon dioxide. However, in earlier work investigating the use of cleaning agents to remove ceria from silica surfaces, SDS was used as a cleaning agent due to the fact that it can be found as a surfactant in many detergent products and it was found to be very effective for cleaning silica surfaces. The silica sample was dipped into ceria slurry at a pH where coulombic attraction occurred for one minute, rinsed with SDS and dried in air. XPS data showed < 1 % atomic concentration of ceria on the silica surface when it was rinsed with SDS. Figure 6-6 shows SEM of the silica surface dipped into ceria slurry at pH 6 then rinsed with 10mmol SDS solution and dried. While it is clear that there are few ceria particles remaining on the surface, SDS seemed to have also adsorbed onto the silica surface. It is believed that the lubrication effect of SDS between the work surface and the abrasive particle decreased the frictional force during polishing and hence lowered the oxide MRR significantly and slightly lowered the nitride MRR.

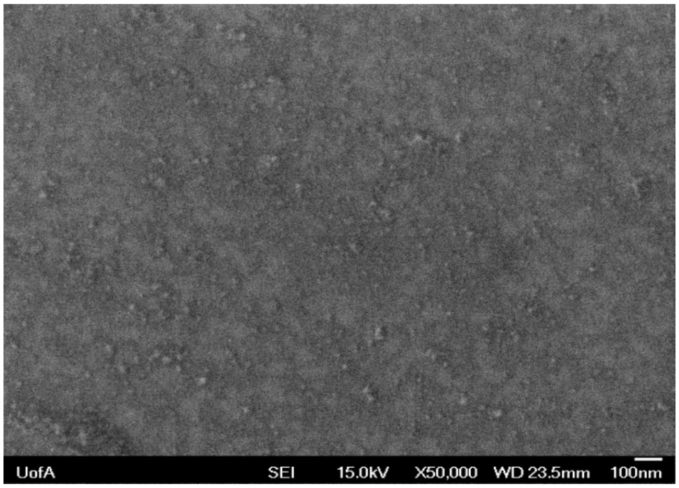

Figure 6-6 SEM of silica surface dipped into ceria slurry at pH 6 and rinsed with 10mmol SDS solution.

In summary, L-proline was the only additive that proved to be effective in suppressing the nitride removal rate when using mixed abrasive particles. The influence of both the weight ratio of the composite particles and pH play a critical role for the suppression of the nitride removal rate. Higher ceria to silica weight ratios ≥ 0.2 are required and a pH of 9 is preferable where the composite particle is near the isoelectric point. The additive was found to be more effective at lower concentrations. The sequence in which the additive is added to the mixed abrasive slurry is also important as the additive seems to interfere with the ceria-silica interactions. It is believed that suppression of the nitride removal occurs through a combination of adsorption of the additive onto the work surface and chemical modification of the abrasive particle.

6.3 CMP Using MAS of Colloidal Ceria and Silica Namely Bindzil EB6040

The primary aim of this work as stated within the Introduction is to develop a novel slurry for STI polish using mixed abrasive slurries. However, mixing ceria abrasives of diameter approximately 5 nm with colloidal silica, namely Bindzil EB6080, of diameter approximately 125 nm, produced not only high silicon dioxide MRR but also higher than expected nitride MRR. While MRR is explained by the chemical interaction between the reactive ceria abrasives and surface to be polished, the silica is used only as a carrier for the smaller ceria particles and is believed not to take part in the actual polish itself. Polishing by silica particles is said to be more mechanical. The larger core silica particles provide a means by which more ceria particle can come in contact with the surface to be polished hence increasing the contact area between abrasive and wafer. However, to better understand the removal mechanism using MAS, smaller silica particles namely Bindzil EB6040, of diameter approximately 81 nm, were utilized in mixed abrasive slurries with ceria of diameter approximately 5 nm.

Figure 6-7 shows the MRR of silicon dioxide and silicon nitride along with the resulting selectivity using MAS of ceria and silica, EB 6040, as a function of ceria-to-silica weight ratio. The data shown is obtained using the polishing conditions described in Experimental section and polishing parameters listed in Table 3-1. The SiO_2 concentration was kept at 5 wt % (the same using EB 6080) while ceria concentration was varied. The pH of all the slurries used was kept constant at pH 4±0.6. The error bars indicate standard deviation in the experimentally measured polish rates.

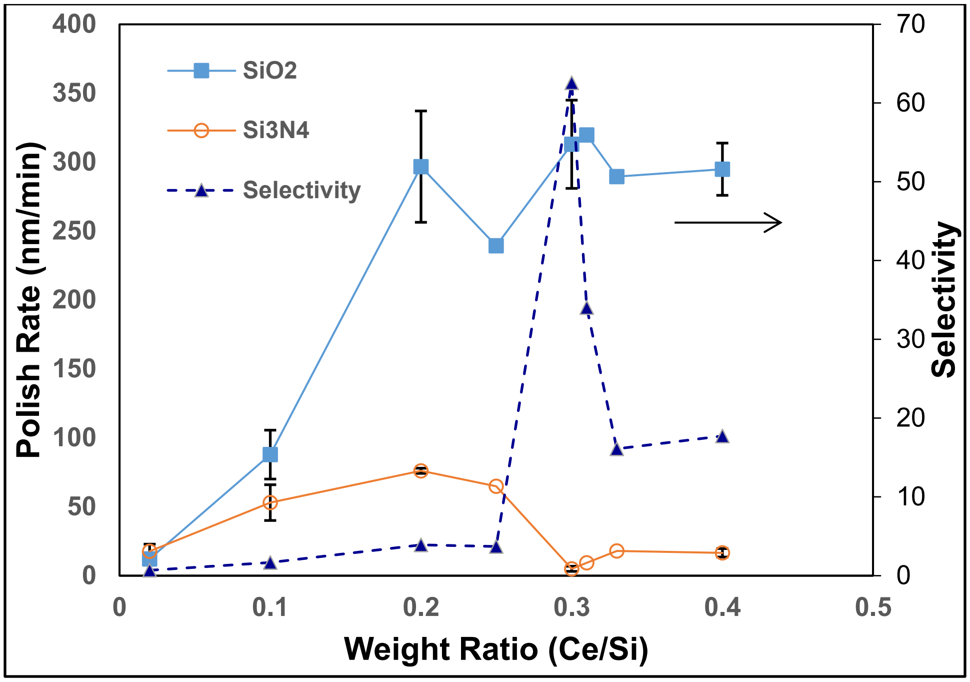

Figure 6-7 Removal rate of silicon dioxide and silicon nitride films as a function of MAS weight ratio using 5 wt% silica EB 6040 (81 nm) at pH 4.

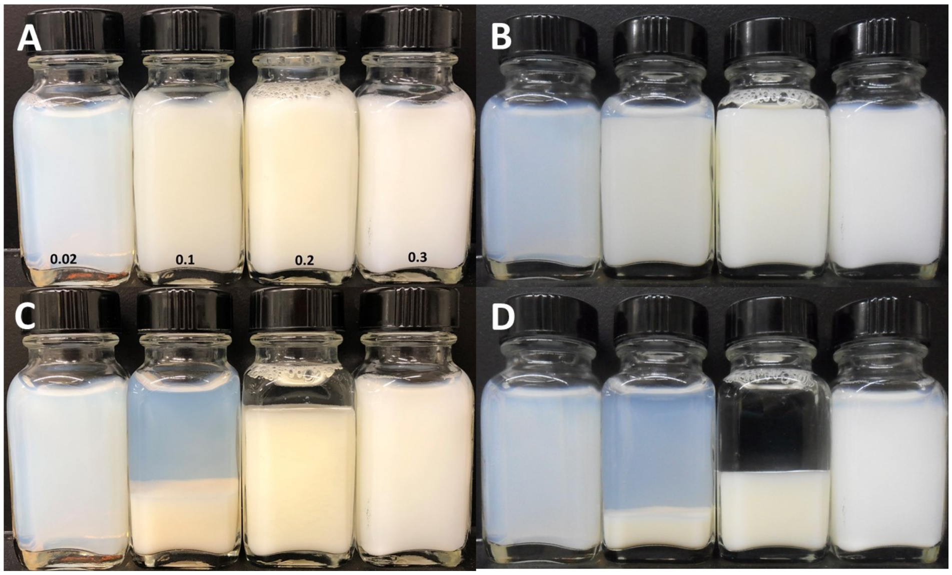

Figure 6-8 Settling of ceria and silica EB 6040 at 0.02,0.1, 0.2 and 0.3 weight ratio over (a) 0 hour (b) 8 hours (c) 24 hours and(d) 1 week. pH was kept at 4 for all samples

The data trend for the polish rates for silicon dioxide and nitride as a function of slurry weight ratio appears to follow the same path as that of the MAS containing ceria and EB 6080 abrasive particles of diameter 125 nm. As the ceria concentration increases, MRR for both oxide and nitride surfaces increases up to a maximum value. However, there is a substantial shift in the Ce/Si weight ratio at which the first maximum polish rate for both oxide and nitride is observed when compared to polishing with ceria and EB 6080 silica particles. A steep increase in both oxide and nitride polish rates was observed from 0.02 to 0.2 Ce/Si weight ratio where a first maximum of approximately 300 nm/min and 76 nm/min were measured for oxide and nitride MRR respectively. We know from Figure 5-10 using silica EB 6080 along with ceria, a maximum polish rate was achieved for both surfaces around 0.07 Ce/Si weight ratio, which corresponded to the IEP of the composite particle. When using silica Bindzil EB6040 instead of silica EB 6080 as the core particle for the attachment of the smaller ceria particles, settling tests at pH 4 showed rapid settling occurring at higher ceria to silica weight ratios between 0.1-0.2(see Figure 6-8) which signifies a shift in the isoelectric point of weight ratio to a higher value. This corresponded well with the zeta potential measurements in Figure 6-9 where the zero zeta potential weight ratio was observed at approximately 0.11. This shift in zero zeta potential weight ratio of the composite particle can be explained by the increase in the total silica surface area as the silica particle size decreases from 125 nm to 81 nm since the same weight percentage of silica was used. From the settling test, it is observed that while settling occurred fastest at a weight ratio of 0.1, which corresponded to the IEP of the composite particle, the MAS slurry still appeared cloudy when compared to the top liquid of that of 0.2 weight ratio MAS. When 5 wt % EB 6040 is used instead of 5 wt % EB 6080, more silica particles are now present in the slurry. At the point of zero net charge, it is believed that all the ceria particles were used to fully cover the silica particles and these zero net charge composite particles settled quickly, however, there still exist silica particles in the MAS that have not been fully covered or not covered at all which remain suspended in the slurry explaining the cloudy appearance. However, with an increase in ceria concentration to 0.2 weight ratio, all the silica particles are now fully covered with ceria particles leaving a transparent liquid at the top of the sediment.

A maximum oxide polish rate of 320 nm/min was observed at weight ratio 0.31 Ce/Si while nitride polish rate was approximately 9 nm/min giving a selectivity of ~35, however, by decreasing the Ce/Si weight ratio by a minute amount to 0.3 Ce/Si, oxide polish rate was approximately 313 nm/min and nitride MRR was at its' lowest of approximately 5 nm/min, almost doubling the selectivity to 63. At this weight ratio, the composite particles are believed to now possess a positive surface charge due to the ceria particles coating the negatively charged silica core changing its surface charge to zero and then to positive at 0.3 weight ratio. The positively charged composite particles are repelled by the similarly charged nitride surface. Settling test of the MAS at 0.3 Ce/Si weight ratio appear to be very stable at pH 4 due to the electrostatic repulsion among the particles. Zeta-potential measurements also showed the MAS at 0.3 weight ratio possessing the same zeta potential as that of pure ceria at pH 4 of approximately +40 mV.

Beyond 0.31 weight ratio MAS, oxide polish rates began to decrease and level off as the ceria concentration increases, as explained before, this may be due to ceria saturation in the suspension at higher concentrations. The same was observed for nitride, where the MRR increased slightly and then leveled off with increasing ceria concentration beyond 0.31 weight ratio.

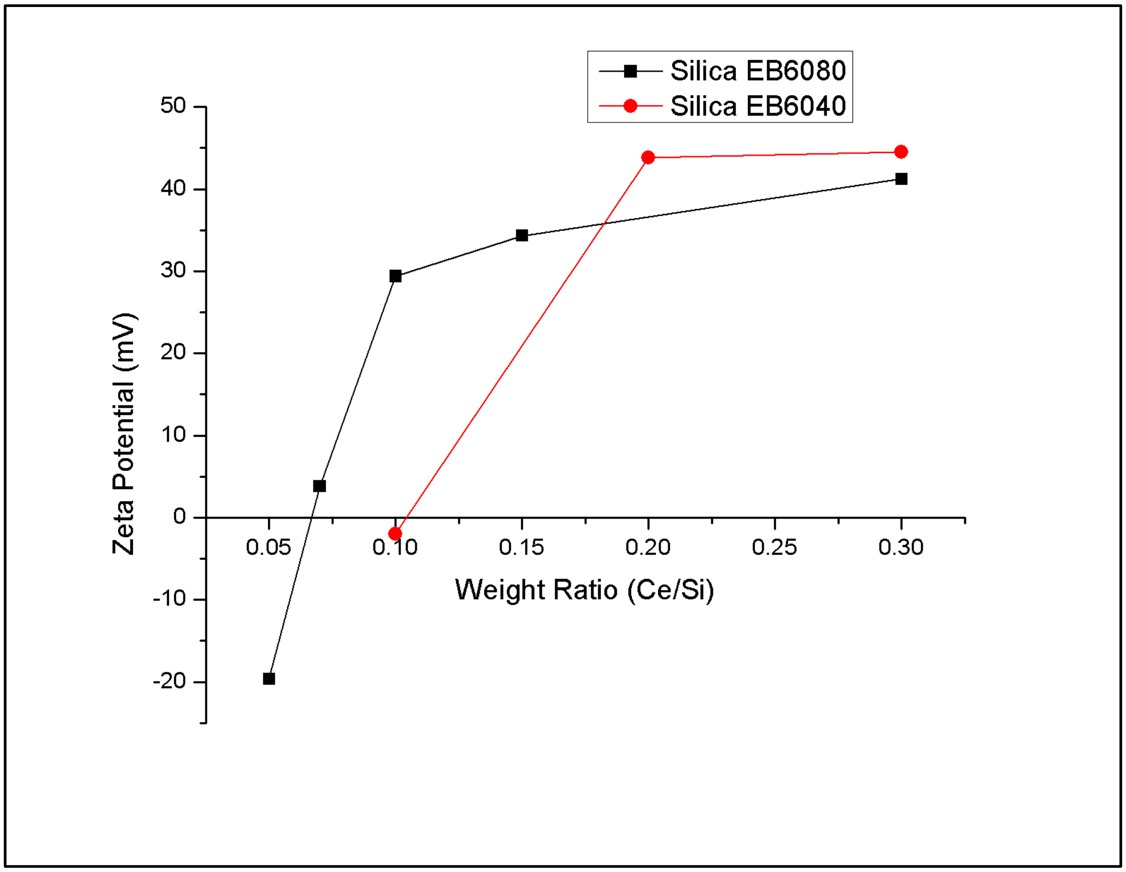

Figure 6-9 Zeta-potential of composite particles using ceria along with silica namely, EB 6080 (125 nm) and EB 6040 (81 nm) as a function of ceria-to-silica weight ratio

CMP of both oxide and nitride surfaces using silica EB 6040 and ceria was investigated at pH 10 at selected weight ratios between 0.1-0.3 and reported in Figure 6-10. Oxide polish rates were initially increased at 0.1 weight ratio Ce/Si when pH was increased from 4 to 10. This may be due to the quicker dissolution of the oxide layer at higher pHs, however, as the weight ratio increases, oxide polish rates dropped due to Coulombic repulsion between the composite particles and the oxide surface. Nitride polish rates also decreased with an increase to pH 10, with a minimum polish rate of approximately 10 nm/min observed at 0.2 Ce/Si weight ratio giving a selectivity of approximately 23. However, surprisingly an increase in polish rate was observed at 0.3 Ce/Si weight ratio at pH 10.

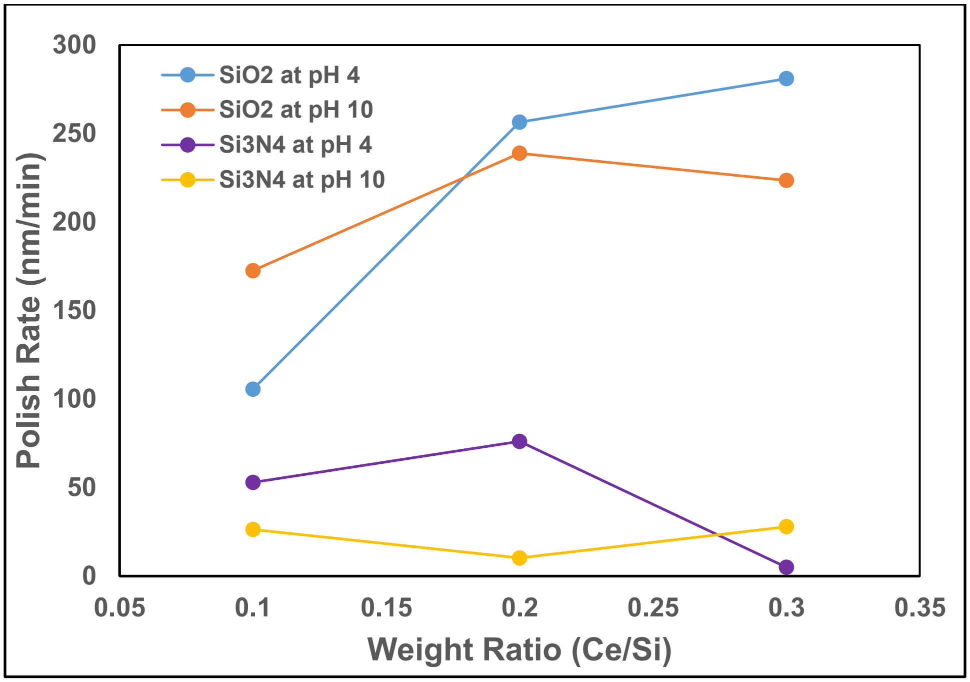

Figure 6-10 A comparison of silicon dioxide and silicon nitride polish rates using EB6040 along with ceria at pH 4 and pH 10 as a function of slurry weight ratio

6.4 CMP with MAS of EB 6040 and Ceria with Additives

Three different additives, L-proline, nicotinic acid and SDS were also added to the MAS utilizing silica EB6040 (diameter 81 nm) with ceria at pH 4 and all proved to be ineffective in suppressing the nitride polish rates as shown in Figure 6-11. In fact, in all cases (with the exception of SDS) when the additives were added to the slurry with weight ratios below 0.2, nitride removal rate increases with the additive.

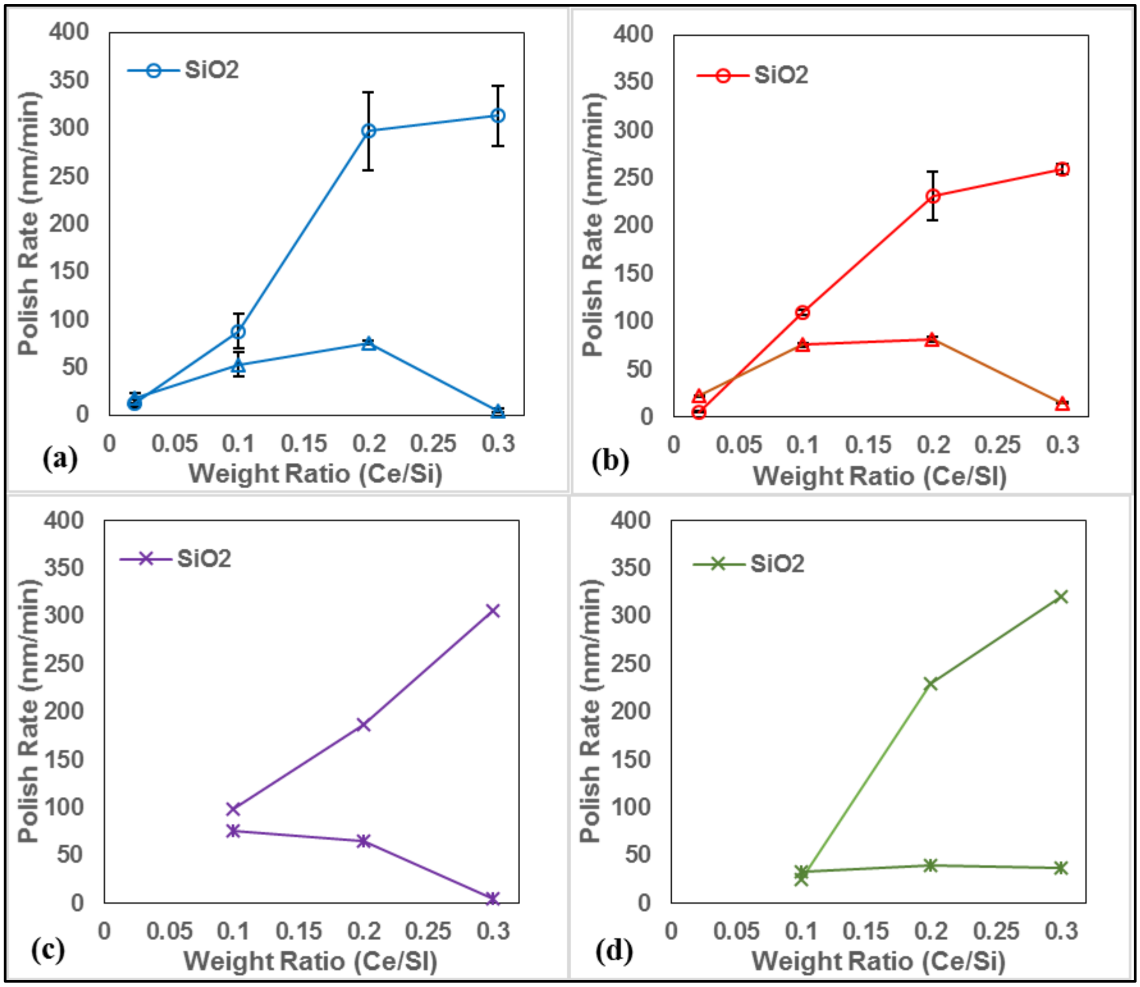

Figure 6-11 Polish rates of silicon oxide and nitride films as a function of ceria-to-silica weight ratio at pH 4, (a) without additive (b) with 0.5 wt % L-proline (c) with 0.1 wt % nicotinic acid and, (d) 10 mmol SDS.

Silicon dioxide polish rates decreased at all weight ratios with the addition of the additives. It is clear that the additives modified the ceria-silica interaction when smaller silica particles were used in the MAS. The highest selectivity achieved using additives with the MAS of ceria and silica EB6040 was approximately 58 at 0.3 Ce/Si weight ratio using 0.1 wt% nicotinic acid (Figure 6-11c) which was still a decrease in selectivity since the highest selectivity reported using these abrasive particles at the same weight ratio without additive was 63 (Figure 6-11a).

6.5 Model Proposal for Material Removal Mechanism using MAS based on IEP of Composite Particles.

Application of mixed abrasive slurries (MAS), such as the ones used in this work, have stimulated interest recently because of higher polish rates (or material removal rate MRR) and better selectivity as compared to single abrasive slurries (SAS). Despite their proven advantages in STI CMP, the material removal mechanism of MAS CMP is not fully understood. Material removal in SAS CMP is modelled as (i) an indentation-based polishing and (ii) a surface area based polishing as reported by Mahajan et al[60]. Using these SAS CMP models, a potential MRR mechanism for $CeO_2 + SiO_2$ MAS CMP is proposed.

In this study, we have made simplifying assumptions that all of the abrasive particles are spherical in shape and that the particle size distribution is such that every ceria and silica particles have diameters d_{CeO} and d_{SiO}, respectively. In a specific pH range, since ceria (+) and silica (-) particles are oppositely charged, the electrostatic attraction between these particles results in a core-shell structure where the negatively charged silica particles forms the core while the positively charged ceria particles ($d_{CeO} \ll d_{SiO}$) are evenly distributed over silica particle surface. The charge neutrality condition at isoelectric point for MAS slurries, allows calculation of the number of ceria particles that surround each silica core from their particle size and relative weight ratio under isoelectric conditions:

$$\left(\frac{\#CeO}{\#SiO}\right)=\left(\frac{\text{Wt. \% CeO}}{\text{Wt. \% SiO}}\right)^{isoelectric}\times\left(\frac{d_{SiO}}{d_{CeO}}\right)^{3}\times\left(\frac{\rho_{SiO}}{\rho_{CeO}}\right) \qquad [20]$$

Figure 6-9 shows that at pH = 4, for MAS1 (ceria and silica EB 6080 with d_{CeO} = 5 nm and d_{SiO} = 125 nm) IEP occurs at relative weight ratio of ~0.068; for MAS2 (ceria and silica EB 6040 with d_{CeO} = 5 nm and d_{SiO} = 81 nm) IEP occurs at relative weight ratio of ~0.11. The relative number of ceria particles per silica particle calculated at IEP conditions for MAS1 and MAS2 are summarized in Table 6-3. With decreasing d_{SiO}, both surface area and net surface charge per silica particle decreases. Consequently the number of ceria particles per silica core also decreases at IEP, as our calculations illustrate.

Table 6-3 Number of ceria particles per silica particle at the iso-electric point weight ratio

Ceria-to-Silica IEP weight ratio	Silica particle size (nm)	Ceria particle size (nm)	$\frac{\# CeO_2}{\# SiO2}$at IEP
0.068	125	5	306
0.11	81	5	135

The particle concentration (C_o) per cubic centimeter of slurry was calculated as:

$$\begin{aligned} C_o\left(1/cm^3\right) &= \frac{\left(0.01\times Wt_{particle}\%\right)\times\rho_{slurry}\left(gm/cm^3\right)}{Volume_{particle}\left(cm^3\right)\times\rho_{bulk}\left(gm/cm^3\right)} \\ &= \frac{Wt_{particle}\%\times10^{19}}{\frac{4}{3}\pi\left(\frac{d_{particle}}{2}\right)^{3}\times\rho_{bulk}} \end{aligned} \qquad [21]$$

where $d_{particle}$ is particle diameter (in nm), ρ_{bulk} is bulk density (in gm/cm^3), ρ_{slurry} is slurry density (in gm/cm^3).

The solid loading (wt %) used for both silica slurries was kept at 5 wt % and the ceria concentration was that calculated at the IEP weight ratio. ρ_{slurry} was assumed to be 1 gm/cc. The particle concentration at the IEP weight ratio are reported in Table 6-4 a and b.

Table 6-4 The particle concentration (C_o) per cubic centimeter of slurry for both silica particles and ceria using the solid loading at the IEP weight ratio

SiO_2 loading	**d_SiO_2**	**ρ_SiO_2**	**C_o_SiO_2**
(wt. %)	(nm)	(g/cm^3)	(1/ cm^3)
5	81	2.2	8.168E+13
5	125	2.2	2.222E+13

CeO_2 loading	**d_CeO_2**	**ρ_CeO_2**	**C_o_CeO_2**
(wt. %)	(nm)	(g/ cm^3)	(1/ cm^3)
0.34	5	7.65	6.7906E+15
0.55	5	7.65	1.0985E+16

According to the surface area based mechanism described by Mahajan et al[60], polishing rate varies with the total effective contact area (A) between the abrasives particles and the wafer. Since this contact area A is dependent on the abrasive concentration C_o and particle size d, MRR in surface area based polishing mechanism is given by:

(a) Surface area based mechanism

$$\begin{aligned} MRR &\propto A \\ &\propto C_o^{1/3} \times d^{-1/3} \end{aligned} \qquad [22]$$

For surface area based polishing mechanism, smaller particles results in higher MRR than larger particles and increasing the C_o also leads to higher MRR due to an increase in the number of particles in contact with the wafer surface.

On the other hand, material removal in indentation based mechanisms results from indentations made into the surface being polished and is expressed by the indent volume, *V* shown below:

(b) Indentation based mechanism

$$\begin{aligned} MRR &\propto V \\ &\propto C_o^{-1/3} \times d^{4/3} \end{aligned} \qquad [23]$$

For an indentation based polishing mechanism, larger particles will produce higher MRRs due to larger indent volume. Also with increasing particle concentrations, the polish rate should decrease as the distributed pressure on each particle is now lower.

Considering both the surface area mechanism, and the indentation mechanism for polishing, calculated ratio of the MRR for MAS1 (ceria + silica EB6080) and MAS2 (ceria+ silica EB6040) were compared with measured polishing rates. Here the effective diameter of abrasive particle in composite slurries MAS_1 and MAS_2 are approximated to d_{SiO} of silica EB6080 and silica EB6040 respectively (i.e. $d_{MAS1} \approx 125$ nm and $d_{MAS2} \approx 81$ nm).

For Surface Area-Based Mechanism, MRR ratio is obtained as:

$$\frac{MRR_{MAS1}}{MRR_{MAS2}} = \frac{(2.222 \times 10^{13})^{1/3}}{(8.168 \times 10^{13})^{1/3}} \times \frac{125^{-1/3}}{81^{-1/3}} = 0.56 \qquad [24]$$

For Indentation Based Mechanism, MRR ratio is obtained as as:

$$\frac{MRR_{MAS1}}{MRR_{MAS2}} = \frac{(2.222 \times 10^{13})^{-1/3}}{(8.168 \times 10^{13})^{-1/3}} \times \frac{125^{4/3}}{81^{4/3}} = 2.75 \qquad [25]$$

6.5.1 Verification of the Proposed Polish Mechanism

Calculated MRR ratios for MAS1 and MAS2 slurries considering (i) Surface area mechanism, and (ii) indentation mechanism are tabulated in Table 6-5. Polishing experiments using MAS1 (silica EB 6080 + ceria) and MAS2 (silica EB 6040 + ceria) at pH 4, showed that the silicon dioxide polish rates (RR) were higher for MAS1 for all CeO/SiO weight ratios investigated except at 0.3 weight ratio where the oxide RR was approximately equal.

Table 6-5 Comparison of the calculated MRR ratios for MAS1 and MAS2 slurries considering (i) Surface area mechanism, and (ii) indentation mechanism against experimental results.

Polish Mechanism	**MRR Ratio**
Surface Area	$\frac{MRR_{MAS1}}{MRR_{MAS2}} = 0.56$
Indentation	$\frac{MRR_{MAS1}}{MRR_{MAS2}} = 2.75$
CMP with MAS1 and MAS2 slurries	$\frac{MRR_{MAS1}}{MRR_{MAS2}} > 1$
CMP with only silica slurry	$\frac{MRR_{EB6080}}{MRR_{EB6040}} < 1$

Similarly silicon nitride RR were also higher for MAS1 at all CeO/SiO weight ratios with the exception at 0.2 CeO/SiO weight ratio, wherein MAS2 gave almost double the nitride RR rate than MAS1. However, it should be noted that at the 0.2 CeO/SiO weight ratio the MAS2 slurry was unstable and lead to agglomeration of the composite particles, whereas at the 0.2 weight ratio MAS1 slurry was stable. This observed MRR dependence on abrasive diameters (d_{MAS1} and d_{MAS2}) indicates that material removal with MAS1 and MAS2 composite slurries follows the indentation based polishing mechanism.

Interestingly, for polishing experiments using 5 wt% silica EB 6040 (d_{SiO} = 81 nm) alone at pH 4, MRR for oxide and nitride were 24.96 nm/min and 29.55 nm/min respectively, whereas the MRR of oxide and nitride using silica EB6080 (d_{SiO} = 125 nm) were 9.71 nm/min and 12.39 nm/min respectively. MRR dependence on diameter d_{SiO} observed in these experiments suggests that CMP using single abrasive slurries follow surface area mechanism for polishing.

Difference in the polishing mechanisms for MAS and SAS slurries may further explain:

(i) Use of surfactants only marginally improve oxide to nitride MRR selectivity for indentation based polishing with colloidal composite as opposed to improvement in selectivity for surface area based polishing

(ii) Surface area based polishing mechanism for silica slurry alone could explain higher nitride MRR compared to oxide MRR from the difference in the electrostatic interactions at similarly charged silica/silicon oxide interface and oppositely charged silica/silicon nitride interface.

Chapter 7 : Polish Rate as Function of Down Pressure and Frictional Force.

Friction monitoring using motor current signals can be used for endpoint detection in STI CMP processes. The friction force measurement between the pad and the wafer provides useful information for tribological analysis. Studies done on the polishing tribology have shown that mechanical interaction between the wafer, pad and slurry can influence the material removal rate. It was shown that the downforce applied on the wafer during polishing was directly proportional to the friction force[78]. Xie and Boning[87] showed that motor current signals were directly proportional to the frictional force between the wafer and pad. It was further suggested that motor current signals are dependent on the pattern structures and the different layered materials on the wafer. A friction model [87] was proposed where it was assumed that the exposure of the nitride layer and CMP induced global topography variations causes a change in the friction force.

Achieving an effective endpoint detection is an important outcome for STI CMP, leading to increased yield, improved throughout and planarity[87]. In Chapter 6, the proposed material removal mechanism of the CMP process using mixed abrasive slurries of colloidal ceria and silica joined together by electrostatic attraction was explained. A number of surfactants were also employed with the objective of stopping the hydrolysis reaction on the nitride surface and hence hindering the polishing of the nitride surface, however, the use of these surfactants proved to be marginally effective. In the absence of surfactants, selectivity was approximately 4 when the nitride MRR was at its' highest of ~ 93 nm/min and approximately 63 when the lowest nitride polish rate was achieved. This shows that silicon dioxide exhibited a much higher material removal rate over the entire weight ratio and pH range investigated. Based on bulk data (www.azom.com), the average hardness of silicon nitride is ~ 19.25 GPa while that of silicon dioxide is ~ 6.5 GPa. The silicon nitride surface is approximately 3 times harder than silicon dioxide, hence, it is not easily abraded by the ceria particles during polishing compared to oxide surfaces. Silicon nitride removal rate is believed to be predominately mechanical and therefore it is believed in our work that the friction force plays a key role in the material removal of silicon nitride.

In this chapter, the table load current (TLC) will be measured (which is directly related to the frictional force, TLC α F_F) while the downforce is varied during the polishing process. All the methods used in this chapter to determine the frictional force is explained in Experimental Procedures in Chapter 3 of this work and the polishing parameters listed in Table 3-1 with the exception of the down force that will be varied . In Chapter 6, the slurry that presented the optimum oxide-to-nitride polish rate selectivity was employed for all the measurements in this chapter (0.3 weight ratio ceria-to-silica EB6040 (diameter 81 nm) at pH 4). It should be noted that this is an exploratory chapter, a preliminary investigation into whether or not friction could be used to lower RR of nitride films.

7.1 Table load current as function of polish time

The motor current for the table was monitored at different down force (down pressure) for both oxide and nitride surfaces CMP with a polishing time of 60 seconds. Figure 7-1 shows the variation of the table load current (TLC) plotted against down force for both oxide and nitride wafer surfaces at a polishing time of 15 seconds (the time at which the maximum value of TLC for oxide surfaces was observed at all down pressures). As expected, increasing the down pressure during polishing increased the friction and hence the TLC. It should be mentioned here that the polishing of nitride surfaces at both 4 psi and 6 psi down pressure produced a very loud distinct noise while at a down pressure of 2 psi hardly any sound was heard. At down pressures > 2 psi, higher friction must be involved in the polishing process. This is most likely due to the indentation of the wafer surface by the abrasives at higher down pressures. The sound got very loud and persistent at 6 psi down force that it shook the entire tool opening the safety window and stopping the polishing process at approximately 25 seconds, a full minute of polishing data could not be attained. This sound was missing when polishing silicon oxide surfaces.

Figure 7-2 (a), (b) and (c) shows a comparison of the change in table load current when polishing oxide surfaces versus nitride surfaces against polishing time at down pressures of 2, 4 and 6 psi, respectively.

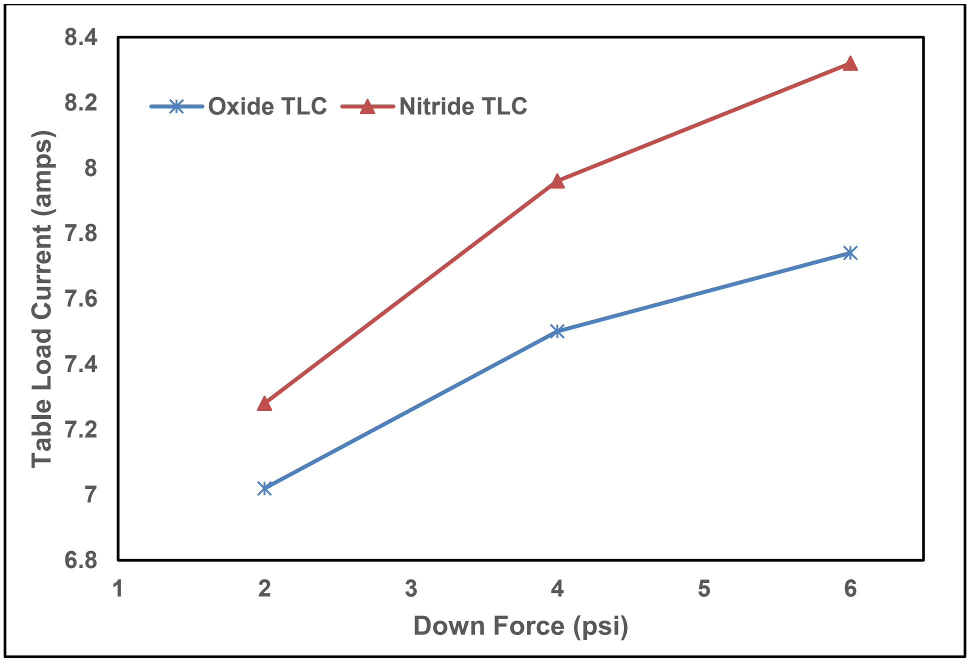

Figure 7-1 Variation of the table load current as a function of down force for both oxide and nitride surfaces at a polishing time of 15 secs.

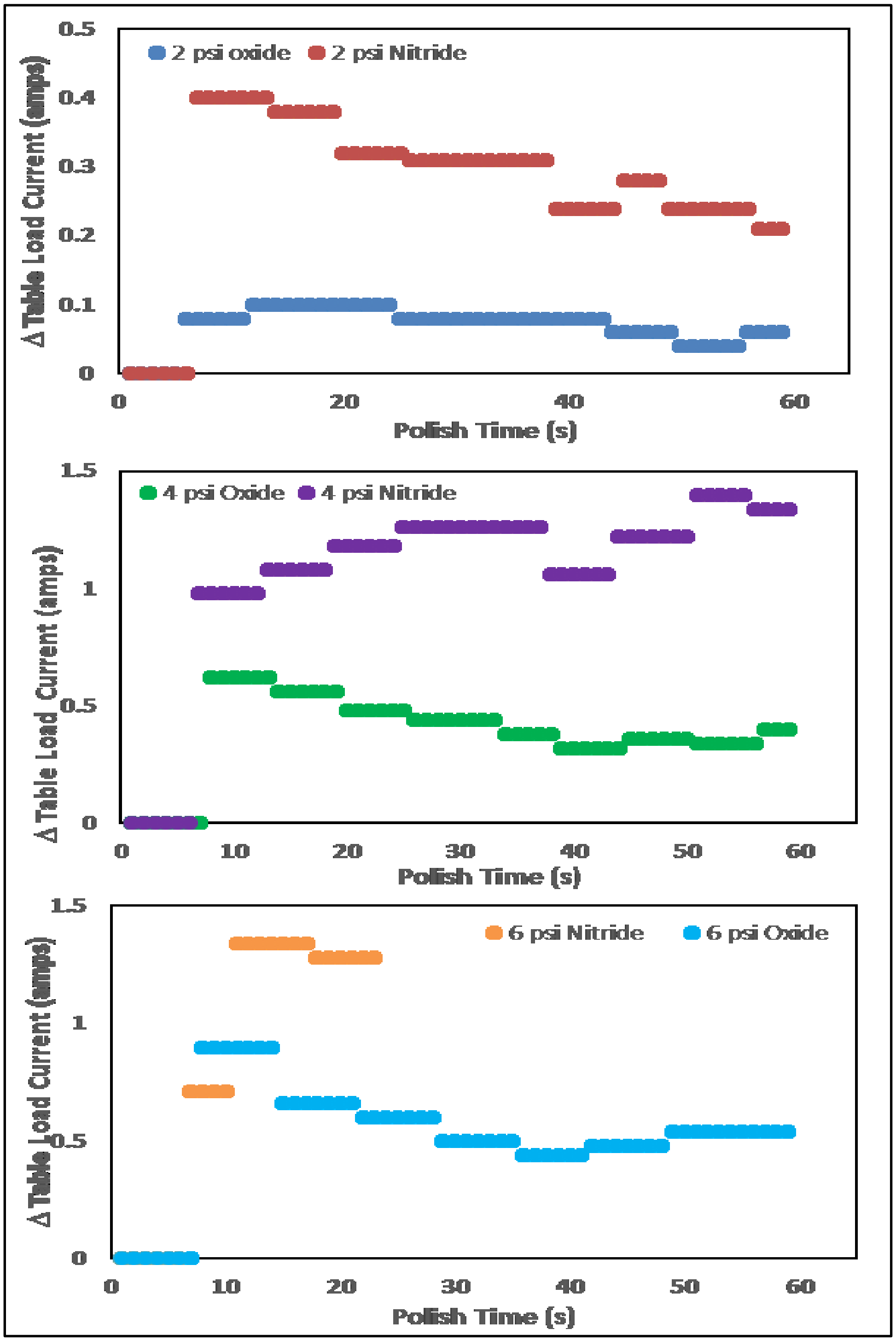

Figure 7-2 Comparison of the table load current as function of polish time when polishing oxide surfaces vs nitride surfaces at a down pressure of (a) 2 psi, (b) 4 psi and (c) 6 psi

At all down pressures, the TLC recorded for the polishing process of nitride surfaces was higher than that of oxide surfaces and TLC for nitride increased more than the TLC for oxide with increased down force. This signifies higher frictional forces for the polishing of nitride surfaces compared to oxide surfaces, however, although the friction is much higher for the polishing of nitride surfaces, polish rate is much lower compared to that of oxide surfaces which has to do with the hardness of the surfaces.

7.2 Polish Rate as function of down pressure

Changing the polish parameters such as pressure and velocity will affect the polish rate. According to Preston's equation, the relationship between the polish rate and PV product is expected to be linear. Here, the velocity was not changed but the down pressure was varied and the polish rates of both oxide and nitride surfaces were measured. It is evident from Figure 7-3, where the polishing rate for both silicon dioxide and silicon nitride are plotted against down pressure, that the highest polish rates were achieved at the higher table load values for both oxide and nitride surfaces. Increasing the down pressure results in a linear increase in the contact area between the pad and the wafer and hence a linear increase in the number of particles at the pad-wafer interface. Polish rates should increase linearly with the increase in down pressure. During polishing at low pressure (2 psi), the down force here has a smaller effect on the polish rate than at higher pressures > 2 psi. It is suggested that[89,110] lower polish rates at lower pressures can be attributed to the fact that there is no solid contact between the wafer–pad-abrasives and the slurry forms a thick boundary between the surfaces which in turn significantly reduces the friction force leading to lower removal rates.

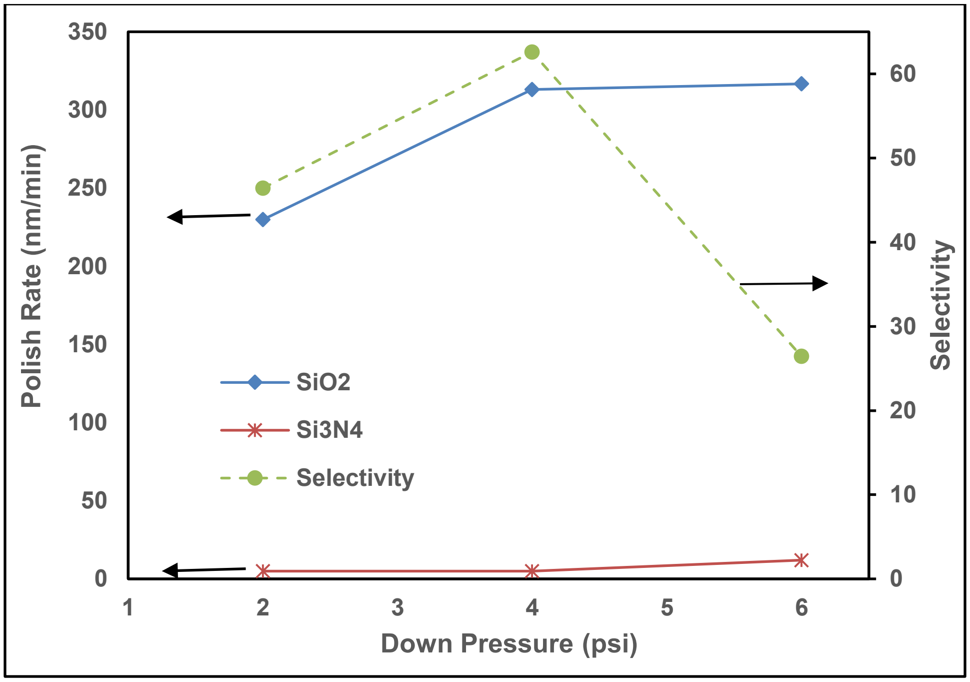

Figure 7-3 Polish rate of oxide and nitride as a function of down pressure and the corresponding selectivity.

7.3 Conclusion

The objective of this chapter was to study the frictional force that exist when polishing both oxide and nitride surfaces and relate this to the material removal rate by varying the down pressure. It was shown that an increase in the down pressure causes an increase in frictional forces, which leads to an increase in table load current and higher material removal rates. At all down pressures studied, the table load current measured was higher for nitride surfaces than oxide surfaces suggesting that the polishing of the nitride surface in this study is mostly mechanical. It is suggested that future work could focus on the addition of a surfactant to lubricate the nitride surface (instead of stopping the hydrolysis reaction as was the aim in Chapter 6) and hence decreasing the frictional force should suppress the nitride removal rate giving a higher oxide-to nitride removal rate selectivity that is needed for STI CMP.

Chapter 8 : Conclusions

It is the aim of this thesis to design a slurry using mixed abrasives of a silica core coated with more reactive colloidal ceria particles joined by electrostatic attraction for STI CMP. In addition, the removal of ceria abrasives from silica surfaces was evaluated using XPS, SEM and AES for the later cleaning of the surface during post-CMP.

Mixed abrasive slurries can be formed by simply mixing two different colloidal slurries if there is sufficient difference in the surface charge characteristics of the particles. Composites particles of a silica core (diameter ~ 125 nm) coated with ceria nanoparticles (diameter 5 nm) were made by simply mixing commercially available silica slurries with ceria slurries at pH 4. The composite particles were formed by electrostatic attraction and are not chemically bonded since at higher pH the particles separate. The colloidal stability of these slurries was studied and found to be dependent on the slurry weight ratio and pH.

The presence of different zones of colloidal stability of the MAS explains the relationship between material removal rate of oxide and nitride surfaces and colloidal stability of the slurry as a function of the slurry weight ratio. At very low ceria concentrations corresponding to low ceria-to-silica weight ratio (0.02), the composite particles possess a high negative net surface charge and the MAS behaves as a partially stable slurry. These mixed abrasive slurries have the least impact on material removal rate of oxide surfaces due to mutual repulsion of the negatively charged composite particles from the similarly charged oxide film surface and the "chemical tooth"[6] effect is limited due to the low ceria solid load. The MAS exhibited a transition in colloidal stability in the ceria to silica weight ratio range of 0.05-0.1. In this range the composite particles approach zero net charge as more ceria particles are attracted to the silica particle modifying the net charge. The particles agglomerate and unstable slurries are formed. Mixed abrasive slurries with weight ratios inside the transition range have the highest synergistic effect on both oxide and nitride polishing producing the highest material removal rates due to agglomerated particles trapped between the wafer and the pad under the polish pressure. MAS with weight ratios above the transition range regain stability as the particles now have a high positive net charge due to the excess of ceria particles and repels surrounding particles. MAS between 0.2-0.3 ceria-to-silica weight ratios possess a zeta-potential close to that of pure ceria particles. High oxide polish rates are obtained at these weight ratios due to the electrostatic attraction of the positively charge particles and the negatively charged oxide surface and the "chemical tooth"[6] effect is stronger here. On the other hand, nitride polish rates were at its' lowest as the particles are repelled by similar charged nitride film surface. At ceria-to-silica weight ratios > 0.3, the slurry becomes saturated and an increase in ceria concentration will not result in further increase in oxide polish rates.

Increasing the pH from 4 to 10 changes the slurry stability and also causes both the oxide and nitride polish rates to decrease. At high pH's, oxide polish rates were still ~200 nm/min due to its' rapid dissolution at higher pH's[82].

The interaction of colloidal ceria and silica abrasive particles in STI CMP is synergistic in nature. Combining ceria and silica lead to oxide polish rates that are over two times higher than the sum of the polish rates of the particles in isolation. Nitride polish rates also increased at lower ceria over silica weight ratios, however, at MAS weight ratios > 0.2 nitride polish rates decreased. Higher oxide and nitride polish rates are likely due to the increased contact of the 5 nm ceria abrasives brought closer to the surface being polished by the bigger silica core particle along with the synergistic combination of the chemical tooth effect of the ceria particles and the mechanical force of larger silica particles. Using MAS of ceria and silica without additives produced oxide RR as high as 420 nm/min at pH 6 using 0.2 ceria-to-silica weight ratio at pH 4 and nitride RR as high as 93 nm/min using 0.15 slurry weight ratio at pH 4. The highest selectivity was 28 when the nitride removal rate was around 7 nm/min using 0.2 ceria-to-silica weight ratio at pH 10. However, at pH 10 this slurry also produced lower oxide removal rates of around 200 nm/min. At pH 4, the highest selectivity was approximately 16 using 0.3 weight ratio MAS.

The second part of this study included the use of selected additives namely, L-proline, nicotinic acid, glycine and SDS with the goal of increasing the oxide-to-nitride selectivity by selective adsorption of the additives onto the nitride surface hindering the hydrolysis reaction and hence suppressing the nitride RR. However, all the additives, with the exception of L-proline, proved to be ineffective with MAS in suppressing the nitride polish rates. L-proline suppressed the nitride polish rates only at MAS weight ratios above the transition range at pH 4. Selectivity was doubled at MAS weight ratios of 0.2 and 0.3, both around 32 with the addition of 0.5 wt % L-proline. L-proline had no effect on the oxide removal rate. Using 0.3 ceria-to-silica weight ratio with 0.5 wt% L-proline at pH 9 (the composite particle is near zero net charge), the highest selectivity of 72 was achieved.

Smaller concentrations of the additives proved to be more effective in suppressing nitride RR when compared to using higher concentrations. The sequence in which the additive was added to the MAS also seemed to affect the polish rates because our study has additional electrostatic interactions between the particles, the additive seems to interfere with the ceria-silica interactions. It is believed that suppression of the nitride RR using additives in our study occurred through a combination of adsorption onto the nitride surface and chemical modification of the abrasive particle.

In Chapter 6, a smaller silica core particle size was employed (diameter 81 nm) and mixed with ceria particles at pH 4 in the same weight ratios reported for the larger silica core particle (diameter 125 nm). There was a shift in the isoelectric point of weight ratio to higher values and rapid settling occurred at higher ceria to silica weight ratios between 0.1-0.2 (transition range). Oxide and nitride polish rates were lower at all weight ratios (the exception being 0.3 where oxide polish rates were approximately the same) using a smaller silica core particle. The selectivity using the smaller silica core particle with ceria was as high as 63 at 0.3 weight ratio without an additive.

Using the polishing results for both MAS systems, and the IEP weight ratios of the composite particles, calculations were carried out and a model was proposed for the material removal mechanism using MAS in our study. Based on the calculations, it would appear that an indentation based mechanism is operational in our study. Our polishing results validated our theory.

To explore other possible routes to improve polish rate selectivity the friction force was analyzed by varying the down pressure. The table load current was higher for nitride polishing compared to oxide at all down force pressures. Given that the oxide polish rates were atleast 4 times higher than the nitride polish rate at the highest nitride RR measured, this suggests that the polishing of the nitride surface in this study is predominately mechanical and that using a surfactant to lower the silicon nitride friction may be a way to further improve polish rate selectivity.

Lastly, it is suggested that for the cleaning process in CMP, pH modification of the slurry may be a useful strategy to enhance cleaning of the wafer. This work demonstrated that the optimum pH for obtaining a clean silica surface, after exposure to a ceria slurry, is pH > 9.6, and we know that the preferred pH for the polishing of silica substrates with ceria is approximately pH 4[7]. To rectify this, one possible approach would be to polish wafers with optimum removal pH, and conclude the last few seconds of the polish process with a high pH slurry by adding potassium hydroxide, for example, to the polishing slurry on the pad. Emphasis should be placed on designing slurries that limit contact between the abrasive and the substrate, at least in the final stage of the polish process.

Future Work

The work carried out here utilized only blanket silicon dioxide or silicon nitride wafers, therefore future work should include the use of these slurries on patterned wafers. Studies on the effect of chemical additives and surfactants within MAS for high selectivity STI CMP needs more work in order to develop slurries with high oxide-to-nitride selectivity with a reduction in defect levels and improved surface finish. In this work, only two types of abrasive particles were utilized with 3 different particle sizes. Further work could include using other kinds of particles for mixed abrasive slurries.

Further work should also be carried out to elucidate the mechanisms of nitride polish rate suppression using surfactants. Nitride surface is harder than oxide surfaces and from our work, the polishing process of nitride appears to be more mechanical producing high frictional forces, therefore, a surfactant should be chosen to lubricate the surface reducing the friction force. Future work should be carried out to study the friction between particles and surfaces under various conditions such as varying the table and chuck velocity during polishing and varying the slurry flow rate to study the lubrication regimes. An in-depth study of the variation in the polish time dependency on the TLC is another area for future work.

Finally, endpoint detection is also a good area of future work for STI CMP performance. Such a study can be conducted through friction measurements using systems that can measure table and carrier motor current.

Bibliography

[1] *"Interconnect" in The International Technology Roadmap for Semiconductors* (2007).

[2] R.K. Singh, S.-M. Lee, K.-S. Choi, G. Bahar Basim, W. Choi, Z. Chen, and B.M. Moudgil, MRS Bull. **27**, 752 (2002).

[3] Y. Li, *Microelectronic Applications of Chemical Mechanical Planarization* (John Wiley, Hoboken, N.J., 2008).

[4] U. Paik and J.-G. Park, in (CRC Press, Boca Raton, 2009), pp. 3–8.

[5] W.. America, R. Srinivasan, and S. V. Babu, Mater. Res. Soc. Symp. Proc **566**, 13 (2000).

[6] L.M. Cook, J. Non. Cryst. Solids **120**, 152 (1990).

[7] F. Lin, L. Nolan, Z. Xu, and K. Cadien, J. Electrochem. Soc. **159**, H482 (2012).

[8] A. Jindal, S. Hegde, and S. V. Babu, Electrochem. Solid-State Lett. **5**, G48 (2002).

[9] A. Jindal, S. Hegde, and S. V. Babu, J. Electrochem. Soc. **150**, G314 (2003).

[10] Y.-J. Seo, S.-W. Park, and W.-S. Lee, J. Vac. Sci. Technol. A Vacuum, Surfaces, Film. **26**, 996 (2008).

[11] R. Manivannan and S. Ramanathan, Microelectron. Eng. **85**, 1748 (2008).

[12] W.G. America and S. V. Babu, Electrochem. Solid-State Lett. **7**, G327 (2004).

[13] W.-M. Lee, T. Katoh, H.-G. Kang, J.-G. Park, U. Paik, and H. Jeon, Korean Phys. Soc. **44**, L796 (2004).

[14] R. Manivannan, S.N. Victoria, and S. Ramanathan, Thin Solid Films **518**, 5737 (2010).

[15] K.-H. Bu and B.M. Moudgil, J. Electrochem. Soc. **154**, H631 (2007).

[16] L.-Y. Wang, B. Liu, Z.-T. Song, W.-L. Liu, S.-L. Feng, H. David, and S.. Babu, Chinese Phys. B **20**, 038102 (2011).

[17] P.R. Dandu Veera, S. Peddeti, and S. V. Babu, J. Electrochem. Soc. **156**, H936 (2009).

[18] N.K. Penta, B.C. Peethala, H.P. Amanapu, A. Melman, and S.V. Babu, Colloids Surfaces A Physicochem. Eng. Asp. **429**, 67 (2013).

[19] S.-H. Lee, Z. Lu, S. V. Babu, and E. Matijević, J. Mater. Res. **17**, 2744 (2002).

[20] Y. Lee, Y.-J. Seo, and H. Jeong, Electron. Mater. Lett. **8**, 523 (2012).

[21] G. Banerjee and R.L. Rhoades, in *ECS Trans.* (ECS, 2008), pp. 1–19.

[22] H.J. Levinson, *Principles of Lithography*, 3rd ed. (SPIE Press, Bellingham, 2010).

[23] R. Doering and Y. (Eds. . Nishi, *Handbook of Semiconductor Manufacturing Technology* (Marcel Dekker, New York, 2000).

[24] D. Apone, C. Gray, C. Rogers, V.P. Manno, C. Barns, M. Moinpour, S. Anjur, and A.Philipossian., Mater. Res. Soc. Symp. Proc. **867**, W2.3.1 (2005).

[25] J.-G. Park and T.-G. Kim, Mater. Res. Soc. Proc. **991**, (2007).

[26] L. Nolan and K. in: N. Cadien, in edited by M. Stepanova and S. Dew (Springer-Verlag/Wien, New York, 2012), pp. 239–274.

[27] K. Cadien, L. Nolan, H. Pirayesh, K. Dawkins, and Z. Xu, *Electrodeposition and Surface Finishing: Fundamentals and Applications, Modern Aspects of Electrochemistry* (Springer, 2014).

[28] R.K. Singh and R. Bajaj, Mater. Res. Soc. Bull. **27**, (2002).

[29] P.B. Zantye, A. Kumar, and A.K. Sikder, Mater. Sci. Eng. R Reports **45**, 89 (2004).

[30] E. Matijević and S.V. Babu, J. Colloid Interface Sci. **320**, 219 (2008).

[31] B. Zhao and F. G. Shi, J. Electrochem. Solid-State Lett. **2**, 145 (1999).

[32] R. Jairath, Mater. Res. Soc. Proc. **337**, 121 (1994).

[33] J.T. Abiade, Dissertation PhD: Characterization of the Chemical Effects of Ceria Slurries for Dielectric Chemical Mechanical Polishing, University of Florida, 2004.

[34] J.M. Steigerwald, S.P. Murarka, and R.J. Gutmann, *Chemical Mechanical Planarization of Microelectronic Materials* (Wiley and Sons, New York, 1997).

[35] S. Hegde and S. V. Babu, Electrochem. Solid-State Lett. **7**, G316 (2004).

[36] Z. Lu, S.-H. Lee, V.R.K. Gorantla, S. V. Babu, and E. Matijević, J. Mater. Res. **18**, 2323 (2003).

[37] J. Seo and U. Paik, in *Adv. Chem. Mech. Planarization* (Elsevier, 2016), pp. 273–298.

[38] W.M. Haynes, *CRC Handbook of Chemistry and Physics*, 92nd ed. (CRC Press, Boca Raton, FL, 2011).

[39] D.E. Speed, in *Adv. Chem. Mech. Planarization* (Elsevier, 2016), pp. 229–269.

[40] J. Dahle and Y. Arai, Int. J. Environ. Res. Public Health **12**, 1253 (2015).

[41] K. Dawkins, B.W. Rudyk, Z. Xu, and K. Cadien, Appl. Surf. Sci. **345**, 249 (2015).

[42] P. Suphantharida and K. Osseo-Asare, J. Electrochem. Soc. **151**, G658 (2004).

[43] T. Wiktorczyk, P. Biegański, and E. Zielony, Opt. Mater. (Amst). **34**, 2101 (2012).

[44] R. Srinivasan, P.V. Dandu, and S. V. Babu, ECS J. Solid State Sci. Technol. **4**, P5029 (2015).

[45] W. Hsu, L. Ronnquist, and E. Matijevic, Langmuir **4**, 31 (1988).

[46] M. Hirano and M. Inagaki, . . J. Mater. Chem. **10**, 473 (2000).

[47] A. TROVARELLI, Catal. Rev. **38**, 439 (1996).

[48] N. Chandrasekaran, MRS Proc. **816**, K9.2 (2004).

[49] Y.K. Hong, Y.J. Kang, J.G. Park, S.Y. Han, S.K. Yun, B.U. Yoon, and C.K. Hong, Solid State Phenom. **134**, 159 (2007).

[50] J.T. Abiade, W. Choi, and R.K. Singh, J. Mater. Res. **20**, 1139 (2005).

[51] P.R.V. Dandu, B.C. Peethala, and S. V. Babu, J. Electrochem. Soc. **157**, H869 (2010).

[52] A. Kelsall, Glas. Tech. **39**, (1998).

[53] T. Kido and K. Ichikawa, US Pat. 6,436,835 (2002).

[54] S. Kim, J.-H. So, D.-J. Lee, and S.-M. Yang, J. Colloid Interface Sci. **319**, 48 (2008).

[55] W. Choi, J. Abiade, S.-M. Lee, and R.K. Singh, J. Electrochem. Soc. **151**, G512 (2004).

[56] R. Jairath, M. Desai, M. Stell, R. Tolles, and D. Scherber-Brewer, MRS Proc. **337**, 121 (1994).

[57] T. Izumitani: in Treatise on Materials Science and Technology, in *Treatise Mater. Sci. Technol.*, edited by M. Tomozawa and R. Doremus (Academic Press, New York, 1979), p. 115.

[58] M. Bielmann, U. Mahajan, and R. K. Singh, Electrochem. Solid-State Lett. **2**, 401 (1999).

[59] W. Choi and R.K. Singh, Jpn. J. Appl. Phys. **44**, 8383 (2005).

[60] U. Mahajan, M. Bielmann, and R.K. Singh, MRS Proc. **566**, 27 (1999).

[61] G.B. Basim, J.J. Adler, U. Mahajan, R.K. Singh, and B.M. Moudgilz, J. Electrochem. Soc. **147**, 3523 (2000).

[62] R.K. Singh and R. Bajaj, MRS Bull. **27**, 743 (2002).

[63] C. Zhou, L. Shan, J.R. Hight, S. Danyluk, S.H. Ng, and A.J. Paszkowski, Tribol. Trans. **45**, 232 (2002).

[64] K. Cooper, J. Cooper, J. Groschopf, J. Flake, Y. Solomentsev, and J. Farkas, Electrochem. Solid-State Lett. **5**, G109 (2002).

[65] Z. Lu, S.-H. Lee, S.V. Babu, and E. Matijević, J. Colloid Interface Sci. **261**, 55 (2003).

[66] A. Jindal, Y. Li, and S. V. Babu, Mat. Res. Soc. Symp. Proc. **671**, (2001).

[67] W. Choi, U. Mahajan, S.-M. Lee, J. Abiade, and R.K. Singh, J. Electrochem. Soc. **151**, G185 (2004).

[68] G.B. Basim, I.U. Vakarelski, and B.M. Moudgil, J. Colloid Interface Sci. **263**, 506 (2003).

[69] K. Pate and P. Safier, in *Adv. Chem. Mech. Planarization* (Elsevier, 2016), pp. 299–325.

[70] F.W. Preston, J. Soc. Glas. Technol. **Vol XI**, 214 (1927).

[71] C. Rogers, J. Coppeta, L. Racz, A. Philipossian, F.. Kaufman, and D. Bramono, J. Electron. Mater. **27**, 1082 (1998).

[72] A. Mazaheri and G. Ahmadi, J. Electrochem Soc **150**, G233 (2003).

[73] S.-Y. Lee, S.-H. Lee, and J.-G. Park, J. Electrochem Soc **150**, G327 (2003).

[74] D. DeNardis, D. Rosales-Yeomans, L. Borucki, and A. Philipossian, Thin Solid Films **518**, 3910 (2010).

[75] Q. Luo, S. Ramarajan, and S.V. Babu, Thin Solid Films **335**, 160 (1998).

[76] A. Bryant, W. Haensch, and Mii T., IEDM Tech. Dig. 671 (1994).

[77] C.F. Lin, W.T. Tseng, M.. Feng, and Wang Y.L., Thin Solid Films **347**, 248 (1999).

[78] Y. Moon, in *Adv. Chem. Mech. Planarization* (Elsevier, 2016), pp. 3–26.

[79] J.. Bondur and H.B. Pogge, United States Patent number 4,104,086 (1978).

[80] Y. Li (Ed.), *Microelectronic Applications of Chemical Mechanical Planarization* (Wiley Interscience, New Jersey, 2007).

[81] E. Zhao and C. Shan, Semicond. Int. (2001).

[82] R.. Iler, *The Chemistry of Silica* (John Wiley & Sons, New York, 1979).

[83] T. Hoshino, Y. Kurata, Y. Terasaki, and K. Susa, J. Non. Cryst. Solids **283**, 129 (2001).

[84] A. Kelsall, Glas. Technol. **39**, (1998).

[85] Y.Z. Hu, R.. Gutmann, and T.. Chow, J. Electrochem. Soc. **145**, 3919 (1998).

[86] ITRS Roadmap: http://www.itrs.net/Links/2012ITRS/Home2012.htm Table FEP14, (n.d.).

[87] X. Xie and D. Boning, in *Proc. WTC2005 (World Tribol. Congr. III). ASME* (2005), p. WTC2005_641.

[88] L. Nolan, Achieving High Rates and High Uniformity in Copper Chemical Mechanical Polishing, University of Alberta, 2012.

[89] H. Pirayesh, Study of the High Rate Chemical Mechanical Polishing of Heavily Boron-Doped Polysilicon for 3D Applications, University of Alberta, 2014.

[90] J.C. Vickerman and I.S. Gilmore, *Surface Analysis - The Principal Techniques: 2nd Ed.* (John WIley & Sons Ltd, United Kingdom, 2009).

[91] G. Friedbacher, *Surface and Thin Film Analysis: A Compendium of Principles, Instrumentation, and Applications.*, Second Edi (Wiley, 2011).

[92] K. Osseo-Asare, J. Electrochem. Soc. **149**, G651 (2002).

[93] M. Nabavi, O. Spalla, and B. Cabane, J. Colloid Interface Sci. **160**, 459 (1993).

[94] P. Burroughs, A. Hamnett, A.F. Orchard, and G. Thornton, J. Chem. Soc. Dalt. Trans. 1686 (1976).

[95] E. Bêche, P. Charvin, D. Perarnau, S. Abanades, and G. Flamant, Surf. Interface Anal. **40**, 264 (2008).

[96] A. Kotani, T. Jo, and J.C. Parlebas, Adv. Phys. **37**, 37 (1988).

[97] F. Larachi, J. Pierre, A. Adnot, and A. Bernis, Appl. Surf. Sci. **195**, 236 (2002).

[98] B.E. Koel, G. Praline, H.-I. Lee, J.M. White, and R.L. Hance, J. Electron Spectros. Relat. Phenomena **21**, 31 (1980).

[99] E.J. Preisler, O.J. Marsh, R.A. Beach, and T.C. McGill, J. Vac. Sci. Technol. B Microelectron. Nanom. Struct. **19**, 1611 (2001).

[100] A.Q. Wang, P. Punchaipetch, R.M. Wallace, and T.D. Golden, J. Vac. Sci. Technol. B Microelectron. Nanom. Struct. **21**, 1169 (2003).

[101] F. Le Normand, J. El Fallah, L. Hilaire, P. Légaré, A. Kotani, and J.C. Parlebas, Solid State Commun. **71**, 885 (1989).

[102] C. Anandan and P. Bera, Appl. Surf. Sci. **283**, 297 (2013).

[103] Q. Xu, W. Lei, X. Li, X. Qi, J. Yu, G. Liu, J. Wang, and P. Zhang, Environ. Sci. Technol. **48**, 9702 (2014).

[104] L. Luo, J. Chen, and X. Wang, Appl. Surf. Sci. **322**, 111 (2014).

[105] J.-G. Yu, H.-G. Yu, B. Cheng, X.-J. Zhao, J.C. Yu, and W.-K. Ho, J. Phys. Chem. B **107**, 13871 (2003).

[106] L.H. Allen and E. Matijević, J. Colloid Interface Sci. **31**, 287 (1969).

[107] F. Lin, A Study of the Colloidal Stability of Mixed Abrasive Slurries of Silica and Ceria Nanoparticles for Chemical Mechanical Polishing, University of Alberta, 2011.

[108] Y. Nagendra Prasad and S. Ramanathan, Electrochem. Solid-State Lett. **9**, G337 (2006).

[109] J.-F. Lambert, L. Stievano, I.. Lopes, M. Gharsallah, and L. Piao, Planet. Sp. Sci. **57**, 460 (2009).

[110] H. Pirayesh and K. Cadien, ECS J. Solid State Sci. Technol. **3**, P213 (2014).